Universitätsklinikum Hamburg-Eppendorf

Klinik und Poliklinik für Pädiatrische Hämatologie und Onkologie

Prof. Dr. med. Stefan Rutkowski

Novel diagnostic methods for central nervous system tumors using liquid biopsies

Dissertation

zur Erlangung des Doktorgrades Dr. rer. biol. hum.

an der Medizinischen Fakultät der Universität Hamburg

vorgelegt von:

Ann-Kristin Afflerbach

aus Hamburg

Hamburg 2023

Angenommen von der

Medizinischen Fakultät der Universität Hamburg am: 15.01.2024

Veröffentlicht mit Genehmigung der Medizinischen Fakultät der Universität Hamburg.

Prüfungsausschuss, der/die Vorsitzende: Prof. Dr. Ulrich Schüller

Prüfungsausschuss, der/die zweite Gutachter/in: Prof. Dr. Klaus Pantel

Datum der Disputation: 15.01.2024

List of Contents

<u>Abbreviations</u>

Abbreviation	Meaning
°C	degrees Celsius
ATRT	atypical teratoid/rhabdoid tumor
bp	basepairs
BSA	bovine serum albumin
cfDNA	(circulating) cell-free DNA
Chr.	chromosome
CNS	central nervous system
CNV	copy number variation
CO_2	carbon dioxide
CSF	cerebrospinal fluid
CTC	circulating tumor cell
ctDNA	circulating tumor DNA
ddPCR	droplet digital PCR
DMEM	Dulbecco's modified eagle medium
DMG	diffuse midline glioma
DNA	deoxyribonucleic acid
DPBS	Dulbecco's phosphate-buffered saline
EGF	epidermal growth factor
EMEM	Eagle's minimum essential medium
ETMR	embryonal tumor with multilayered rosettes
EV	extracellular vesicle
FAM	fluorescein amidite
FCS	fetal calf serum
FFPE	formalin fixed, paraffin embedded
FGF	fibroblast growth factor
FISH	fluorescence in-situ hybridization
Gb	gigabases

Abbreviation	Meaning
gDNA	genomic DNA
h	hour(s)
H_2O	water
H3	histone 3
HEX	hexachloro-fluorescein
hg38	human genome, assembly 38
IDH	isocitrate dehydrogenase
k	thousand(s)
M	million(s)
Mb	megabases
MB	medulloblastoma
min	minute(s)
mL	milliliter(s)
MRD	minimal residual disease
mut	mutant
NA / n.a.	not available / not applicable
ng	nanogram(s)
NGS	next-generation sequencing
P/S	penicillin/streptomycin
PA	pilocytic astrocytoma
PCR	polymerase chain reaction
PF	posterior fossa
RNA	ribonucleic acid
sec	second(s)
SHH	Sonic Hedgehog
SNV	single nucleotide variant
TSO	TruSight Oncology, gene panel
UMAP	uniform manifold approximation and projection

Abbreviation	Meaning
VAF	variant allele frequency
WGS	whole genome sequencing
WHO	World Health Organization
WNT	wingless
WT	wildtype
x g	x gravity
μL	microliter(s)

1. Introduction

1.1. Tumors of the central nervous system

Conforming to the most recent guidelines of the World Health Organization (WHO), brain tumors can be classified into more than 100 different entities with varying characteristics, prognoses and outcomes [1,2]. Most entities can be divided into further subgroups and -types, according to their, often molecular, but also clinical characteristics – such as medulloblastoma with its subgroups wingless (WNT), sonic hedgehog (SHH), group 3 and group 4 [3,4]; or atypical teratoid/rhabdoid tumors (ATRT) with the subgroups tyrosinase (TYR), SHH, MYC and SMARCA4 [5,6]. Entities, incidences, symptoms, treatment and outcome vary between pediatric and adult patients. Generally, primary brain tumors are rare diseases, however they represent the most commonly occurring solid tumor type in pediatric patients, whereas other solid cancers like prostate cancer in male and breast cancer in female patients predominate in adults [7].

Considering this great variety of primary central nervous system (CNS) tumors, it is important to diagnose a tumor as accurately as possible. Especially in the still developing pediatric brain, treatment decisions need to be based on an accurate diagnosis. While radiotherapy is beneficial for some tumors [8], long-term risks for several issues such as cognitive impairments [9,10], hearing loss [9,11], hormone deficiencies [12] and cerebrovascular disease [13] are well known, showing that this treatment should only be utilized when absolutely necessary.

1.1.1. Diagnostics of CNS tumors

Historically, tumor diagnoses were made based on the histology of tumor biopsies and clinical features. While still important today, molecular characteristics are now ingrained into the diagnostic process, and for some tumor entities are even required to make the exact diagnosis [1,2]. For example, ependymoma are grouped based on their location within the CNS – with occurrences in the spinal cord, posterior fossa (PF) or supratentorial locations; on their histopathological features such as myxopapillary

features for the subgroup of myxopapillary ependymoma, as well as based on their molecular features, for example fusions such as RELA or YAP1 for the subgroups of ependymoma, RELA-fusion, or ependymoma, YAP1-fusion, respectively [1,2,14].

In recent years, the use of methylation profiling has become a widely respected method to classify brain tumors and their exact entities. Thousands of CpG sites of isolated DNA are analyzed in respect for their methylation status on arrays. The resulting data can be compared to a vast reference cohort using a random forest algorithm, which in turn classifies the sample with a probability score to the best fitting tumor entity [15,16]. This classifier, often referred to as the 'Heidelberg classifier', developed by Capper *et al.* [15,16] has been integrated into clinical routines in many neuropathologies and supports the diagnostic process immensely. This method allows for very robust and exact classification of brain tumors, and has already been adapted for other tumor entities, namely sarcoma [17,18]. Although it has great advantages, this method still has drawbacks. One of them is the long hands-on protocol, as the turn-around time from DNA isolation from samples to final methylation results is roughly five days. Another drawback this method shares with many others currently employed in the routine neuropathological diagnostic process is the availability of tumor tissue. Especially in cases with difficult to reach anatomical sites, such as the brainstem, or in the pediatric setting where neurosurgery would preferably not be performed, tumor tissue is not always available for the use in established methods. In cases where the surgeon cannot safely remove a piece of sufficient size of the tumor for biopsy, these methods are also often not applicable as they usually require hundreds of nanogram of DNA, leaving the patients with the risks of the surgery but no secured diagnosis. In addition to these drawbacks, knowing the tumor entity beforehand can influence the surgery and course of treatment. For example, the identification of the glioblastoma subgroup before surgery is able to influence the extent of resection necessary as patients with glioblastoma subclasses RTKI and RTKII benefit from extended resections, while patients with the mesenchymal subclass do not [19]. Similarly, if the diagnosis of an ependymoma compared to a medulloblastoma

is secured before the surgery takes places, neurosurgeons might preferably maximize the resection as residual tumor is one of the key risk factors in ependymoma [20], whereas it only plays a minor role in medulloblastoma [21]. For pre-surgery diagnosis, new diagnostic methods are needed that do not rely on the availability of tumor tissue. For this, the field of liquid biopsies opens great possibilities.

1.2. Liquid biopsies

The concept of liquid biopsies as the analysis of bodily fluid, namely plasma and bone marrow, for circulating tumor cells (CTCs) and disseminated tumor cells was coined in 2010 by Pantel and Alix-Panabières [22]. The range of analytes considered in the field of liquid biopsies expanded to cell-free DNA (cfDNA) or circulating tumor DNA (ctDNA) [23], as well as circulating RNAs [23,24] and extracellular vesicles (EVs) [25] (Figure 1.1).
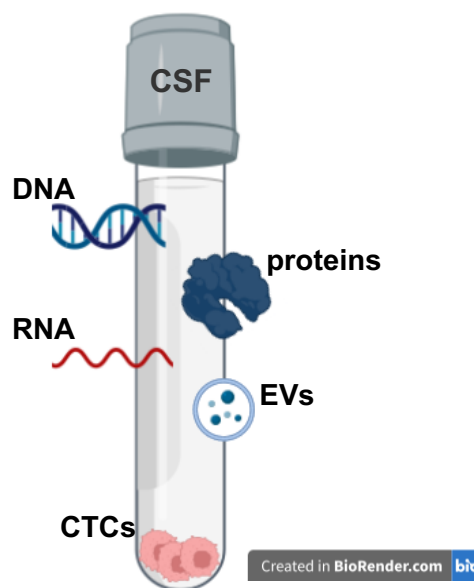
Figure 1.1 Analytes such as DNA, RNA, EVs, proteins and CTCs are found in liquid biopsies of the cerebrospinal fluid. CSF – cerebrospinal fluid, CTCs - circulating tumor cells, EVs - extracellular vesicles. Created in BioRender.com.

In the fast-growing field, many entities found uses for liquid biopsies, for initial diagnostics, biomarker evaluation or minimal residual disease (MRD) detection, as they contain valuable information and are collected minimally invasively compared to

surgical biopsies. Most cancers exhibit detectable levels of a liquid biopsy biomarker, such as ctDNA [26] that can be used for clinical decision making. Liquid biopsy studies in cancer types with relatively large cohorts, such as castration-resistant prostate carcinoma, allowed for the development of specific prognostic markers, like the CTC count in plasma [27]. In other cancer types, like breast cancer, specific cancer-associated mutations can be found in the plasma at early stages already, improving the initial diagnosis [28]. Liquid biopsies have become popular areas of research in many entities and are integrated in a great variety of clinical trials across many entities [29,30].

1.2.1. Cerebrospinal fluid

For neurooncological research and eventual diagnostics of brain tumors, finding appropriate liquids for the use as liquid biopsies proves somewhat more difficult. Cerebrospinal fluid (CSF) is in direct contact to the brain, which makes it an attractive fluid to use, however it is usually collected via lumbar puncture, and more rarely via shunt or extraventricular drainage, which is more invasive than a blood draw. However, these draws are routine procedures in the clinic and justifiable in regards to the possible benefits.

CSF is mainly produced by the choroid plexus, a structure in the ventricles. In adults, a total of about 150 mL of CSF is present in subarachnoid spaces in the cranium and spine, with a production of up to 600 mL per day. The CSF contains electrolytes such as Na^+, Cl^-, Mg^{2+}, K+ and Ca^{2+}, proteins, glucose and lactic acid, amongst other components [31,32]. Healthy CSF contains less than five cells per mL [31]. Circulation of the CSF follows the flow depicted by the arrows in Figure 1.2. It flows from the lateral ventricle through the interventricular foramen to the third and fourth ventricle, where it enters the subarachnoid space through the median aperture. Within the subarachnoid space, it follows either a rostral path until absorbed, or a caudal path into the spine, from where it circulates back towards the cranium [31,33].
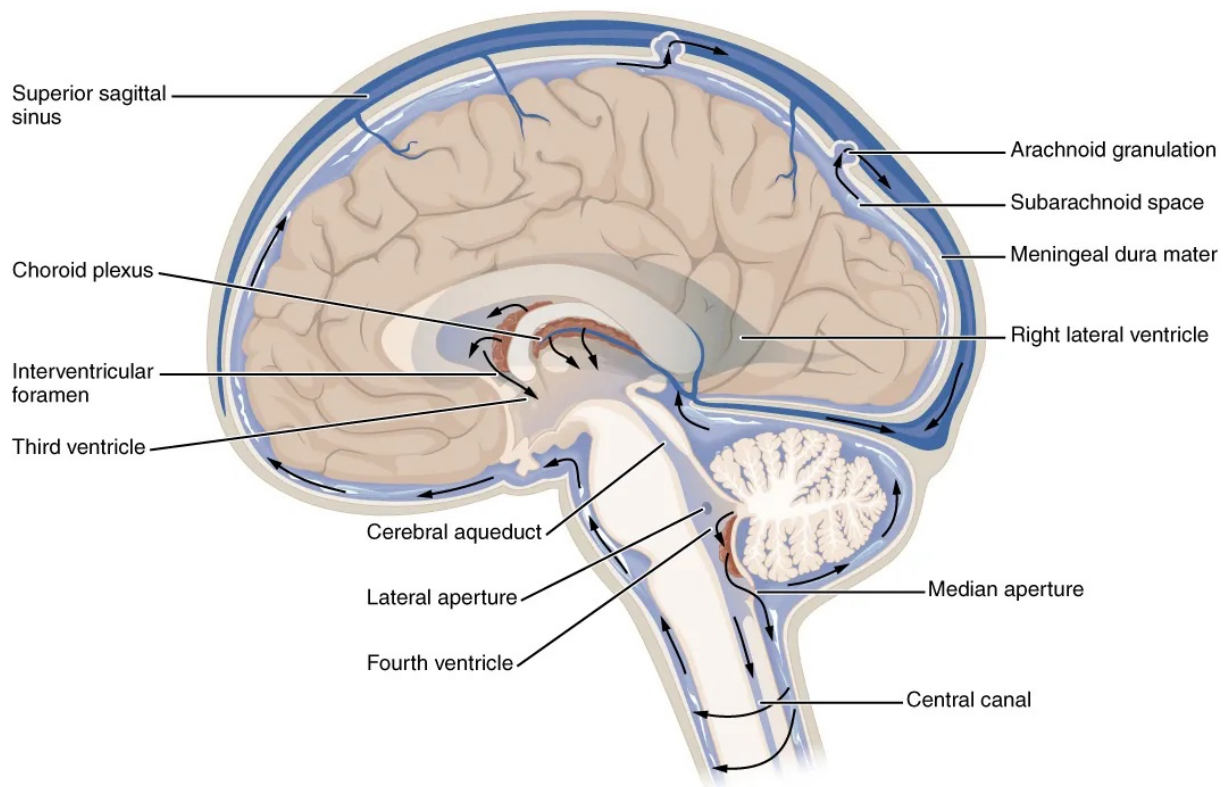
Figure 1.2 CSF circulation within the brain and skull. CSF flows from the choroid plexus through the lateral ventricles towards the third and fourth ventricles. It enters the subarachnoid space through the median aperture, where it either flows rostrally until it is absorbed, or caudally into the spine and back towards the cranium. CSF - cerebrospinal fluid. Figure from Betts et al. [33], access for free at https://openstax.org/books/anatomy-and-physiology/pages/1-introduction.

It has also been shown that CSF is the preferable fluid of choice for CNS tumors as detection rates of tumor-derived markers are higher than in other fluids [34–36], although biomarker detection is still possible in plasma [26,37]. One routine scenario of basic liquid biopsy analysis that is already adapted into clinical practices is the microscopic analysis of CSF for the presence of tumor cells after surgery for medulloblastoma patients to determine disease status. Molecular analyses of CSF and its analytes, however, are still experimental and not yet implemented into the routine.

1.2.2. Cell-free DNA

cfDNA is particularly interesting as analyte as it remains relatively stable for long periods of time and is easily isolated with commercially available kits [38,39]. After isolation, it can simply be stored at -20 °C and does not require special handling,

12

making it an attractive analyte for routine applications in the clinical diagnostic setting. In addition to delivering information on the sequence of the DNA itself, cfDNA also carries epigenetic modifications, opening up further possibilities of analysis and thus diagnostic paths [40]. The exact origins of cfDNA are still debated, with apoptosis being widely proposed as the main contributor to cfDNA fragmentation and release, however also necrosis and active secretion are possible origins for cfDNA [41]. The main characteristic distinguishing cfDNA from genomic DNA (gDNA), apart from it being cell-free, is its size: cfDNA is highly fragmented, with size ranges of 140-180 bp. In healthy cells, 143 bp is the length of DNA wrapped around the histone octamer, and 166 bp including the histone H1, which gives the cfDNA its characteristic length when cut by a nuclease (Figure 1.3) [42]. The fragmentation profile of tumor-derived cfDNA is possibly being influenced by chromatin modifications due to the inherent biological mechanisms of cancer [43–45], and often shows mean fragment lengths below 166 bp [46,47].
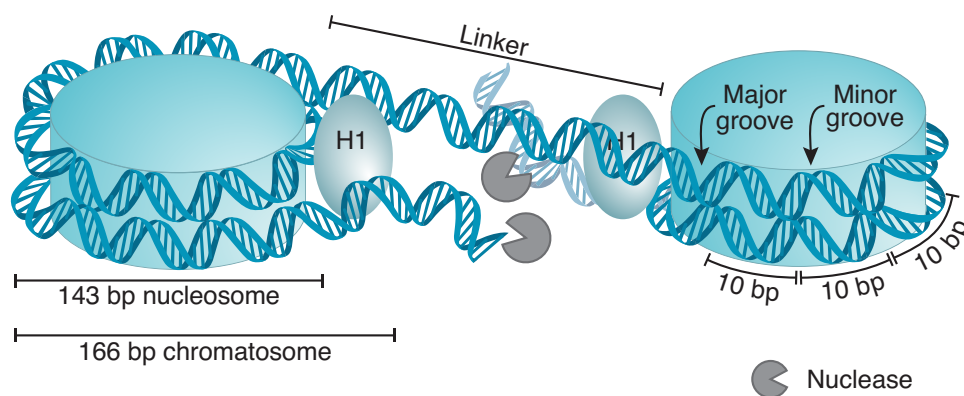
Figure 1.3 DNA is wrapped around the histone complex, forming nucleosomes. DNA wrapped around the histone complex and additionally the H1 forms the chromatosome. Nucleases target the DNA during for example apoptosis, and cut the DNA at the specific lengths of 143 bp for the nucleosome and at 166 bp for the chromatosome. bp - basepairs, H1 - histone 1. Adapted from Lo et al. [42].

cfDNA from the CSF does not differ in those characteristics and has the additional advantage of low background compared to plasma, as only few cells shed into the CSF – resulting in low DNA amounts in healthy people [39]. Another advantage of using cfDNA for molecular analysis over tissue biopsies is the possibility to interrogate the

tumor heterogeneity that might be lost in the tissue biopsy due to sampling bias. Tumor-derived biomarkers in the CSF recapitulate those in the tumor [34,35,48], yet sometimes they offer additional information regarding aberrations than the tumor biopsy itself [34,49]. Longitudinal studies for the detection of MRD using cfDNA from CSF are also successful [50].

1.2.3. Current approaches

CSF analysis, especially the analysis of CSF-derived cfDNA, is already performed using a variety of methods. The most prominent methods are polymerase chain reaction (PCR)-based methods, such as droplet digital PCR (ddPCR), and sequencing approaches. ddPCR is a highly sensitive method that randomly divides DNA fragments into thousands of singular water-in-oil droplets that all serve as an individual reaction tube [51]. Detection is fluorescence-based, and assays investigating single nucleotide variants (SNVs) and copy number variations (CNVs) are already commercially available. SNV detection has been demonstrated especially successful for diffuse midline glioma (DMG) that harbor a histone 3 (H3) K27M mutation [52,53]. Sequencing approaches involve next-generation sequencing (NGS), either targeted deep-sequencing approaches or low-coverage (shallow) whole genome sequencing (WGS). Low-coverage approaches are mostly used for CNV detection [50,54], whereas deep-sequencing approaches are more focused on SNV detection [55,56]. Both the target-informed and the broad, target-uninformed approaches have shown their utility in brain tumor diagnostics in these various studies.

The recent emergence of third generation sequencing approaches such as Nanopore sequencing has made sequencing approaches more widely accessible as it is less complicated in terms of handling and less expensive than previous classical sequencing approaches. Instead of depending on sequencing by hybridization or by synthesis, Nanopore sequencing works via the detection of changes in ionic current produced by nucleic acid strands passing through nanopores, derived from bacteria,

embedded in a membrane [57,58]. These signals are translated to the sequence in real-time, with the additional advantage of being able to detect epigenetic modifications, such as 5-methylcytosine and 5-hydroxymethylcytosine, on the strands [59,60]. With recent improvements to kit chemistries, flow cells and software, the method has outgrown its original purpose of long reads only, and is now also applicable for short read sequencing, such as that of cfDNA. Pioneer work for oncological research using Nanopore sequencing has been performed, showing that it is indeed possible to detect CNVs and perform methylation analysis from cfDNA [61,62]. For neurooncological purposes, Nanopore sequencing has been employed for methylation-based classification of brain tumors using tissue biopsies, showing robust classification results demonstrating that performing these kinds of analyses with the novel Nanopore method are feasible [63].

1.3. Aim of the work

The aim of this study was to develop a novel, minimally invasive diagnostic approach using liquid biopsies for brain tumors, especially in the pediatric setting.

Brain tumor diagnostics rely more heavily on molecular analysis in addition to histopathological analyses for exact tumor identification [1,2], however this still requires invasive neurosurgical biopsies. Pediatric patients and their developing brains experience additional risks with these surgeries. Liquid biopsies have gained popularity for tumor diagnostics and have been shown to also deliver promising results in the neurooncological setting [50,52–56]. However, the methods developed and experimentally used were often focused on singular entities, which is not ideal for routine clinical settings. The aim was to develop a method that would work for the majority of brain tumors, resulting in the most information possible for an integrated diagnosis.

First, ddPCR was employed as an informed approach to verify cfDNA as analyte of choice and to develop a method that would allow confirmation of ctDNA presence with known tumors.

As methylation arrays are already routinely performed in the local neuropathology as well as in many other centers, the routine protocol was investigated for improvement with the use of cfDNA isolated from CSF.

Next, sequencing approaches were investigated. As an uninformed approach, they could potentially work with samples of unknown tumors and thus perform as tools for delivering an initial diagnosis. In this part, traditional next-generation deep-sequencing approaches were investigated as well as novel third-generation sequencing approaches that allow a combinatorial analysis of sequence and methylation.

2. Materials & Methods

2.1. Reagents & chemicals, kits and consumables

Table 2.1 Reagents and chemicals used in this study.

Reagent / chemical	Specification	Manufacturer
Blunt/TA Ligase Master Mix		New England BioLabs Inc., USA
ddPCR supermix for probes	no dUTP	Bio-Rad Laboratories, USA
DMEM/F-12 + GlutaMAX		Gibco, Thermo Fisher Scientific, USA
DPBS (Dulbecco's phosphate-buffered saline)	without calcium chloride and magnesium chloride	Gibco, Thermo Fisher Scientific, USA
Droplet generator oil		Bio-Rad Laboratories, USA
Droplet reader oil		Bio-Rad Laboratories, USA
EGF (epidermal growth factor)	human, recombinant	PeproTech Inc., Thermo Fisher Scientific, USA
Ethanol	analysis grade, 96-100%, EMSURE	Supelco, Merck KGaA, Germany
FCS (fetal calf serum)		Gibco, Thermo Fisher Scientific, USA
FGF (fibroblast growth factor)	human, recombinant	PeproTech Inc., Thermo Fisher Scientific, USA
Formamide		Sigma-Aldrich, Merck KGaA, Germany
Glutamine		Life Technologies, Thermo Fisher Scientific, USA
Laminin		Sigma-Aldrich, Merck KGaA, Germany
Native barcoding expansion	EXP-NBD104, 1-12, PCR-free	Oxford Nanopore Technologies, UK
NEBNext FFPE DNA Repair Mix		New England BioLabs Inc., USA
NEBNext Quick Ligation Module	T4 Ligase	New England BioLabs Inc., USA

Reagent / chemical	Specification	Manufacturer
NEBNext Ultra II End Repair/dA-Tailing Module		New England BioLabs Inc., USA
NeuroCult	NS-A Basal	STEMCELL Technologies Canada Inc.
Penicillin/Streptomycin	5000 U / mL	Gibco, Thermo Fisher Scientific, USA
Restriction enzyme	FastDigest *Hind*III	Thermo Fisher Scientific, USA
Seraseq ctDNA Complete Mutation Mix		SeraCare, LGC Clinical Diagnostics, Inc., UK
Trypsin/EDTA	0.25%	Gibco, Thermo Fisher Scientific, USA

Table 2.2 Kits used in this study.

Kit		Manufacturer
BioAnalyzer High Sensitivity DNA kit		Agilent Technologies, USA
DNA Clean & Concentrator-5		Zymo Research Corp., USA
EZ DNA Methylation kit		Zymo Research Corp., USA
Flow cell wash kit	EXP-WSH004 / EXP-WSH004-XL	Oxford Nanopore Technologies, UK
Infinium HD FFPE DNA Restore kit		Illumina, USA
Ligation sequencing kit	SQK-LSK109 / SQK-LSK110 / SQK-LSK114	Oxford Nanopore Technologies, UK
MagMAX Cell-Free DNA Isolation kit		Thermo Fisher Scientific, USA
NEBNext Enzymatic Methyl-seq kit		New England BioLabs Inc., USA
NucleoMag kit for clean up and size selection of NGS library prep reactions		Macherey-Nagel GmbH + Co. KG, Germany
NucleoSnap cfDNA kit for cell-free DNA from plasma		Macherey-Nagel GmbH + Co. KG, Germany
NucleoSpin Tissue, Mini kit for DNA from cells and tissue		Macherey-Nagel GmbH + Co. KG, Germany

Kit	Manufacturer
QIAamp Circulating Nucleic Acid kit	Qiagen GmbH, Germany
Qubit High Sensitivity DNA assay	Invitrogen, Thermo Fisher Scientific, USA
TruSight Oncology 500 ctDNA kit	Illumina, USA

Table 2.3 Consumables used in this study.

Consumable	Specification	Manufacturer
96-well plates		Bio-Rad Laboratories, USA
Cartridges	DG8	Bio-Rad Laboratories, USA
Centrifuge tubes	15 mL / 50 mL	Greiner Bio-One GmbH, Austria
Centrifuge tubes	LoBind, 15 mL	Eppendorf SE, Germany
Filter pipette tips	10 μL / 100 μL / 200 μL / 1000 μL	Sarstedt AG & Co. KG, Germany
Flow cells	R9.4.1 / R10.4.1	Oxford Nanopore Technologies, UK
Gaskets	DG8	Bio-Rad Laboratories, USA
Methylation array	EPIC	Illumina, USA
Microcentrifuge tubes	1.5 mL / 2 mL	Eppendorf SE, Germany
Microcentrifuge tubes	LoBind, 1.5 mL	Eppendorf SE, Germany
PCR tubes	0.2 mL	Sarstedt AG & Co. KG, Germany
Pierceable heat foil		Bio-Rad Laboratories, USA
Pipette tips	10 μL / 100 μL / 1000 μL	Sarstedt AG & Co. KG, Germany
Qubit assay tubes		Invitrogen, Thermo Fisher Scientific, USA
Serological pipets	2 mL / 5 mL / 10 mL	Sarstedt AG & Co. KG, Germany
Tissue culture flasks	T75, adherent & suspension	Sarstedt AG & Co. KG, Germany

2.2. ddPCR assays

Table 2.4 ddPCR assays used, all by Bio-Rad Laboratories, USA.

Target	Type	Length	Unique Assay ID
AP3B1	CNV detection	60 bp	dHsaCP2500315
Myc	CNV detection	121 bp	dHsaCP2507112
MycN	CNV detection	64 bp	dHsaCP2506554
BRAF V600E	SNV detection	91 bp	dHsaMDV2010027
H3-3A K27M	SNV detection	129 bp	dHsaMDV2510510

2.3. Equipment

Table 2.5 Equipment used for this study.

Equipment	Model	Manufacturer
BioAnalyzer	2100	Agilent Technologies, USA
Centrifuges	Heraeus Multifuge 3 S-R / Megafuge ST Plus	Thermo Fisher Scientific, USA
Centrifuge for CSF	Rotofix 32 A	Andreas Hettich GmbH & Co. KG, Germany
CO_2 incubator	HERAcell 240	Heraeus GmbH & Co. KG, Germany
Droplet generator	QX200	Bio-Rad Laboratories, USA
Droplet reader	QX200	Bio-Rad Laboratories, USA
Magnet for tubes	IMag Cell Separation Magnet	BD Biosciences, Becton, Dickinson and Company, USA
	Dynal MPC-E	Thermo Fisher Scientific, USA
Microarray scanner	iScan	Illumina Inc., USA
Microcentrifuge	Heraeus Pico 17 / Heraeus Fresco 17	Thermo Fisher Scientific, USA
Nanopore sequencer	MinION Mk1b / MinION Mk1c / GridION	Oxford Nanopore Technologies, UK
NGS Sequencer	NovaSeq	Illumina Inc., USA
PCR Plate Sealer	PX1	Bio-Rad Laboratories

Equipment	Model	Manufacturer
Pipetor	Pipetus	Hirschmann Laborgeräte, Germany
Pipette	10 µL / 200 µL / 1000 µL	Gilson Inc., USA
Pipette	100 µL	Eppendorf SE, Germany
Qubit	3.0	Invitrogen, Thermo Fisher Scientific, USA
Rotator mixer	Rotator SB3	Stuart, Thermo Fisher Scientific, USA
Tabletop centrifuge	C1301 B	Labnet International, Corning Inc., USA
	Rotilabo	Carl Roth GmbH + Co. KG
Thermocycler	Biometra TAdvanced	Analytik Jena GmbH + Co. KG, Germany
Thermocycler for 96-well plates	Biometra TOne	Analytik Jena GmbH + Co. KG, Germany
Vacuum manifold	Vac-Man	Promega GmbH, Germany
Vacuum pump	Laboport	KNF DAC GmbH, Germany
Vortex	vortex mixer	Stuart, Thermo Fisher Scientific, USA
	MS2	IKA-Werke GmbH + Co. KG, Germany
Water bath	WB 10	P-D Industriegesellschaft mbH, Germany

2.4. Software

Table 2.6 Software used for this study.

Software	Version	Source
2100 Expert	B.02.11.SI811	Agilent Technologies, USA
Guppy	6.1.5 / 6.3.8	Oxford Nanopore Technologies, UK
Inkscape	1.2	open source, https://inkscape.org
MinKNOW	21.11.6 - 23.07.12	Oxford Nanopore Technologies, UK
PyCharm	2021.3.3	JetBrains s.r.o., Czech Republic
Python	3.9.7	open source, https://www.python.org
QuantaSoft	1.7.4	Bio-Rad Laboratories, Inc., USA
R	4.2.2	open source, https://www.r-project.org
RStudio	2022.02.3 492 "Prairie Trillium"	Posit Software, USA

2.5. Cerebrospinal fluid sample collection

CSF was collected via lumbar puncture, ventricular puncture or external ventricular drainage when clinically indicated from patients with brain tumors or suspected brain tumors for routine diagnostics. The use of the CSF biopsies for this research upon anonymization was in line with the local ethical standards, as well as guidelines and regulations at the Universitätsklinikum Hamburg-Eppendorf.

Samples were collected in standard CSF tubes or in Eppendorf LoBind tubes. Typically, 1-10 mL were collected. Samples were processed in the Department of Neuropathology for cytology analysis by centrifuging for 10 min at 750 x *g*. The sediment was used for cytospin preparation in the routine diagnostic, the supernatant

was either used immediately for cfDNA isolation or stored in LoBind tubes at -20 °C until it was used in further experiments.

2.6. Cell culture

In Table 2.7, cell lines are described with their origins, culture specifications and characteristics. Adherent cells were cultured with their respective medium in T75 flasks for adherent cells in an incubator at 37 °C with 5% CO_2 and 86% humidity. For continuous culture, cells were grown until they were confluent. Cells were washed with 5 mL of DPBS. To detach the cells from the flask, 2 mL of Trypsin-EDTA was added, and flask was incubated in the incubator for 3 – 5 min. If cells had not detached, flask was tapped on the bench to manually detach the cells. To the detached cells, 5 mL of medium was added. Cells were pelleted by centrifugation for 5 min at 350 x g and then diluted and seeded as desired in a fresh flask.

Flasks for PBT-04 were coated with laminin for 1 h in the incubator and washed twice with DBPS before cells were seeded into them.

D341 cells were cultured similarly to adherent cells described above, but in T75 flasks for suspension cells. For splitting, they were transferred with their medium to a 15 mL tube and centrifuged for 5 min at 350 x g. Pelleted cells were washed with 5 mL DPBS. Cells were diluted accordingly with medium, and then seeded in a fresh flask.

For the isolation of reference or control cfDNA, aspirated medium was collected in 15 mL tubes and centrifuged for 10 min at 750 x g. Supernatant was transferred and stored in LoBind tubes at -20 °C until isolation of cfDNA. Pelleted cells were transferred to 1.5 mL tubes and stored at -20 °C until gDNA was isolated.

Table 2.7 Cell lines used as references and their characteristics.

Cell line	Origin	Culture specification	Media	Characteristics
HEK293T	human embryonic kidney	adherent	DMEM + 10% FCS + 1% P/S	used as wild-type control
SF8628	diffuse intrinsic pontine glioma	adherent	DMEM + 10% FCS + 1% P/S	*H3-3A* K27M mutation
Malme-3M	melanoma	adherent	DMEM + 10% FCS + 1% P/S	*BRAF* V600E mutation
D341	medulloblastoma	suspension	EMEM + 20% FCS + 1% P/S	*Myc* amplification
PBT-04	high-grade glioma	adherent	NeuroCult + 1% P/S + 20 ng/mL EGF + 20 ng/mL FGF	*MycN* amplification
LN-229	glioblastoma	adherent	DMEM + 10% FCS + 1% P/S + 1% glutamine	*p53* mutation, CNV aberrations

2.7. DNA isolation & characterization

2.7.1. cfDNA

Liquid biopsy samples were thawed at room temperature, if necessary, and centrifuged at 11,000 x *g* for 10 min. Then, cfDNA was isolated with the ThermoFisher MagMAX Cell-free DNA Isolation Kit, the Qiagen QIAamp Circulating Nucleid Acid Kit or with the Macherey-Nagel NucleoSnap cfDNA kit from plasma according to the respective manufacturer's instructions. In short, samples were lysed, cell-free DNA was bound to either beads or silica membrane, then samples were washed, and finally cell-free DNA was eluted.

For most samples, the Macherey-Nagel NucleoSnap cfDNA kit was used. Here, the sample was incubated with 15 µL Proteinase K per mL sample for 5 min. Then, an equal volume of lysis buffer was added. The mixture was vortexed and incubated for 5 min in a water bath at 56 °C. A to the initial sample equal volume of 96-100% ethanol

was added, the mixture was thoroughly vortexed. The purification column was assembled with a connector on the vacuum manifold. 500 µL column conditioner was added to the column, then vacuum was applied. After 1-5 min, sample mixture was added to the column and vacuum was applied. When sample had fully passed through the column, silica membrane was washed with 1000 µL wash buffer VW1 first, and second with 500 µL wash buffer. Then, upper part of the column was snapped off and discarded, lower part was centrifuged for 3 min at 11,000 x g in a collection tube to dry the silica membrane. The column was then transferred to a fresh collection tube and 50 µL of elution buffer was added. After a 3 min incubation time, cfDNA was eluted by centrifugation of the column for 1 min at 11,000 x g.

Total DNA was quantified using the Qubit High Sensitivity DNA assay with the Qubit 3.0 according to the manufacturer's instructions (see 2.7.3).

2.7.2. gDNA

gDNA was isolated from cultured cells using the Macherey-Nagel NucleoSpin Tissue kit. In brief, cells were lysed, DNA was bound to the silica membrane, which was then washed and lastly, gDNA was eluted. Total DNA was quantified using the Qubit High Sensitivity DNA assay with the Qubit 3.0 according to the manufacturer's instructions (see 2.7.3).

2.7.3. Qubit

The Qubit 3.0 was used to determine total DNA concentration within a sample. The Qubit High Sensitivity DNA assay was used according to the manufacturer's instructions. Standards were read once daily. 1 µL of sample was quantified twice and the mean was calculated.

2.7.4. BioAnalyzer

Distribution of fragment sizes from isolated DNA was analyzed using the Agilent BioAnalyzer with the High Sensitivity DNA kit according to the manufacturer's

instructions. For determination of cfDNA proportion, the region of calculation within the 2100 Expert software was set to 75-400 bp. For molarity calculation, region was not specified and all fragments were considered.

2.8. ddPCR

2.8.1. Single nucleotide variation detection

Assays used are listed in Table 2.4. Mastermix for ddPCR was prepared according to Table 2.8. Restriction enzymes were used as recommended and compatible for assays, which was *Hind*III in all assays used. For wildtype controls, cfDNA or gDNA from HEK293T cells was used. For the mutation control in the *H3-3A* K27M assay, DNA from SF8628 cells was used, for the *BRAF* V600E assay DNA isolated from Malme-3M cells was used. Generally, 10 ng of input were preferred for controls as well as for the sample of interest, but depending on sample concentration, higher or lower input amounts were also used, with a minimum of 1 ng input per well. All samples and controls were measured in duplicates.

Table 2.8 Mastermix for ddPCR for SNV detection.

Reagent	Per 1x reaction [μL]
2x ddPCR supermix for probes (no dUTP)	10
primer/probe mix – if WT and mutant as a single combined assay	1
primer/probe mix – if WT and mutant as two separate assays	1 (per assay)
restriction enzyme	0.5
H$_2$O	add to 15
total	15

Mastermix was mixed well by pipetting and briefly centrifuged. 15 μL of mastermix were added to PCR tube strips, 10 μL sample or control were added and mixed thoroughly by pipetting. 25 μL of combined sample-mastermix was added to each of the sample well of the cartridge. Then, 70 μL of droplet generator oil was added to the

oil wells of the cartridge. If any sample well remained empty, the matching oil well was nonetheless filled with droplet generator oil. Gasket was put in place over the cartridge and droplets generated using the droplet generator. Gasket was removed carefully and droplets then transferred to a 96-well plate. Plate was sealed with pierceable foil using the plate sealer, turned 180 degrees, and sealed again. PCR was run according to the scheme in Table 2.9 with the heated lid on.

Table 2.9 PCR settings for ddPCR for SNV detection.

Step	Temperature [°C]	Time	Ramp rate	Cycles
enzyme activation	95	10 min	2 °C/sec	1
denaturation	94	30 sec		40
annealing/extension	55	1 min		
enzyme deactivation	98	10 min		1
hold	4	∞	1 °C/sec	1

After cycling, plate was kept at 4 °C until reading, for 24 h at most. Plate layout was replicated in the software, with H_2O wells set as no template controls.

For analysis in QuantaSoft, all measurements of the same color, either FAM or HEX, across all wells were analyzed together. Threshold was set in a way that all empty droplets were below the threshold. A well was considered to have a positive signal when at least three droplets were positive, a sample was considered positive when both replicates were positive. When the H_2O no template control exhibited any positive signal, ddPCR run was considered a technical failure.

2.8.2. Copy number variation detection

For copy number variation assays, protocol as described in 2.8.1 was followed with minor changes. Specific assays are listed in Table 2.4. As wildtype control, HEK293T derived DNA was used, for *Myc* amplification control DNA from D341 cells was used. For *MycN* amplification control, PBT-04 cells were used. For both assays, the reference gene was *AP3B1*. PCR cycling was carried out as described in Table 2.10. Analysis was

carried out with QuantaSoft by setting the threshold for the fluorescent signal for both FAM and HEX individually above that of empty droplets and running the copy number calculation.

Table 2.10 PCR settings for ddPCR for CNV analysis.

Step	Temperature [°C]	Time	Ramp rate	Cycles
enzyme activation	95	10 min	2 °C/sec	1
denaturation	94	30 sec		40
annealing/extension	60	1 min		
enzyme deactivation	98	10 min		1
hold	4	∞	1 °C/sec	1

2.9. Methylation arrays

2.9.1. *Illumina Infinium MethylationEPIC – bisulfite conversion*

Standard methylation arrays were performed in the Institute of Neuropathology in the routine diagnostic laboratory. Isolated DNA was processed as described in the manufacturer's instructions. In brief, 100-500 ng of DNA was converted using the Zymo EZ DNA Methylation kit. DNA was processed with the Zymo DNA Clean & Concentrator-5 and Illumina Infinium HD FFPE DNA Restore kit, all according to manufacturer's instructions. DNA was fragmented and precipitated, then resuspended and finally hybridized to the EPIC methylation array. Chips were washed and stained, and lastly imaged using the iScan device to evaluate the methylation status of the CpG sites. Generated data were analysed using the Heidelberg classifier (https://www.molecularneuropathology.org/mnp/) [15].

2.9.2. *Illumina Infinium Methylation EPIC – enzymatic conversion*

To reduce input needed for methylation arrays and to perform conversion of the DNA more gently, enzymatic conversion was used.

Using the NEBNext Enzymatic Methyl-seq kit, the cfDNA was enzymatically converted introduced into the normal EPIC array workflow from hybridization to the array. Manufacturer's instructions were followed from oxidation of 5-methylcytosines and 5-hydroxymethylcytosines onwards.

TET2 buffer was prepared freshly by adding 100 µL of TET2 reaction buffer to TET2 reaction buffer supplement. 28 µL isolated cfDNA was transferred to a tube on ice. Then, 10 µL of the prepared TET2 buffer, 1 µL of oxidation supplement, 1 µL of DTT, 1 µL of oxidation enhancer and 4 µL of TET2 were added. Mix was vortexed briefly. 1 µL of Fe(II) solution was diluted in 1,249 µL of water. 5 µL of this was added to the DNA-enzyme mix and thoroughly vortexed, before being incubated for 1 h at 37 °C in a thermal cycler with the heated lid on. After incubation, tube was transferred to ice and 1 µL of stop reagent was added. This was then again incubated for 30 min at 37 °C. 90 µL of resuspended sample purification beads were added to the sample, thoroughly mixed by pipetting and incubated for 5 min at room temperature. Beads were pelleted on a magnetic stand and supernatant was removed and discarded. Bead pellet was washed twice with 200 µL freshly prepared 80% ethanol. After the final wash, beads were air dried for 2 min before DNA was eluted with 17 µL elution buffer. Beads were incubated with the elution buffer for 1 min at room temperature and then placed in the magnetic stand to pellet the beads. Supernatant containing the elution was collected in a fresh PCR tube. DNA was then denatured by adding 4 µL of formamide to it. The tube was placed into a pre-heated thermal cycler at 85 °C for 10 min, with the heated lid on. After the incubation, sample was immediately placed on ice. The denatured DNA was supplemented with 68 µL of water, 10 µL of APOBEC reaction buffer, 1 µL of BSA and 1 µL of APOBEC and mixed by pipetting. The mixture was incubated at 37 °C for 3 h in a thermal cycler with the heated lid on. After the incubation time, 100 µL of resuspended sample purification beads were added to the DNA-enzyme mix and pipetted up and down several times. The bead mix was incubated for 10 min at room temperature. Beads were then pelleted on a magnetic stand and supernatant was discarded. Pellet was washed twice with 200 µL freshly

prepared 80% ethanol. To thoroughly remove all residual ethanol, beads were air dried for 90 sec before adding 21 μL of elution buffer. Beads were resuspended with the elution buffer and incubated for 1 min at room temperature. Beads were then pelleted on the magnet again and supernatant was removed and collected in a fresh tube. Samples were frozen at -20 °C overnight and introduced into the EPIC array workflow at the hybridization step the next day.

2.10. Sequencing

2.10.1. TruSight Oncology 500 ctDNA

cfDNA with a sufficient DNA amount, a relatively clean BioAnalyzer profile (showing expected cfDNA peaks) and known mutations were chosen. Additionally, some samples with lower input, less distinct cfDNA peaks in the fragmentation profile and unknown, but expected, mutations were chosen to test the utility of the panel for the variety of routine samples.

cfDNA was sequenced with the TruSight Oncology (TSO) 500 ctDNA panel by Illumina, which covers 523 genes. Sample handling and sequencing was performed by Illumina according to the kit's instructions. In brief, cfDNA samples first underwent end repair and A-tailing. Then, adapters were ligated to the repaired prepared cfDNA and reaction was cleaned up. After that, an index PCR was performed. Then, for enrichment, samples were hybridized overnight and targets were captured. After a second hybridization and capturing of targets, the enriched library was amplified and cleaned. As a reference control, the SeraCare ctDNA Complete Mutation Mix was used and handled accordingly. Libraries were quantified and normalized before being sequenced on an Illumina NovaSeq sequencer as a paired-end 2 x 151 run. Data was analyzed with Illumina's own DRAGEN TSO 500 ctDNA workflow, giving out run details, CNVs, fusions and small variants.

2.10.2.   *Nanopore sequencing – standard sequencing*

cfDNA was sequenced using either the SQK-LSK110 kit along with R9.1 flow cells or the SQK-LSK114 along with R10.4 flow cells, all by Oxford Nanopore Technologies. The manufacturer's protocol for genomic DNA by ligation was followed, with minor changes in the bead ratios according to Martignano *et al.* [61]. Input ranges can be found in Supplementary Table 1.

Library preparation using SQK-LSK110 kit

Samples sequenced with the SQK-LSK110 kit were adjusted to 47 µL with water to the desired input. 1 µL of DNA CS, 3.5 µL NEBNext FFPE DNA Repair buffer and 2 µL of the respective enzyme mix, 3.5 µL Ultra II End-Prep Reaction buffer and 3 µL of the respective enzyme mix was added to the sample and mixed thoroughly by pipetting. Mixture was incubated at 20 °C for 5 min and at 65 °C for 5 min in a thermal cycler. It was then transferred to a 1.5 mL LoBind tube. 108 µL resuspended NucleoMag kit beads were added, and bead-mix was incubated at room temperature for 5 min. Beads were then pelleted on a magnet, supernatant was discarded and pellet was washed twice with 200 µL freshly prepared 70% ethanol. After the second wash, pellet was allowed to air dry for ~ 30 sec before being resuspended in 61 µL of water. Beads were incubated for 2 min at room temperature, then pelleted again on a magnet and supernatant was collected in a fresh tube. 1 µL of the eluate was quantified using the Qubit 3.0 (2.7.3).

60 µL of sample was then combined with 25 µL of ligation buffer, 10 µL of NEBNext Quick T4 Ligase and 5 µL of Adapter Mix F and incubated for 10 min at room temperature. 72 µL of resuspended beads were added after the incubation time, and then the mixture was held for 5 min on a rotator mixer. Beads were then pelleted and washed twice by resuspending with 250 µL Short Fragment Buffer. After the final wash, the beads were pelleted again on a magnet, any liquid residue was discarded and beads were dried for ~30 sec. Pellet was then resuspended in 15 µL elution buffer

and incubated for 10 min at room temperature. The beads were collected on a magnet, and supernatant was transferred to a new LoBind tube. 1 µL was again quantified using the Qubit.

To prepare the flow cell (exemplarily depicted in Figure 2.1) for loading, 30 µL Flush Tether was mixed into one tube of Flush Buffer, creating the priming mix. Flow cells of type R9.1 was put into position under the clip in either the MinION Mk1B or Mk1C device. Priming port was opened, and any air bubbles were removed before introducing 800 µL of the priming mix. Priming mix was let to sit for 5 min. In the meantime, 37.5 µL Sequencing Buffer II and 25.5 µL well-mixed Loading Beads II were added to the prepared DNA library. After the incubation time of the flow cell, 200 µL remaining priming mix were introduced through the priming port while the sample port was open. Immediately after, prepared DNA library was loaded onto the flow cell in a dropwise manner through the sample port. All ports were closed and sequencing was started within the MinKNOW software.
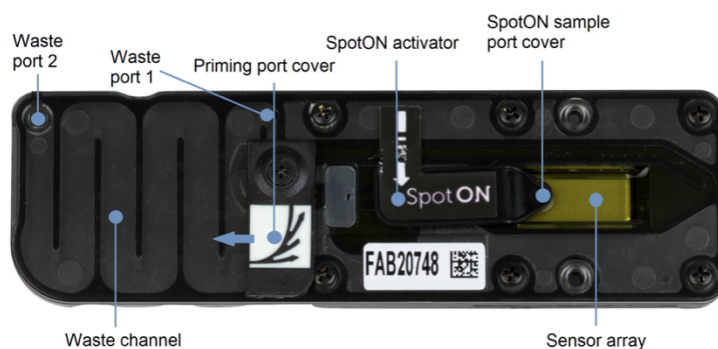
Figure 2.1 Depiction of a flow cell from Oxford Nanopore Technologies, with sensor array and ports for sample and waste. Adapted from Flow Cell Wash Kit EXP-WSH004 protocol by Oxford Nanopore Technologies.

Library Preparation using SQK-LSK114 kit

DNA sequenced with the SQK-LSK114 was prepared for sequencing in the same way as described above for SQK-LSK110. DNA CS was not used, instead an additional 1 µL water or sample was added. Reagents used in this kit carry the same names as those in the older kit LSK-SQK110, except for the Adapter Mix F, which is called Ligation Adapter in the new kit, and Loading Beads II, which are called Library Beads in the

SQK-LSK114 kit. For the magnetic beads, the provided AMPure XP beads were used instead of the NucleoMag kit beads. Washes of the beads after DNA repair was carried out using freshly prepared 80% ethanol. Amounts of reagents used remained the same between the two kits. Prepared libraries were then loaded onto flow cells of type R10.4.

Sequencing Settings

After the selection of the kits and flow cells used within the MinKNOW software, runs were started. Run time for unused flow cells was 24 h, for previously used and washed flow cells, run time was set to 48 h. Whenever possible, runs of samples that achieved 2 M reads were stopped regardless of time that had passed. The minimum read length was set to 20 bp for all samples run after feature was made available. For samples sequenced on MinION devices, the fast basecalling model was employed; for those sequenced on the GridION device, the high accuracy basecalling model was employed.

2.10.3.   Nanopore sequencing – barcoding

For multiplex sequencing on Nanopore devices, the SQK-LSK109 kit was used in combination with the EXP-NBD104 barcoding kit on R9.1 flow cells, all by Oxford Nanopore Technologies. 100 ng of cfDNA was used as input for all experiments.

For each sample individually

Isolated cfDNA volume was adjusted to 48 µL with water in a PCR tube. 3.5 µL NEBNext FFPE DNA Repair buffer, 3.5 µL Ultra II End-prep reaction buffer, 3 µL Ultra II End-prep enzyme mix and 2 µL NEBNext FFPE DNA Repair mix was added to the cfDNA. Reagents and cfDNA were mixed well by pipetting. The mix was incubated at 20 °C for 5 min and at 65 °C for 5 min in a thermal cycler. The sample was transferred to a 1.5 mL LoBind tube. 108 µL of NucleoMag kit beads were added to the sample and the mix was incubated on a rotator mixer for 5 min at room temperature. Sample was pelleted on a magnet until supernatant was clear. Supernatant was discarded, pellet was washed twice with 200 µL freshly prepared 70% ethanol. After

the second wash, bead pellet was allowed to dry for ~ 30 sec and any residual ethanol was removed. Pellet was then resuspended in 25 µL water and incubated for 2 min at room temperature. Beads were re-pelleted on magnet until supernatant was clear. 25 µL supernatant was transferred to a novel LoBind tube. Elution was quantified using the Qubit 3.0.

22.5 µL of the eluted sample was combined with 2.5 µL of individual native barcode for each processed sample and 25 µL Blunt/TA Ligase Master Mix. This was mixed well by pipetting and then incubated for 10 min at room temperature. 50 µL of NucleoMag kit beads were added and mixture was incubated on a rotator mixer for 5 min. Sample was pelleted on a magnet until the supernatant was clear, which was then discarded. Pellet was washed twice with 200 µL freshly prepared 70% ethanol. Bead pellet was allowed to dry for ~30 sec and any residual ethanol was removed. Pellet was then resuspended in 26 µL water and incubated for 2 min at room temperature. Tube was again introduced to the magnet and beads were pelleted. 26 µL of clear and colorless supernatant was collected in a fresh LoBind tube. Elution was quantified using the Qubit 3.0.

For each sample to be run in a multiplex sequencing assay, a BioAnalyzer run was performed, as described in 2.7.4. Here, molarity of the total sample content calculated by the software was considered. Samples were diluted and pooled equimolarly and adjusted to 65 µL with water.

For pooled library

5 µL Adapter Mix II, 20 µL 5x NEBNext Quick Ligation Reaction buffer and 10 µL Quick T4 Ligase was added to the 65 µL of pooled samples. Components were mixed by pipetting and incubated for 10 min at room temperature. 50 µL of NucleoMag beads were added and mixture was incubated on a rotator mixer for 5 min at room temperature. Beads were pelleted on a magnet and supernatant was discarded. Pellet

was resuspended and washed twice with 250 µL Short Fragment Buffer. After the second wash, beads were pelleted again and dried for ~ 30 sec. Bead pellet was then resuspended in 15 µL Elution Buffer and incubated for 10 min at room temperature. Beads were pelleted on magnet and supernatant was collected in a fresh LoBind tube. 1 µL of eluate was quantified using the Qubit.

Flow cell and library were prepared for sequencing as described in 2.10.2. The same sequencing settings were applied, with SQK-LSK109 and barcode kit EXP-NBD104 specified in the software. Reads were automatically sorted and stored in different folders with their respective barcodes.

2.10.4. *Nanopore sequencing – flow cell wash*

Nanopore flow cells are reusable. In between sequencing runs, flow cell washes are performed using the Flow Cell Wash kit (EXP-WSH004 or EXP-WSH004XL). The protocol was applied in the same way for R9.1 and R10.4 flow cells.

Flow cell wash mix was prepared by adding 2 µL of Wash Mix to 398 µL Wash Diluent per flow cell to be washed. Mixture was mixed thoroughly, but carefully by pipetting. All waste liquid from the flow cell was removed through the waste port 1. 400 µL prepared flow cell wash mix was introduced into the flow cell through the priming port after removing any air bubbles. Flow cell was incubated with the mix for 60 min at room temperature. All waste liquid was removed through the waste port 1 after the incubation time was up. Flow cell was then either reloaded with a sequencing library immediately, starting with the priming of the flow cell, or stored with 500 µL Storage Buffer, introduced through the priming port, at 4 °C until further use.

2.11. Bioinformatics

2.11.1. *Read length of Nanopore data*

Read length of Nanopore sequencing reads was determined by NanoPlot [64] using Python 3.9.7.

2.11.2.   CNV analysis of Nanopore data

Samples sequenced on the MinION Mk1b generated fastq files using Guppy 6.1.5, samples sequenced on the MinION Mk1c generated them using Guppy 6.3.8. Remaining samples that were sequenced on the GridION generated fastq files with Guppy 6.5.7. Fastq files that passed Guppy internal quality filters were aligned to the human reference genome hg38 with -ax map-ont settings in Minimap2.17 [65,66]. Resulting sam files were transformed into bam files and sorted using samtools 1.15.1 [67]. Bam files were then used for CNV analysis with Control-FREEC 11.6 [68]. For CNV analysis, configuration depended on the number of reads. If the number of reads was > 500 k, then window size was set to 150 k bp; if the number of reads was < 500 k, window size was set to 500 k bp. Calculated ratios from Control-FREEC were plotted in R. Briefly, packages dplyr, magrittr, tidyverse, karyoploteR and scales. A list of regions with ambiguous and difficult to align regions was removed from the data prior to plotting. Each dot in the plot is a window and the median ratio of the segment defines its color. Threshold were set empirically at > 1.1 for a gain and at < 0.9 for a loss.

2.11.3.   Calculation of tumor fraction from Nanopore data

From in 2.11.2 generated bam files, tumor fractions were calculated using ichorCNA [69]. Window size was set to 1 Mb as recommended by ichorCNA and analysis was configured for the reference genome hg38. The tumor fraction with the highest log likelihood was used for further analysis and comparison.

2.11.4.   NanoDx analysis of Nanopore data

NanoDx pipeline [63] was used for methylation analysis of Nanopore data. Data generated on R9.1 flow cells was analyzed in collaboration with Christian Rohrandt and Prof. Franz-Josef Müller at the Integrative Center for Psychiatry in Kiel. For this, raw data was basecalled using Guppy 4.4.2 and then analyzed with nanopolish 0.13.2 [70] to perform methylation calling. Then, the NanoDx pipeline v0.5.0 [63] was

employed. Raw data generated on R10.4 flow cells, as well as all data generated on the GridION device, were analyzed with the NanoDx v0.6.0. Here, Guppy version 6.4.6 was employed and performed the basecalling directly. Samples were classified by methylation according to the Heidelberg reference set [15]. Minimum threshold for analysis performance was 1,000 CpG sites analyzed. A score of ≥ 0.07 was set as threshold for reliable classification.

2.11.5.   *UMAP visualization*

For visualization purposes, uniform manifold approximation and projection (UMAP) was employed by mapping binary methylation values calculated by NanoDx [63] into the brain tumor reference set's [15] preprocessed beta values from methylation arrays. 3,837 reference tissue samples were included, beta value cut-off was 0.4. UMAPs were calculated with settings of n_neighbors = 10 and min_dist = 0.1 using R packages umap, ENmix, fs, minfi and plotly.

2.12.   Statistics

All statistical tests were performed in R using the packages base and stats. Normal distribution was assumed for cohort sizes of > 30. Tests used were t-test, Wilcoxon test, Fisher's exact test and Kruskal-Wallis test, depending on the question. Exact tests and the respective p-values are described in the figures or the text accordingly.

3. Results

3.1. ddPCR

3.1.1. SNV detection

ddPCR is a sensitive PCR-based method to detect SNVs and CNVs with many commercially available assays. For this work, hallmark hotspot mutations were analyzed to confirm suspected diagnoses, for example *H3-3A* K27M as an indicator for DMGs [71,72], or to find potentially targetable mutations, such as *BRAF* V600E in low grade gliomas [73]. Firstly, ddPCR was established with cfDNA from the medium of cell lines to evaluate whether the assays would work on cfDNA as the analyzed fragments are short and might not harbor the whole region necessary for the annealing of the ddPCR specific probes and/or primers. The limit of detection for the SNV assays had to be evaluated, which is exemplarily shown in Figure 3.1 for the *BRAF* V600E assay. *BRAF* V600E mutant cfDNA from Malme-3M cell line was spiked into wildtype cfDNA from HEK293T cell line, with a total input of 1 ng cfDNA. Mutant cfDNA was detectable with 0.01 ng input in 1 ng total DNA (1% of total DNA). This was true for all tested SNV assays.

ddPCR could then be employed for patient samples where mutational status held clinical relevance, either to confirm a diagnosis or to help make an initial diagnosis. An exemplary sample of a patient with a craniopharyngioma, analyzed with the *BRAF* V600E assay, is shown in Figure 3.2. The ddPCR worked without technical issues, with no template detection in the blank H_2O wells, wildtype only detection for the wildtype control and mutation only for the mutation control. The patient cfDNA sample contained both *BRAF* V600E mutations and wildtype sequences. This hints towards a heterozygous mutation, or the presence of background DNA from sources other than the tumor carrying the mutation. The mutation found in the cfDNA was also confirmed in the tumor tissue in the routine diagnostic workflow. With a total of 27 analyzed samples with all SNV assays used in this study, only one sample was a technical failure (4%) and none showed false-positive results. For 4/27 samples (14.8%), a mutation was expected, but not detected. All others showed the expected results of

wildtype or mutation, as known from the tumor tissue from the routine diagnostic workflow.
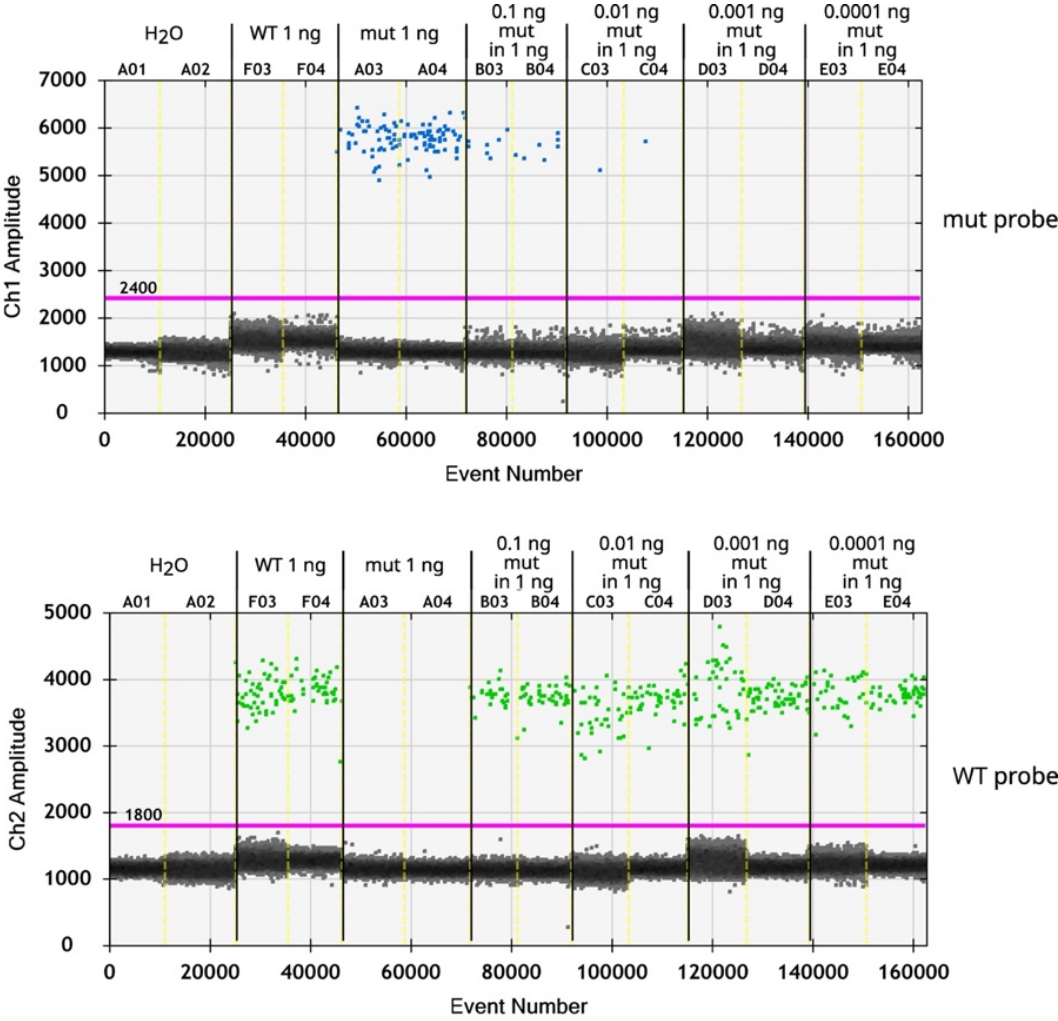
Figure 3.1 ddPCR results for dilution series of BRAF V600E mutation assay with cfDNA from Malme-3M cell line (mut) spiked into HEK293T cfDNA (WT). Mutant probe detected droplets on top in blue; WT detected droplets below in green. Mutant DNA can still be detected with 0.01 ng input spiked into 1 ng total DNA. cfDNA - cell-free DNA, ddPCR - droplet digital PCR, mut - mutant, WT - wildtype.
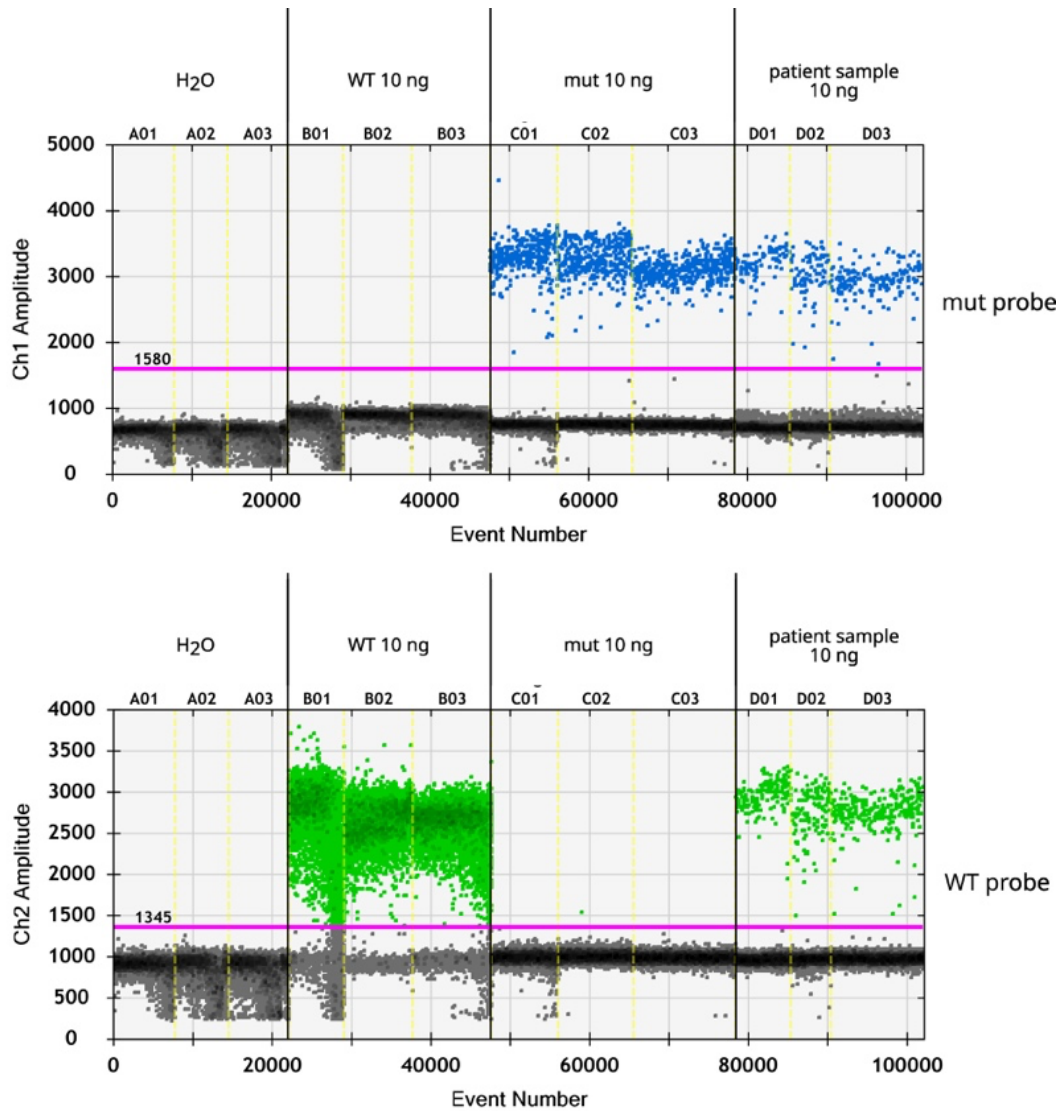
Figure 3.2 ddPCR results for cfDNA derived from patient CSF sample, positive for BRAF V600E mutation. Mutant probe detected droplets on top in blue; WT detected droplets below in green. Sample and controls were measured in triplicates, with 10 ng input each. Patient sample exhibits mutant and WT signals. cfDNA - cell-free DNA, CSF - cerebrospinal fluid, ddPCR - droplet digital PCR, mut - mutant, WT - wildtype.

3.1.2. CNV detection

CNV detection is often relevant for the prognosis of the disease, such as *Myc* or *MycN* amplification in medulloblastoma, which is accompanied with a poor prognosis [74–76]. First, cfDNA from *Myc* amplified and *MycN* amplified cell lines (D341 and PBT-04, respectively) were tested with the CNV assays to investigate whether the assays were useable for cfDNA. HEK293T cfDNA was used as wildtype DNA for both assays. For the *Myc* amplification assay, analysis of wildtype DNA resulted in a calculated

copy number of 2.36 and 2.42, which amounts roughly to the expected two copies present in any cell (Figure 3.3 A). cfDNA from D341 cells showed a clear amplification, with calculated copy numbers of 16.1 and 18 at 10 ng input; and 15.7 and 18 at 1 ng input. DNA from *MycN*-amplified PBT-04 cells did not result in a cross-signal and copy number was calculated at 1.03 and 2.03.

The same was tested for the *MycN* assay (Figure 3.3 B). Wildtype DNA analysis resulted in calculated copy numbers of 1.52 and 1.45. cfDNA from PBT-04 with *MycN* amplification showed a definitive amplification, with calculated copy numbers of 124 and 149 at 10 ng input, and of 170 and 200 at 1 ng input. DNA from D341 cells with *Myc* amplification only had 1.62 and 1.72 calculated copies, showing the high specificity of this assay.

Two exemplary patient samples have then been analyzed with the *Myc* amplification assay to determine the use in clinical samples (Figure 3.3 C). Both patients were diagnosed with a medulloblastoma. The ddPCR worked well technically, no template was detected in the H_2O control. Wildtype control cfDNA from HEK293T showed a copy number of 1.9 and 2.5, mutation control cfDNA from D341 had an amplification calculated at 18.5 and 18.1. Patient sample 1 showed a slight amplification, with calculated copy numbers of 6.6 and 6.4. The matching tumor tissue showed only occasional *Myc* amplification in a few cells by fluorescence in-situ hybridization (FISH) (Supplementary Figure 1), matching the relatively low but amplified copy number in the liquid biopsy.

Patient 2 showed a clear amplification with copy numbers of 156 and 148. This amplification was known from the primary tumor, yet not detectable in the relapse, after which this specific CSF sample was collected.
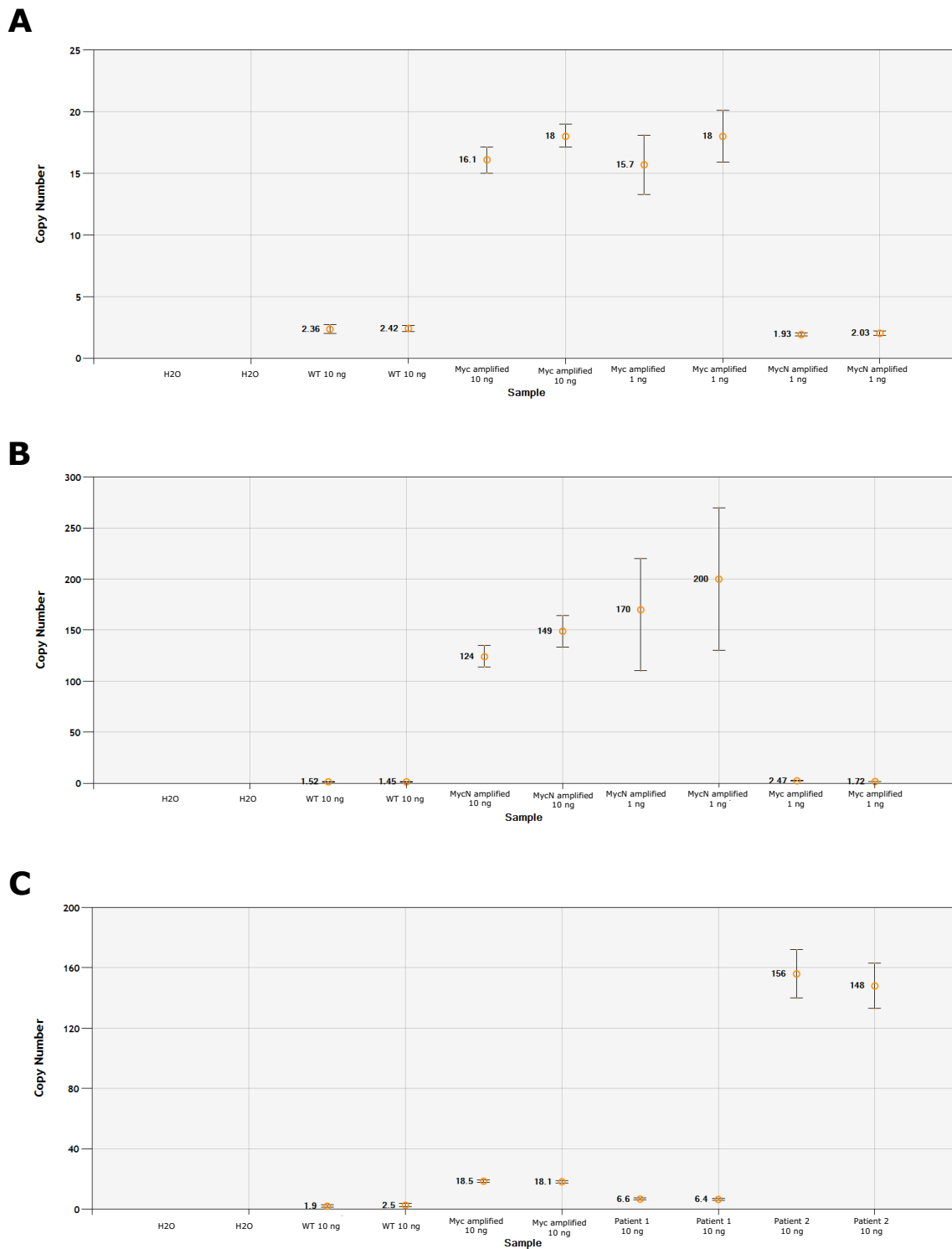
Figure 3.3 Calculated copy numbers by ddPCR using CNV assays. (A) CNV calculated for cfDNA from cell lines using the Myc CNV assay, with HEK293T as wildtype, D341 as Myc-amplified and PBT-04 as MycN-amplified. D341 show clear Myc amplifications, while HEK293T and PBT-04 do not. (B) CNV calculated for cfDNA from cell lines using the MycN CNV assay, with HEK293T as wildtype, PBT-04 as MycN-amplified and D341 as Myc-amplified. PBT-04 show clear MycN amplifications, while HEK293T and D341 do not. (C) CNV calculated for patient cfDNA samples from CSF, both from medulloblastoma, with HEK293T as wildtype and D341 as Myc-amplified. Both patient samples exhibit a Myc amplification. cfDNA - cell-free DNA, CNV - copy number variation. ddPCR - droplet digital PCR, mut - mutant, WT - wildtype.

3.2. Methylation arrays

As methylation analysis using the Illumina EPIC arrays is already established in the routine diagnostics for tissue samples, implementing an adapted workflow for cfDNA would be preferred over establishing a completely novel method. To reduce harshness of the reagents used in the workflow, the DNA was converted using an enzymatic conversion kit (2.9.2) instead of the conventional bisulfite conversion method (2.9.1). This also allows the use of a smaller amount of DNA as less of it gets heavily degraded. For initial establishment of the enzymatic conversion workflow, DNA from a tissue sample of an IDH-mutant glioma that had also been analyzed in the routine bisulfite workflow, was processed with the enzymatic workflow with three differing input amounts: 250 ng, 50 ng and 10 ng. Data generated were evaluated with the Heidelberg classifier [15]. All three amounts of DNA were sufficient to be classified as the correct entity, IDH mutant glioma. Samples with 250 ng and 50 ng input achieved a score of 1.0, that with 10 ng input achieved a score of 0.9, all of which would be above the threshold of 0.9 for neuropathological diagnosis. Looking at the CNV plots generated from the methylation data, a slight decline in quality with decreasing amount of input can be observed (Figure 3.4) as the plots get noisier, but are still well interpretable and show the previously observed losses in Chr. 1 and 19.
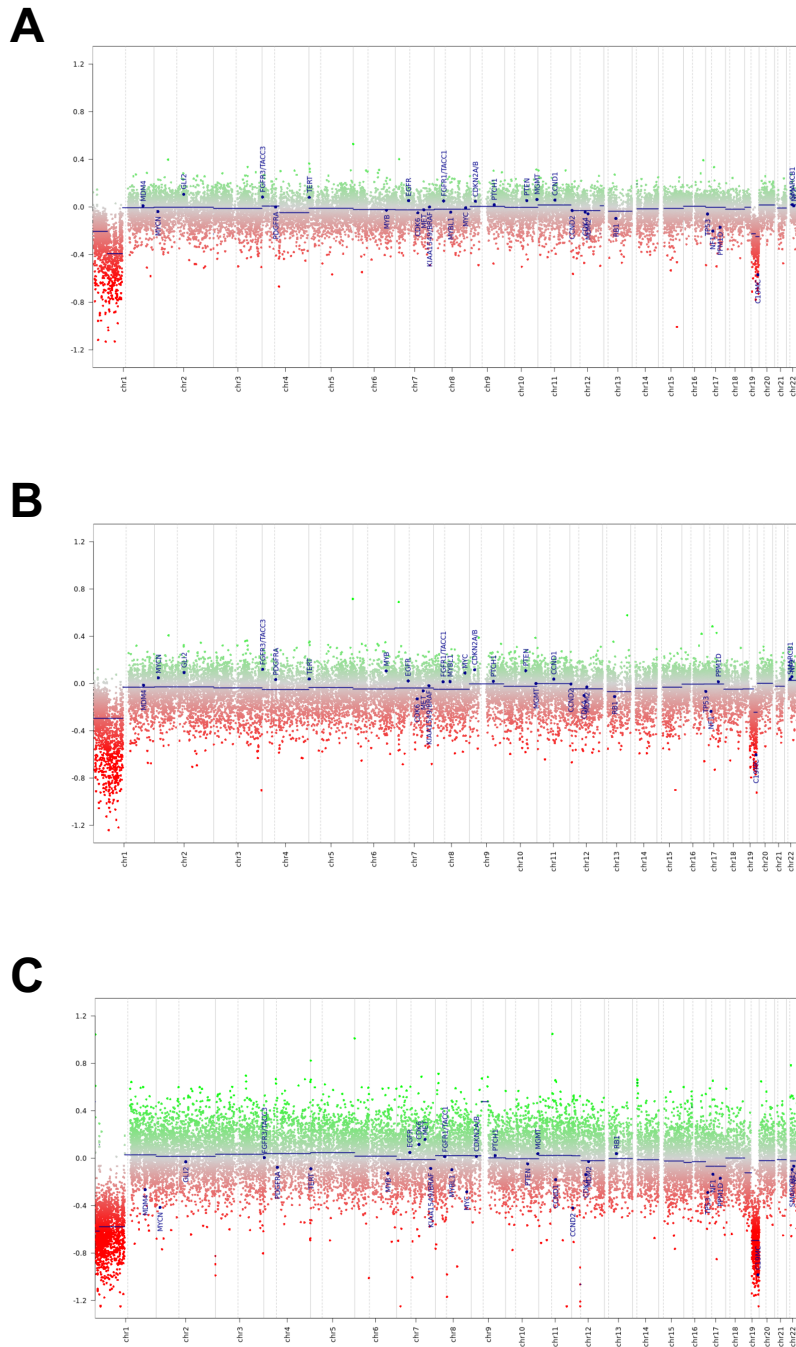
Figure 3.4 CNV plots inferred from methylation data of gDNA from an IDH mutant glioma, processed by enzymatic conversion with (A) 250 ng, (B) 50 ng, and (C) 10 ng input. A slight decline in plot quality is observable with lower input. CNV - copy number variation, gDNA - genomic DNA.

As the results were comparable even at low input amounts, the protocol was tested on cfDNA. First, three cfDNA samples from CSF that had matching tissue analyses available were tested and results were compared. Sample M1 was a medulloblastoma group 4 sample, with a 0.99 match for medulloblastoma group 4 in v11 of the Heidelberg classifier and aberrations in the CNV plot such as Chr. 1q and 17 gains, as well as losses on Chr. 8, 10, 16 and 22. The analysis of the cfDNA by the methylation array resulted in a noisy CNV plot that allude to the same aberrations in Chr. 8, 10 and 17, however none can be identified clearly. The analysis using the Heidelberg classifier resulted in a score of 0.3 for medulloblastoma group 3/4, and 0.23 for the subclass medulloblastoma group 4 in v11. Using the updated classifier v12, the score improved to 0.97 for medulloblastoma non-WNT, non-SHH and 0.85 for the subclass medulloblastoma group 4. Samples M2 and M3 belonged to the same patient with an ATRT-SHH. The tissue DNA could clearly be classified as an ATRT with a score of 1.0 and the respective CNV plot showed a characteristic loss of Chr. 22. The two cfDNA samples did not yield convincing results. Both CNV plots were noisy and the loss of Chr. 22 was not visible. Sample M2 showed a score of 0.45 for plexus tumor in the classifier v11, and a score of 0.32 for ATRT-SHH in the classifier v12, which, albeit true, is below the threshold of 0.9 that is usually used in the routine diagnostic. Sample M3 was not classifiable in the classifier v11 and showed a score of 0.37 for medulloblastoma in classifier v12.

As these initial results were not conclusive about the applicability of this method, it remained to be investigated whether the developed protocol worked for a majority of cfDNA samples or not. Thus, 17 other samples (M4-M20) were investigated, with detailed results listed in Table 3.1. Out of all 20 cfDNA samples, only 6 (30%) matched highest with their respective tumor entity in the v12 of the Heidelberg classifier. The older, but more widely used, v11 only matched 4/20 (20%) correctly. When only the samples that were correctly classified above the threshold of 0.9 were considered, only 3/20 (15%) were classified correctly, all by v12 of the classifier. CNV analysis from the

methylation data revealed noisy plots as observed for samples M1-M3. Only the CNV plots of samples M5, M13, M14, M17, M19 and M20 allowed an interpretation regarding possible aberrations in the genome. Samples M5 and M17 are exemplarily depicted in Figure 3.5 for samples that had interpretable CNV plots, and samples M2 and M15 for samples that resulted in CNV plots that were too noisy to interpret.
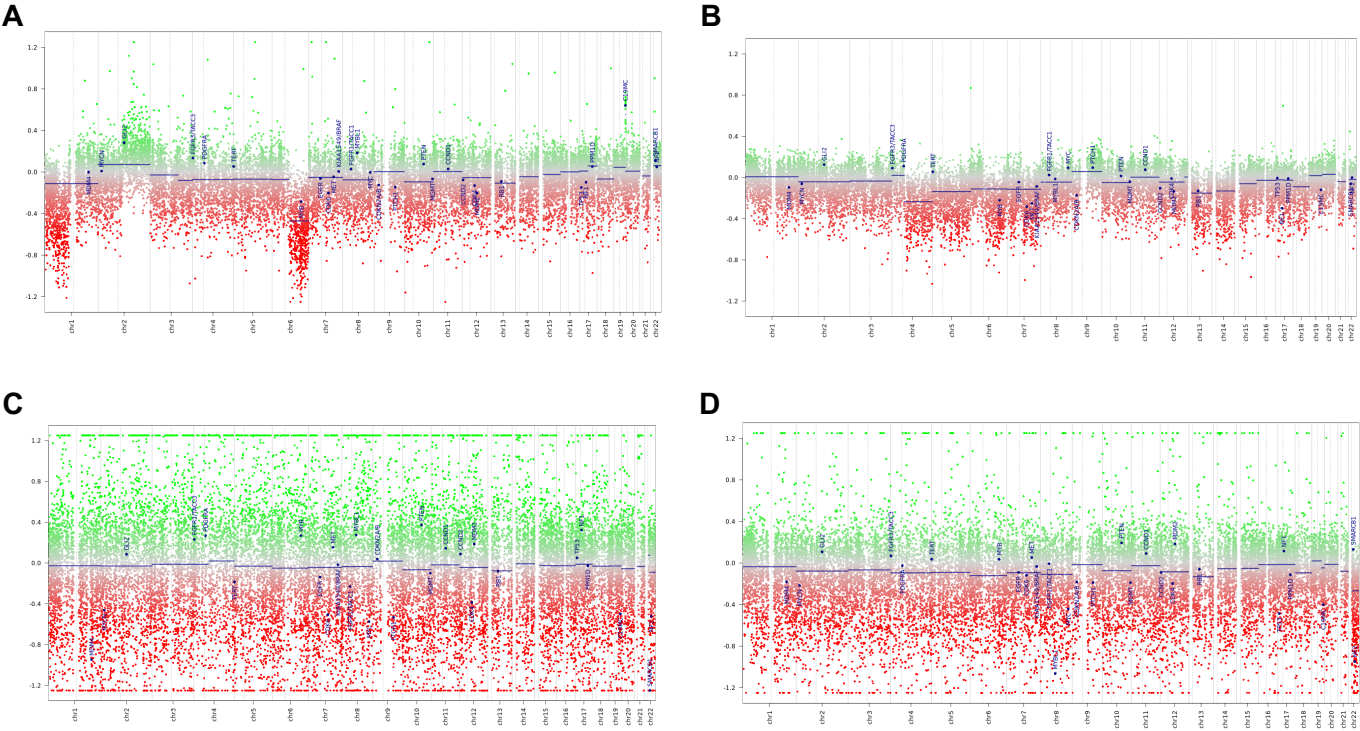
Figure 3.5 CNV plots inferred from methylation data of cfDNA from (A) an ETMR (sample M5), (B) a DMG (sample M17), (C) an ATRT (sample M2), and (D) another ATRT (sample M15). CNV plots in (A) and (B) are interpretable and show gains and losses, whereas those in (C) and (D) do not as the plot is too noisy. ATRT - atypical teratoid/rhabdoid tumor, cfDNA - cell-free DNA, CNV - copy number variation, ETMR - embryonal tumor with multi-layered rosettes, DMG - diffuse midline glioma.

Table 3.1 Brain tumor classifier results of cfDNA from patient CSF samples, analyzed by methylation array with enzymatic conversion.

sample ID	diagnosis	v11b4 score		v12.5 score		match
M4	cranio-pharyngioma	plexus tumor	0.51	control blood	0.46	no
M5	ETMR	ETMR	0.61	ETMR atypical	0.93	yes
M6	PA	plexus tumor	0.53	not classifiable	-	no
M7	MB, SHH	plexus tumor	0.45	germ cell tumor	0.67	no
M8	PA	plexus tumor	0.54	not classifiable	-	no
M9	lymphoma	plexus tumor	0.41	not classifiable	-	no
M10	PA	plexus tumor	0.44	MB Gr 3	0.48	no
M11	MB, SHH	plexus tumor	0.42	not classifiable	-	no
M12	MB, WNT	control tissue, inflammatory tumor micro-environment	0.54	not classifiable	-	no
M13	cranio-pharyngioma	control tissue, inflammatory tumor micro-environment	0.8	not classifiable	-	no
M14	MB, group 3/4	not classifiable	-	not classifiable	-	no
M15	ATRT	ATRT	0.49	other embryonal CNS tumors	0.84 (ATRT subclass 0.52)	yes, too low for diagnosis
M16	ETMR	ETMR	0.41	other embryonal CNS tumors	0.94 (ETMR subclass 0.94)	yes
M17	DMG	not classifiable	-	control tissue	0.42	no
M18	ependymoma, PF-A	plexus tumor	0.36	ependymal tumors	0.36 (ependymoma, PF-A subclass 0.21)	yes, too low for diagnosis
M19	MB, SHH	plexus tumor	0.51	control tissue	0.99	no
M20	ependymoma, PF-A	control tissue, inflammatory tumor micro-environment	0.99	control tissue	0.95	no

3.3. TruSight Oncology 500 ctDNA

As another approach to identify and classify CNS tumors from a CSF sample, sequencing of cfDNA was investigated. A total of 16 samples with varying quality and input were analyzed with the TruSight Oncology 500 ctDNA sequencing panel for SNVs, fusions and CNVs (Table 3.2). A range of different samples was used to mimic the situation in the diagnostic routine where samples of different entities, qualities and characteristics arrive on a daily basis. Samples with known point mutations and gene fusions were chosen, as well as samples where specific mutations were unknown, but nonetheless expected. The manufacturer recommends an input of 30 ng or higher, but as this is not always feasible for cfDNA from CSF, it was tested whether samples with lower input were still suitable for analysis. For this, three samples of good quality and sufficient amount of DNA were analyzed twice with different inputs (TSO4 and TSO5 as well as TSO15 and TSO16, both with 30 and 10 ng input, respectively; and TSO7 and TSO8 with 10 and 31 ng input, respectively). Median coverage recommendation for reliable mutation calling was ≥ 1,300 x. Only 6/16 (37.5%) samples achieved the recommended coverage, however four additional samples (TSO2, TSO7, TSO11 and TSO15) had a coverage over 1,000 x, which could still be considered a successful sequencing, meaning 62.5% of sequenced samples were a technical success. Samples TSO3 and TSO9 both showed 0% cfDNA of total DNA, and median exon coverage was < 10 x for both samples. Input for those samples was also low, however low input itself was not a measure for success or failure of the sequencing. For instance, both sample pairs TSO4 and TSO5, and TSO7 and TSO8 showed that a lower input of the same samples can still achieve a higher coverage. For sample pair TSO15 and TSO16, this was the inverse and tripling the input resulted in a coverage almost 9 x as high. For all samples, analysis issued lists of SNVs, possible fusions and CNVs. The number of SNVs per sample ranged from 398 in sample TSO3 (a technical failure) to 1,578 in TSO14. Samples that do not have any mutations or aberrations reported in Table 3.2 did not show any that were considered relevant or matching to the known entity.

Table 3.2 TSO500 ctDNA sequencing result summary for cfDNA from patient CSF samples.

Sample	Patient sample info	Entity	Input [ng]	Bio-Analyzer cfDNA content [% of total DNA]	Median coverage	Expected mutations	Found mutations (VAF)
TSO1	same patient	MB, WNT	21.4	87%	2016 x	*CTNNB1* S37A	*CTNNB1* S37A (0.48)
TSO2		MB, WNT	13.6	59%	1223 x		*CTNNB1* S37A (0.48)
TSO3		ATRT	6.5	0%	4 x	*SMARCB1*	-
TSO4	same sample	ATRT	30	89%	1913 x	*SMARCB1*	-
TSO5		ATRT	10		2183 x		-
TSO6		MB, SHH	10.7	42%	72 x	*TERT* C228T, *KMT2C*	-
TSO7	same sample	PA	10	81%	1187 x	*KIAA-BRAF* fusion	-
TSO8		PA	31		640 x		-
TSO9		meningeosis carcino-matosa	7.3	0%	7 x	unknown	-
TSO10		germ cell tumor	30	89%	2180 x	unknown	-
TSO11		pineo-blastoma	30	92%	1244 x	unknown	*ATRX* H865Q (0.99)
TSO12		prostate carcinoma	30	99%	1791 x	unknown	*ERG-TMPRSS2* fusion (0.18), *BRCA1*, *BRCA2*, *p53*

Sample	Patient sample info	Entity	Input [ng]	Bio-Analyzer cfDNA content [% of total DNA]	Median coverage	Expected mutations	Found mutations (VAF)
TSO13		MB, WNT	20	75%	3333 x	*CTNNB1* S33F, *SMARCA4* H884R	*CTNNB1* S33F (0.08), *SMARCA4* H884R (0.093)
TSO14		MB, WNT	20	56%	490 x	*CTNNB1* S33C	-
TSO15	same sample	MB, WNT	30	84%	1185 x	*CTNNB1* S33F, *p53* G113V, *Myc* amplification in primary tumor	*CTNNB1* S33F (0.46), *p53* G245V (0.93), *Myc* amplification (113.5x)
TSO16		MB, WNT	10		132 x		*CTNNB1* S33F (0.47), *p53* G245V (0.90) and P72R (0.97), *Myc* amplification (121.3x)

In samples TSO1 and TSO2, the *CTNNB1* S37A mutation known from the tissue was found in the cfDNA samples as well, both times with a VAF of 0.48. Even though input and cfDNA content was lower in TSO2 than in TSO1, both samples delivered the same result. Samples TSO3 through TSO5 all came from patients with ATRTs, where a *SMARCB1* or *SMARCA4* mutation is expected [5,6,77,78]. These mutations were found in neither of the samples, but with a retrospective analysis of the matching tissue of

TSO4 and TSO5, a broad deletion spanning the region of *GNAZ* to *SMARCB1* on Chr. 22 was found. This cannot be detected with this method due to the short-read sequencing's nature and the analysis performed. Sample TSO13 performed well and replicated the known single nucleotide variation from the tumor with VAFs of 8% and 9% for *CTNNB1* and *SMARCA4*, respectively. Samples TSO15 and TSO16 showed comparable results, even though coverage for sample TSO16 was significantly lower. Both samples revealed the known *CTNNB1* S33F mutation with 0.46 and 0.47 VAF. For the *p53* mutation, instead of the known G113V mutation, the G245V mutation was found with VAFs of 0.9 and 0.93. In sample TSO16, the additional *p53* P72R mutation was found with a VAF of 0.97. None of these were present in the tumor tissue. The patient of this CSF sample had experienced a relapse, which was biopsied. In the initial tumor, a *Myc* amplification was found, but not in the relapse. The CSF sample was taken after relapse, and yet cfDNA analysis here in samples TSO15 and TSO16 showed a *Myc* amplification of 113.5 x and 121.3 x, respectively. This was also found in ddPCR analysis of the same sample (3.1.2, Figure 3.3 C – patient 2). For sample TSO12, specific mutations were unknown, however an *EGR-TMPRSS2* fusion was observed, which is a very prominent fusion in prostate carcinoma [79]. Additionally, *p53* mutations were found, which are frequent in prostate carcinoma [80,81], as well as *BRCA1/2* mutations that, although rare in prostate carcinoma, are in line with aggressive variants of the entity [82,83]. Other samples that exhibited a fusion in the tumor tissue (TSO7 and TSO8), although successfully sequenced, did not show those in this analysis. For other samples (TSO9, TSO10 and TSO11) with unknown mutations, no mutation that would match the diagnosis or be informative of the diagnosis was found, except for an *ATRX* mutation in sample TSO11 with a high VAF. This, however, could not be confirmed in a retrospective analysis of the tumor tissue.

3.4. Nanopore sequencing

3.4.1. Nanopore sequencing – native sequencing

To simultaneously analyze the sequence and the methylation of cfDNA, Nanopore sequencing was explored. In total, 197 cfDNA samples isolated from CSF were analyzed in this study (Figure 3.7). Analysis of a smaller subcohort of 129 cfDNA samples has been published in Afflerbach *et al.* [84].

31 different entities are represented in the full cohort, with medulloblastoma dominating the numbers with 65/197 samples (33% of total samples). Ependymoma (n=20, 10.2% of samples), ATRT (n=14, 7.1% of samples), lymphoma (n=12, 6.1% of samples), pilocytic astrocytoma (n=12, 6.1% of samples) and glioblastoma (n=11, 5.6% of samples) follow as the five next largest groups of entities. Other tumors, including rare entities, are also included, albeit in lower numbers – such as ETMR with three samples (1.5% of total samples) or plexus papilloma with two samples (1% of total samples). cfDNA from samples with brain metastases or CNS involvement have also been included, such as breast carcinoma (n=5, 2.5% of samples), lung carcinoma (n=2, 1% of samples), prostate carcinoma (n=2, 1% of samples) or leukemia (n=1, 0.5% of samples), amongst others. These remain the minority, but were included as these samples play an important role in the neuropathological diagnostic routine, where questions arise whether a tumor might have metastasized to the CNS or if it could be an additional CNS primary tumor. For some patients, several samples were available, leading to 197 samples from 158 individual patients. Patients with multiple samples are marked with capital letters in Figure 3.7. Mean age of the patients was 22.2 years, yet most patients were children or adolescents with 65% under 18 years of age. All samples were collected when clinically indicated and only those with sufficient supernatant material after routine microscopic evaluation in the neuropathology were analyzed in this study. This results in a mixed cohort of samples that were collected prior to surgery (n=50, 25.4%), early post-surgery (less than 14 days after surgery, n=28, 14.2%), post-surgery (n=72, 36.6%) and also samples where exact sampling and surgery time were unclear (n=47, 23.9%), for example when the sample was sent from

a different clinic. In only 10/197 cases (5.1% of samples), tumor cells were detectable through standard microscopy in the routine evaluation of the CSF. The isolated DNA amount had a wide range, from 1.5 ng to 3,835 ng per mL CSF, with a mean of 74.3 ng DNA per mL CSF. Of note, 89% of samples contained less than 150 ng DNA per mL CSF. For Nanopore sequencing, input covered 3 ng to 618 ng, with a mean of 19.2 ng. For 17 samples, input value was not available due to either diverging Qubit measurements that did not allow a clear quantification of the sample, or the concentration being too low for quantification via Qubit. Nanopore sequencing of samples was shallow, with a mean coverage of 0.62 x and an average of 1.99 Gb data generated per sample. The mean read length was 461.2 bp, which is in line with the expected short fragmentation profile of cfDNA. cfDNA proportion was measured in samples with sufficient material with the BioAnalyzer, and the mean proportion across all measured samples was 36.7% of cfDNA from total DNA. Exemplary fragment size profiles of the cfDNA as seen in BioAnalyzer analysis and the respective read length distribution of Nanopore data is depicted in Figure 3.6. Overall, sequenced samples achieved 57.8% passed reads, with 53,416 CpG sites overlapping between sample and reference detected on average in those reads.

Details for each sample are listed in Supplementary Table 1.
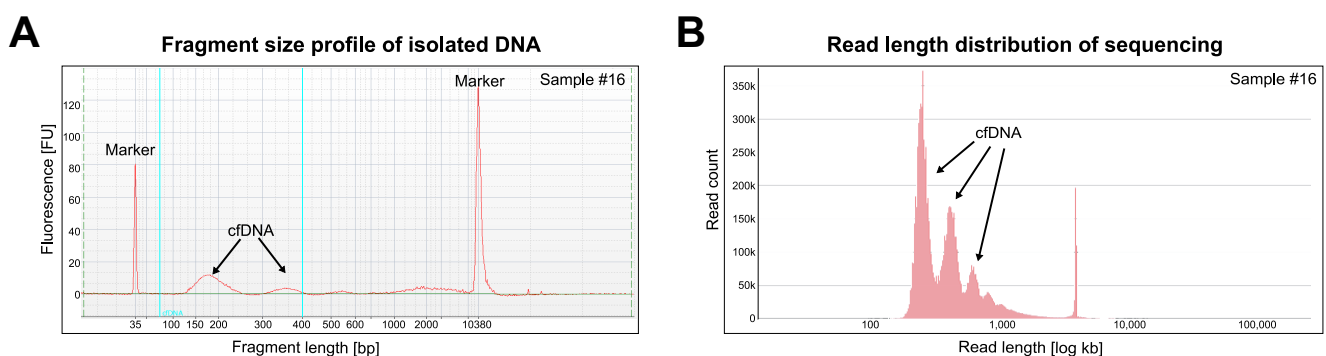
Figure 3.6 cfDNA shows short fragments in the BioAnalyzer read-out (A) and in the read length distribution of the Nanopore sequencing data (B). Both show sample 16. Adapted from Afflerbach et al. [84].
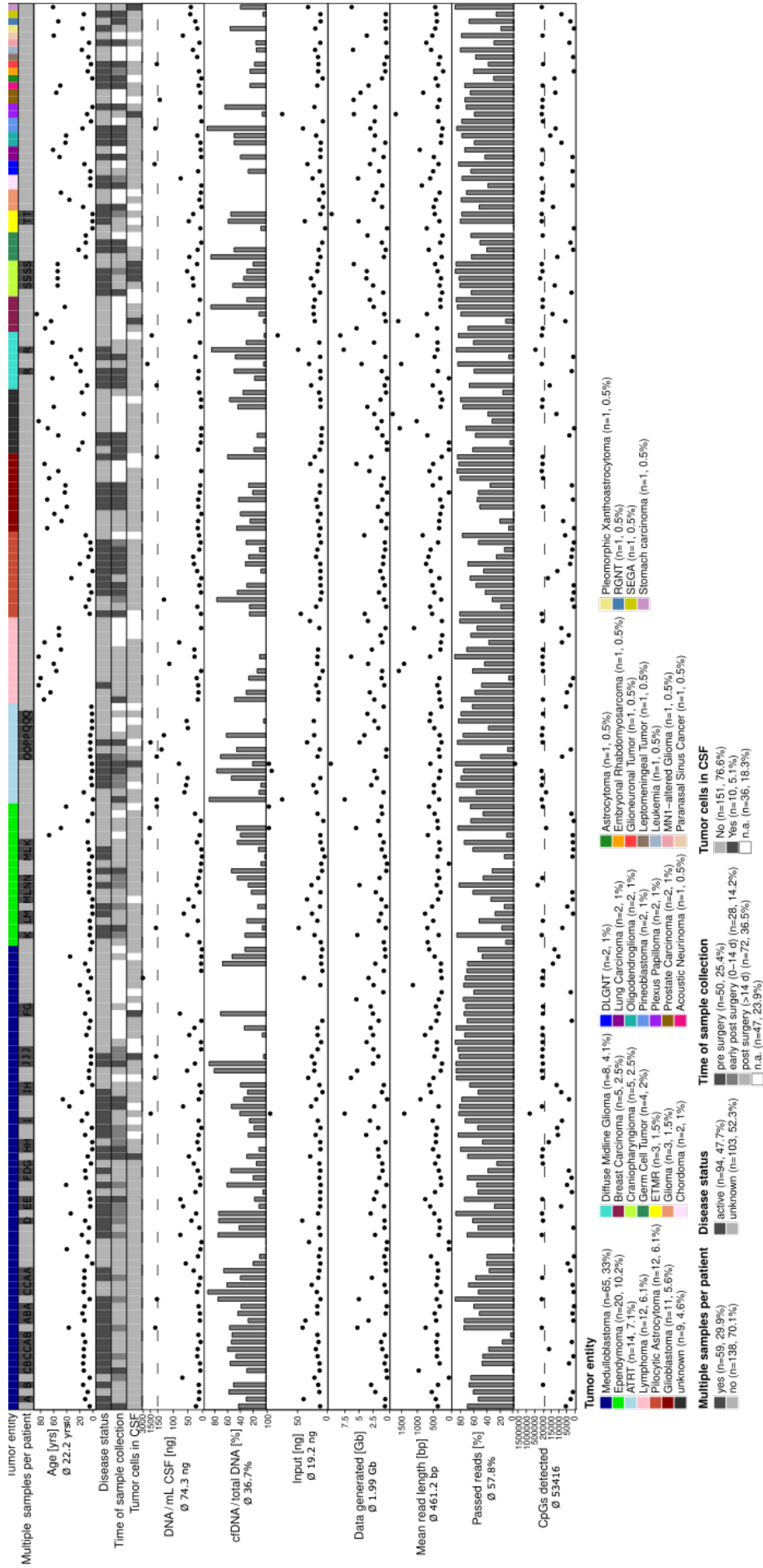
Figure 3.7 Sample overview of all 197 analyzed cfDNA samples from CSF of patients with clinical characteristics as well as cfDNA and sequencing information. Samples are grouped by tumor entity, multiple samples of the same patient are denoted with a capital letter. Input was capped at 100 ng and Data generated was capped at 10 Gb for display purposes, exact data can be found in Supplementary Table 1. cfDNA - cell-free DNA, CSF - cerebrospinal fluid.

54

Firstly, all 197 sequenced samples were analyzed together as the full cohort. In Figure 3.8 A, the results of ctDNA detection are depicted per sample. ctDNA was detected in 86/197 samples (43.7%), in 91/197 samples (46.2%) analysis was performed but no ctDNA was detected, and 20/197 samples (10.2%) were technical failures that did not yield enough data for either CNV or methylation analysis. For methylation analysis with the random forest classifier NanoDx [63], 45/197 samples (22.8%) did not have sufficient CpG sites for analysis, yet the majority of those samples could still be analyzed via CNV analysis.

When technical failures were not considered in the analysis, ctDNA detection was successful in 86/177 samples (48.6%) (Figure 3.8 B). All samples could be analyzed by CNV analysis, with ctDNA detection by CNV in 43.5% of samples (n=77). NanoDx analysis could be performed in 85.9% of cases, with successful entity classification in 41/177 samples (23.2%). CNVs detected in the cfDNA recapitulated those found in the tumor, if known, with only minor differences. In a few cases, additional aberrations private to either tissue or CSF were found, with the overall profile still overlapping and matching (as seen in Afflerbach *et al.* [84], Supplemental Figure 1).

Exemplary analyses are depicted in Figure 3.9 [84]. In Figure 3.9 A, glioblastoma sample 127 shows matching CNV profiles between tissue biopsy and CSF biopsy with Chr. 7, 12, and 17 gains. Methylation analysis with NanoDx reached a score of 0.072 and is thus classified as glioblastoma. UMAP visualization of the methylation data also shows clustering to the glioblastoma reference, specifically the RTKI subgroup. Medulloblastoma sample 16 (Figure 3.9 B) shows matching CNV profiles between tissue and CSF, with additional aberrations only visible in tissue as well as only in the CSF. Both biopsies show losses on Chr. 8, 10, 16 and 22, as well as gains on Chr. 1 and 17. A gain on Chr. 2 was found private to the CSF, and a loss on Chr. 3 private to the tissue. Methylation analysis of the Nanopore data of the cfDNA resulted in a score of 0.39 for medulloblastoma, group 4 and clustering to the respective reference in the UMAP visualization. CNV analysis of ETMR sample 167 showed matching profiles between the tissue and the analyzed CSF, with a specific focal amplification of the

C19MC cluster on Chr. 19 (Figure 3.9 C, inset). This shows that also small and focal aberrations that are relevant for diagnosis can be inferred from Nanopore data when sufficient data is available. The sample also achieved a classification score of 0.148 by the NanoDx algorithm and was clearly classified as an ETMR, highlighted also by the clustering to the reference in UMAP visualization of the data.

7/177 cases (3.95%) were wrongly classified with the NanoDx algorithm, meaning they received a score above the set 0.07 threshold for an incorrect entity. In 4 out of these 7 cases, the highest score was for meningioma, hinting a bias towards this group when classification is unclear or difficult with the algorithm. Classification scores of incorrectly classified samples ranged from 0.07 to 0.09, with a singular outlier with a score of 0.11.

High detection rates of ctDNA were found in the groups of medulloblastoma (32/57, 56.1%), ATRT (7/14, 50%) and lymphoma (7/12, 58.3%). Glioblastoma and diffuse midline glioma were detected at lower rates, with 44.4% (4/9 samples) and 42.9% (3/7 samples), respectively. Of note, ctDNA of ependymoma was detected in only 4/17 samples (23.5%) and that of pilocytic astrocytoma was detected in none of the samples analyzed in this cohort (0/11, 0%) with either analysis method. A statistically significant difference of ctDNA detection rates between samples from benign and malignant entities could be observed (Figure 3.10 B, Fisher's exact test, p = 0.0011). 52% of malignant samples contained detectable ctDNA, whereas only 25% of samples of patients with benign tumors. Additional differences between the groups of samples with detectable and undetectable ctDNA were their read lengths and cfDNA proportion (Figure 3.11). The mean read length of samples that were positive in ctDNA analysis was statistically significantly shorter than that of those samples not containing detectable ctDNA (Figure 3.11 A). This was also supported by the cfDNA proportion, so the proportion of total DNA that falls within the size range of 75-400 bp determined by BioAnalyzer analysis, in samples with detectable ctDNA being significantly higher than those without (Figure 3.11 B). To investigate whether the detection method played a role, the proportion of cfDNA was split into the respective methods (CNV,

methylation or both) in Figure 3.11 C. A statistically significant difference regarding the proportion of cfDNA was only observed between samples that were detected by both CNV and methylation analysis and those that contained no detectable ctDNA. Lastly, groups of tumor entities with $n \geq 10$ were observed for differences in proportion of cfDNA (Figure 3.11 D; only samples with available BioAnalyzer data were included). No statistically significant difference could be observed between the groups (Kruskal-Wallis, $p = 0.32$), indicating that the tumor entity itself is not responsible for the proportion of the cfDNA contained in the sample. Calculated probabilities of tumor fraction by ichorCNA proved to be significantly different between samples with positive ctDNA results, as well as statistically significant between detection methods (Supplementary Figure 2). However, as the ichorCNA algorithm's estimation of tumor fraction is based on the prediction of CNVs, statistical differences between samples with detectable ctDNA by at least CNV analysis and those with methylation only detection and no detection were unsurprising. Yet, it is an additional marker in favor of CNV analysis, and demonstrates that samples with ctDNA detected by both CNV and methylation had the highest tumor fraction.

It remains to note that samples within the cohort belonging to carcinoma entities, such as breast, prostate, stomach or paranasal sinus cancer, as well as the leukemia case were analyzed in the same workflow as all other samples, however due to the current limitations of the reference cohort to brain tumors in the NanoDx algorithm, they could not be correctly classified in the methylation analysis. In the same regard, some samples such as the craniopharyngioma cases 158-160 did not exhibit any CNVs in the tumor tissue, so no CNVs were expected in the CSF either.

A

Sample ID
Tumor entity
Disease status
Time of sample collection
Tumor cells in CSF
ctDNA
CNV analysis
NanoDx analysis

Tumor entity
- Medulloblastoma (n=65)
- Ependymoma (n=20)
- ATRT (n=14)
- Lymphoma (n=12)
- Pilocytic Astrocytoma (n=12)
- Glioblastoma (n=11)
- Unknown (n=9)
- Diffuse Midline Glioma (n=8)
- Breast Carcinoma (n=5)
- Craniopharyngioma (n=5)
- Germ Cell Tumor (n=4)
- ETMR (n=3)
- Glioma (n=3)
- Chordoma (n=2)
- DLGNT (n=2)
- Lung Carcinoma (n=2)
- Oligodendroglioma (n=2)
- Pineoblastoma (n=2)
- Plexus Papilloma (n=2)
- Prostate Carcinoma (n=2)
- Acoustic Neurinoma (n=1)
- Astrocytoma (n=1)
- Embryonal Rhabdomyosarcoma (n=1)
- Glioneuronal Tumor (n=1)
- Leptomeningeal Tumor (n=1)
- Leukemia (n=1)
- MN1-altered Glioma (n=1)
- Paranasal Sinus Cancer (n=1)
- Pleomorphic Xanthoastrocytoma (n=1)
- RGNT (n=1)
- SEGA (n=1)
- Stomach Carcinoma (n=1)

Disease status
- active (n=94, 47.7%)
- unknown (n=103, 52.3%)

Time of sample collection
- pre surgery (n=50, 25.4%)
- early post surgery (0–14 d) (n=28, 14.2%)
- post surgery (>14 d) (n=72, 36.5%)
- n.a. (n=47, 23.9%)

Tumor cells in CSF
- No (n=151, 76.6%)
- Yes (n=10, 5.1%)
- n.a. (n=36, 18.3%)

ctDNA
- ctDNA not detected (n=91, 46.2%)
- ctDNA detected (n=86, 43.7%)
- insufficient data for ctDNA analysis (n=20, 10.2%)

CNV analysis
- CNV not detected (n=100, 50.8%)
- CNV detected (n=77, 39.1%)
- insufficient data for CNV analysis (n=20, 10.2%)

NanoDx analysis
- Tumor class not detected by NanoDx (n=111, 56.3%)
- Tumor class detected by NanoDx (n=41, 20.8%)
- insufficient data for NanoDx analysis (n=45, 22.8%)

B

Sample ID
Tumor entity
Disease status
Time of sample collection
Tumor cells in CSF
ctDNA
CNV analysis
NanoDx analysis

Tumor entity
- Medulloblastoma (n=57)
- Ependymoma (n=17)
- ATRT (n=14)
- Lymphoma (n=12)
- Pilocytic Astrocytoma (n=11)
- Glioblastoma (n=9)
- Unknown (n=6)
- Diffuse Midline Glioma (n=7)
- Breast Carcinoma (n=5)
- Craniopharyngioma (n=5)
- Germ Cell Tumor (n=4)
- ETMR (n=2)
- Glioma (n=3)
- Chordoma (n=2)
- DLGNT (n=2)
- Leukemia (n=1)
- Lung Carcinoma (n=2)
- Oligodendroglioma (n=2)
- Pineoblastoma (n=2)
- Plexus Papilloma (n=2)
- Prostate Carcinoma (n=2)
- Acoustic Neurinoma (n=1)
- Astrocytoma (n=1)
- Embryonal Rhabdomyosarcoma (n=1)
- Glioneuronal Tumor (n=1)
- Leptomeningeal Tumor (n=1)
- MN1-altered Glioma (n=1)
- Paranasal Sinus Cancer (n=1)
- RGNT (n=1)
- SEGA (n=1)
- Stomach Carcinoma (n=1)

Disease status
- active (n=85, 48%)
- unknown (n=92, 52%)

Time of sample collection
- pre surgery (n=44, 24.9%)
- early post surgery (0–14 d) (n=26, 14.7%)
- post surgery (>14 d) (n=60, 33.9%)
- n.a. (n=47, 26.6%)

Tumor cells in CSF
- No (n=131, 74%)
- Yes (n=10, 5.6%)
- n.a. (n=36, 20.3%)

ctDNA
- ctDNA not detected (n=91, 51.4%)
- ctDNA detected (n=86, 48.6%)

CNV analysis
- CNV not detected (n=100, 56.5%)
- CNV detected (n=77, 43.5%)

NanoDx analysis
- Tumor class not detected by NanoDx (n=111, 62.7%)
- Tumor class detected by NanoDx (n=41, 23.2%)
- insufficient data for NanoDx analysis (n=25, 14.1%)

Figure 3.8 (Figure legend on following page)

58

Figure 3.8 Results of ctDNA detection by Nanopore sequencing analysis of cfDNA for (A) all sequenced samples and (B) only technically successful samples. (A) ctDNA was detected in 46.2% of all cases, in 39.1% of all cases by CNV analysis and in 20.8% of all cases by methylation analysis with NanoDx. (B) For all technically successful samples, ctDNA detection was positive in 48.6% of samples. CNV analysis detected ctDNA in 43.5% of samples and methylation analysis with NanoDx detected ctDNA in 23.2% of samples. cfDNA - cell-free DNA, CNV - copy number variation, ctDNA - circulating tumor DNA.
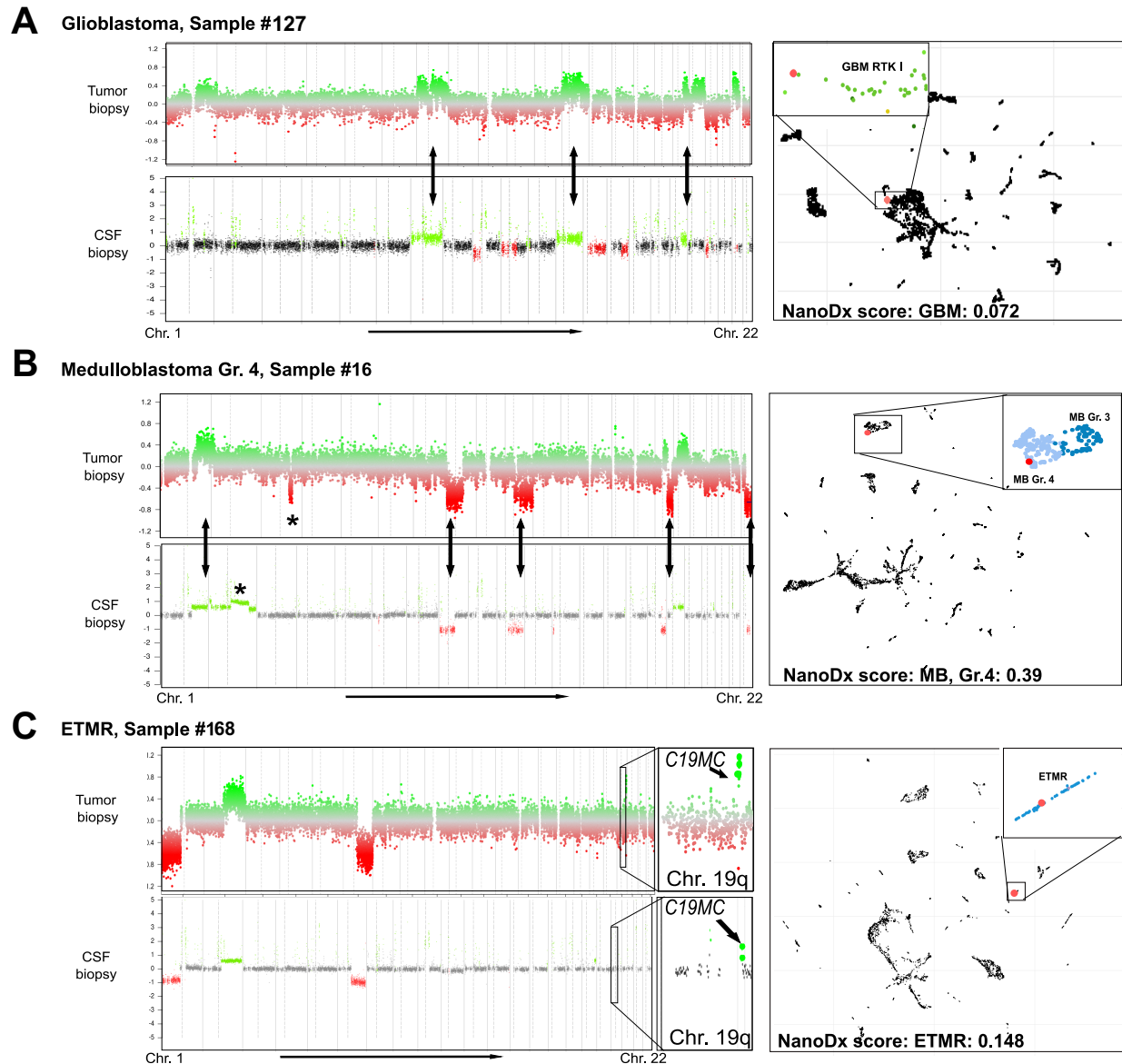
Figure 3.9 CNV and methylation analyses for (A) glioblastoma sample 127, (B) medulloblastoma sample 16, and (C) ETMR samples 168. CNV plots derived from cfDNA match those of the tissue biopsy, with additional private gains marked by an asterisk in (B). (C) Focal amplifications of C19MC on Chr. 19 can be seen in an inlet. All samples shown match with the correct class in the methylation analysis, which is visualized by a UMAP, showing the samples clustering to their respective tumor entities in the inlets. cfDNA - cell-free DNA, CNV - copy number variation, Chr - chromosome, ETMR - embryonal tumor with multi-layered rosettes, UMAP - uniform manifold approximation and projection. Adapted from Afflerbach et al. [84] to represent accurate sample IDs and patient letters.
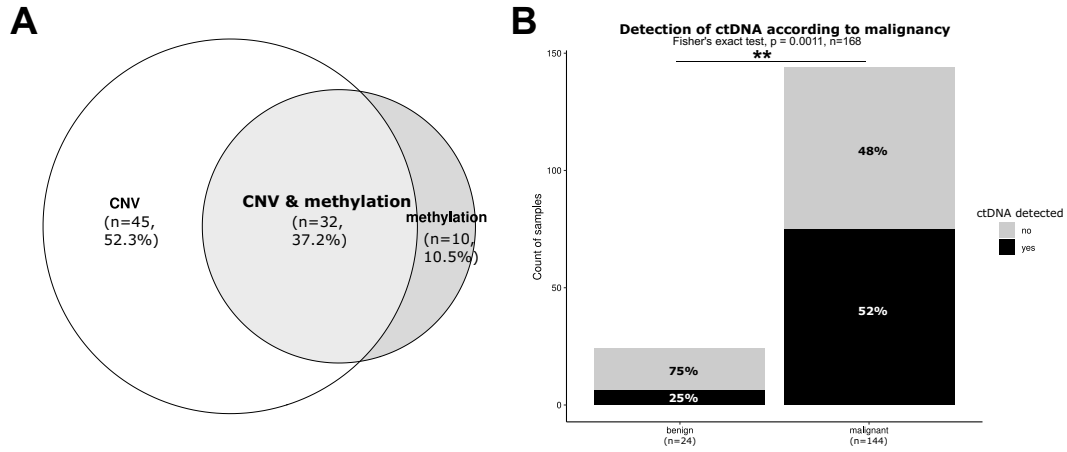
Figure 3.10 (A) Weighted Venn-diagram with ctDNA detection rates according to the method by which ctDNA was detected, CNV analysis or methylation analysis. (B) Detection rates of ctDNA according to the malignancy of the tumor. A statistically significant difference could be observed between the detection rates of malignant and benign tumors (Fisher's exact test, p=0.0011, n=168). CNV - copy number variation, ctDNA - circulating tumor DNA.
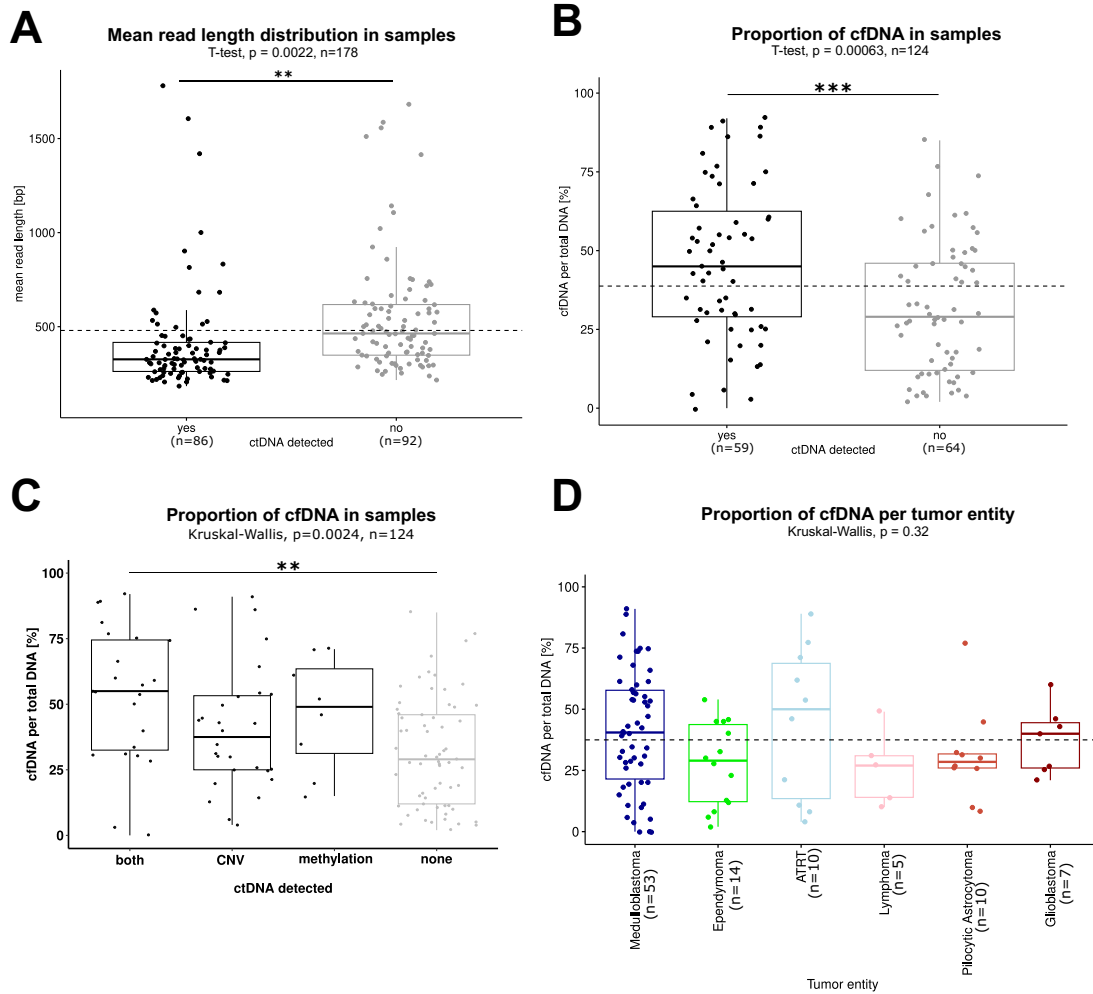
Figure 3.11 (Figure legend on the following page)

Figure 3.11 Statistical differences between samples with detectable and undetectable ctDNA. (A) Mean read length was statistically significantly shorter in samples with detectable ctDNA (t-test, p=0.0022). In accordance with this, cfDNA proportion was statistically significantly higher in samples where ctDNA was detected (B). The detection of ctDNA according to the proportion of cfDNA was not statistically different between the different methods, only between detection by both methods and no detection (p=0.0033) (C). No statistical significant difference could be observed between cfDNA proportion of the six largest groups of entities (Kruskal-Wallis, p=0.32). cfDNA - cell-free DNA, ctDNA - circulating tumor DNA.

Next, samples were divided into two groups: samples collected pre-surgery plus early post-surgery, and samples collected post-surgery (Figure 3.12). In the group of samples collected pre-surgery and early post-surgery (< 14 days after surgery), detection of ctDNA was expected to be higher as tumor was present or residues after surgery were expected to only be partially degraded. 70 technically successful samples fell into the subcohort of pre-surgery and early post-surgery, with 62.9% collected pre-surgery (n=44) and 37.1% collected less than 14 days after surgery (n=26) (Figure 3.12 A). In total, 35/70 samples (50%) contained detectable tumor-derived DNA. 32/70 (45.7%) of samples were detected by CNV, 20/70 (28.6%) were detected by NanoDx analysis. Two cases with detected ctDNA by methylation remained undetected by CNV analysis. 10/70 samples (14.3%) were technically successful but only yielded data for CNV analysis, and methylation analysis could not be performed. Conventional microscopy was only positive for tumor cells in 4/70 cases (5.7%).

For the subcohort of post-surgically collected samples, ctDNA detection was positive for 27/60 samples (45%) (Figure 3.12 B). These samples include long-term post-surgery samples where disease status was unknown, which is in line with the lower number of detected ctDNA cases compared to pre- and early post-surgery samples. CNV analysis detected ctDNA in 22/60 post-surgery samples (36.7%), methylation was able to correctly classify the tumor in 13/60 cases (21.7%). Five of the methylation-detectable cases were undetected by CNV analysis.

Splitting the whole cohort according to their time of sample collection shows the validity of the method for all kinds of samples. Pre-surgery and early post-surgery as well as post-surgery samples were successful with similar success rates, indicating that

the developed method is both valid for initial diagnosis as well as longitudinal monitoring.
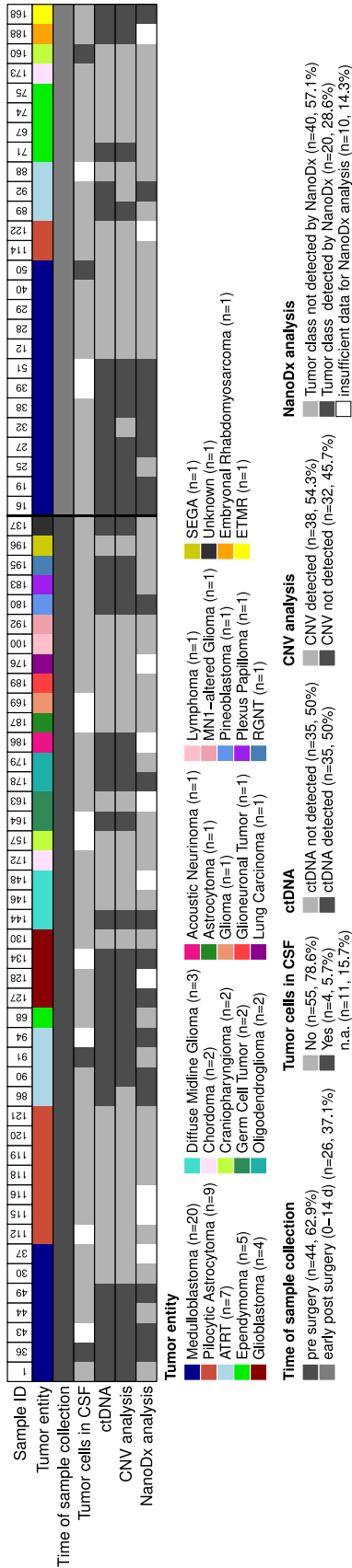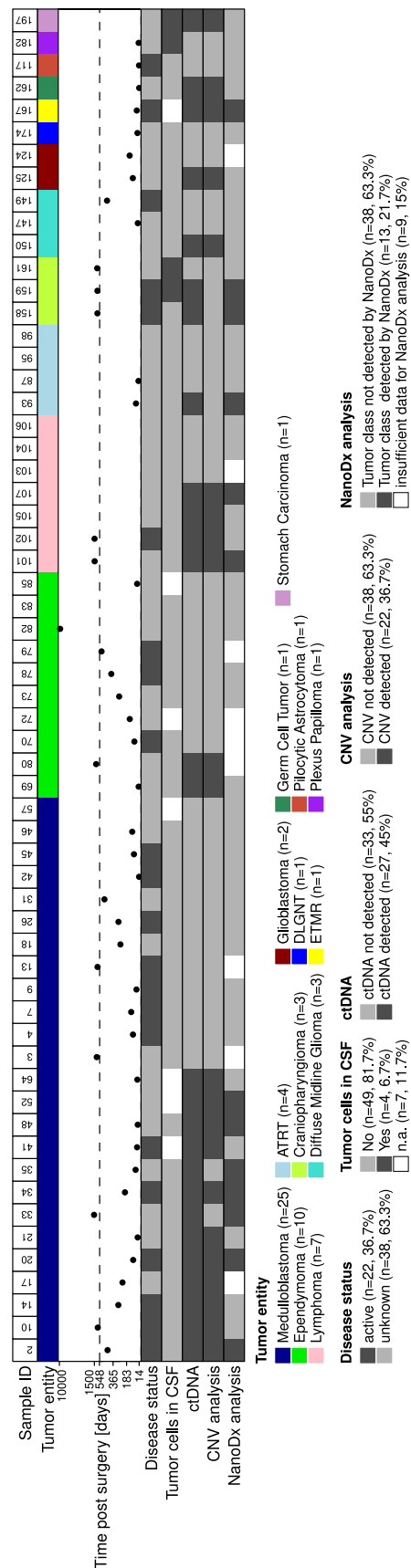
Figure 3.12 (A) Results of ctDNA detection by Nanopore sequencing analysis of 70 cfDNA samples from CSF collected pre- and early post-surgery (< 14 days after surgery). ctDNA was detected in 50% of cases, with 45.7% of cases being detected by CNV analysis and 28.6% of cases being detected by methylation analysis with NanoDx. (B) Results of ctDNA detection by Nanopore sequencing analysis of 60 cfDNA samples from CSF collected post-surgery. ctDNA was detected in 45% of cases, in 36.7% of cases by CNV analysis and in 21.7% of cases by methylation analysis with NanoDx. cfDNA - cell-free DNA, CNV - copy number variation, CSF - cerebrospinal fluid, ctDNA - circulating tumor DNA.

Low-coverage sequencing of cfDNA from CSF has been successfully used as monitoring tool, mainly for medulloblastoma, as shown by Liu *et al.* [50]. In this study, this could be anecdotally reproduced for two cases, a medulloblastoma patient (patient A) and an ependymoma patient (patient L) (Figure 3.15, published and adapted from Afflerbach *et al.* [84], with patient letters and sample numbers reflecting those used in the full cohort of Figure 3.8). Patient A was initially diagnosed with a medulloblastoma with a *CTNNB1* p.S37A mutation that was subtyped as WNT by tissue analysis, but also scored highly for group 3, depending on the Heidelberg classifier version used. The tissue biopsy showed several CNVs visible, namely gains in Chr. 3, 6, 14, 17 and 19. The patient experienced a metastasis roughly half a year after diagnosis, and a CSF biopsy was taken 1.2 years after initial diagnosis, which showed the same CNVs as the initial tissue biopsy as well as an additional loss on Chr. 10. Methylation classified the cfDNA sample as medulloblastoma, group 3 with a score of 0.16. A CSF sample taken during a phase of partial response to treatment showed a noisier CNV plot, with aberrations not visible as clearly as before. Methylation analysis classified the sample as control with a score of 0.038. After second resection of the tumor, a changed CNV profile was found in the tissue sample. A gain in Chr. 2, as well as the loss on Chr. 10 that was already visible in the CSF biopsy before, were now visible. The last analyzed CSF sample of this patient was taken three months after the second surgery and showed very clearly a replication of the CNV profile of the tumor tissue. Additionally, methylation classified the sample as medulloblastoma, group 3 with a score of 0.16.

For patient L, shown in Figure 3.13 B, CSF analysis showed high risk factors before they became apparent in the tumor. Initial tumor biopsy showed a Chr. 1q gain and a Chr. 8 gain. Only three weeks later, a CSF biopsy was taken that showed a diverging CNV profile, with the Chr. 1q gain, but an additional Chr. 6q loss, which is known for being a high-risk factor [85]. Methylation analysis was inconclusive for this sample, yet the highest score was 0.05 for ependymoma, posterior fossa group A. When the patient experienced a local relapse half a year after initial surgery, the tissue biopsy revealed

the CNV profile already detected in the CSF. During a phase of remission, another CSF sample was taken, which showed a flat CNV profile and methylation analysis only revealing control tissue, matching this status of disease.
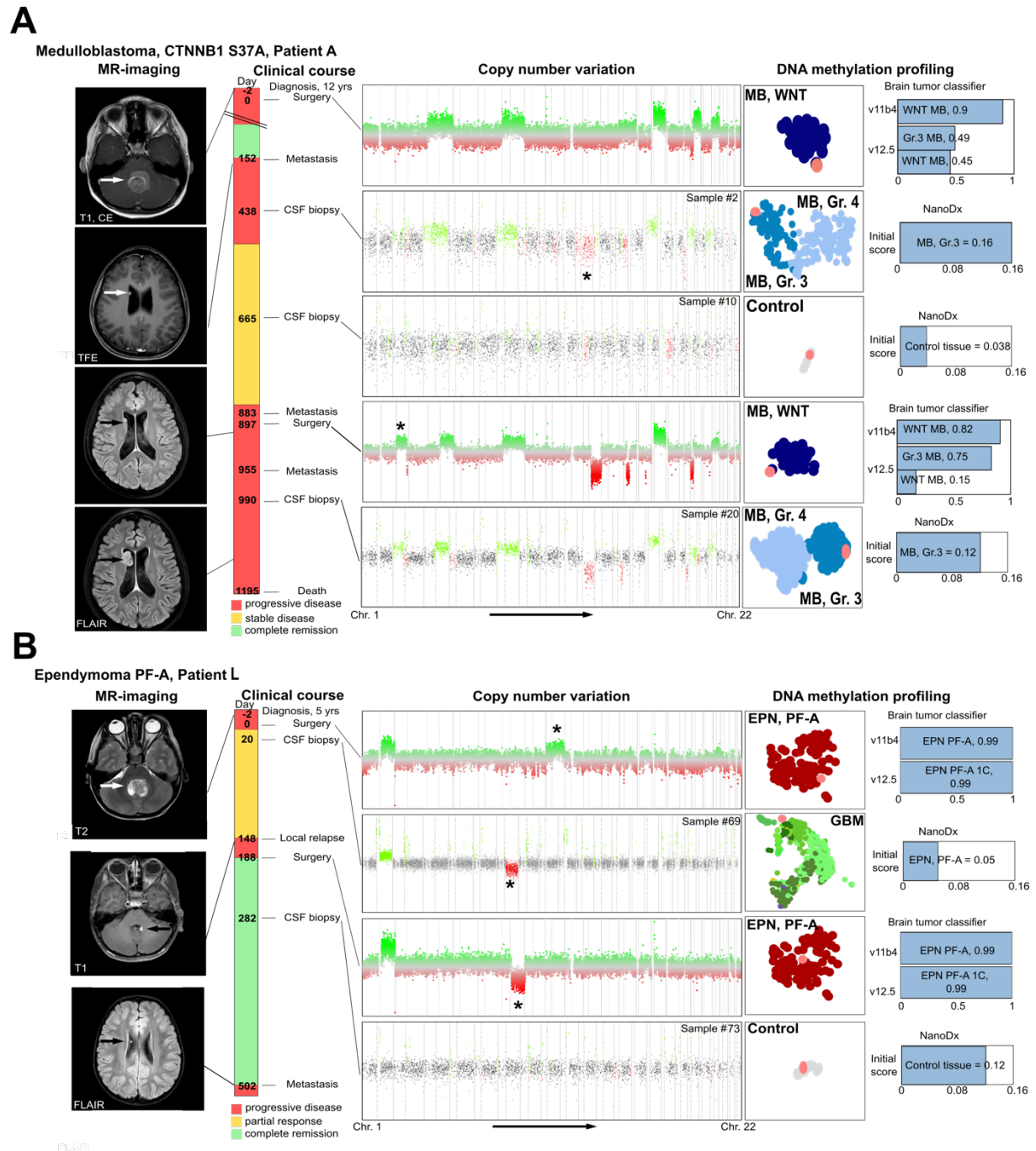
Figure 3.13 Longitudinal results of Nanopore sequencing analysis of cfDNA samples. (A) Course of disease of medulloblastoma patient A with MR-images (far left), clinical events (left), tissue and CSF biopsy derived CNV plots (middle), matching methylation analysis visualized in a UMAP (right) and classifier scores (far right). The CSF sample 2 taken 438 days after surgery showed an additional Chr. 10 loss, not seen in the tissue biopsy. Re-resection of the tumor after 897 days revealed the Chr. 10 loss with an additional Chr. 2 gain, which was also seen in CSF sample 20 taken on day 990. (B) Course of disease of ependymoma PF-A patient L with MR-images (far left), clinical events (left), tissue and CSF biopsy derived CNV plots (middle), matching methylation analysis

visualized in a UMAP (right) and classifier scores (far right). Chr. 1q gain was seen in the initial surgery, CSF sample 69 taken 20 days after surgery revealed an additional Chr. 6q loss, which was confirmed in the tissue of a relapse after 188 days. Aberrations marked with asterisks are private to either the CSF biopsy or the tissue biopsy. cfDNA - cell-free DNA, Chr. - Chromosome, CNV - copy number variation, CSF - cerebrospinal fluid, MR - magnetic resonance, PF - posterior fossa, UMAP - uniform manifold approximation and projection. Adapted from Afflerbach et al. [84] to represent accurate sample IDs and patient letters.

3.4.2. Nanopore sequencing – barcoded sequencing

To make the method more convenient for routine diagnostics as well as more economically viable, Nanopore sequencing was tested with barcoded samples. In an initial test of the protocol, DNA from cell lines were tested in a multiplex assay. cfDNA from SF8628 and LN-229 cell lines were barcoded and pooled, with an input of 100 ng each. Reads were demultiplexed automatically by the MinKNOW sequencing software. Individual CNV plots for the barcodes were constructed and no mixing between the data sets could be observed, both plots are distinct from each other (Figure 3.14).
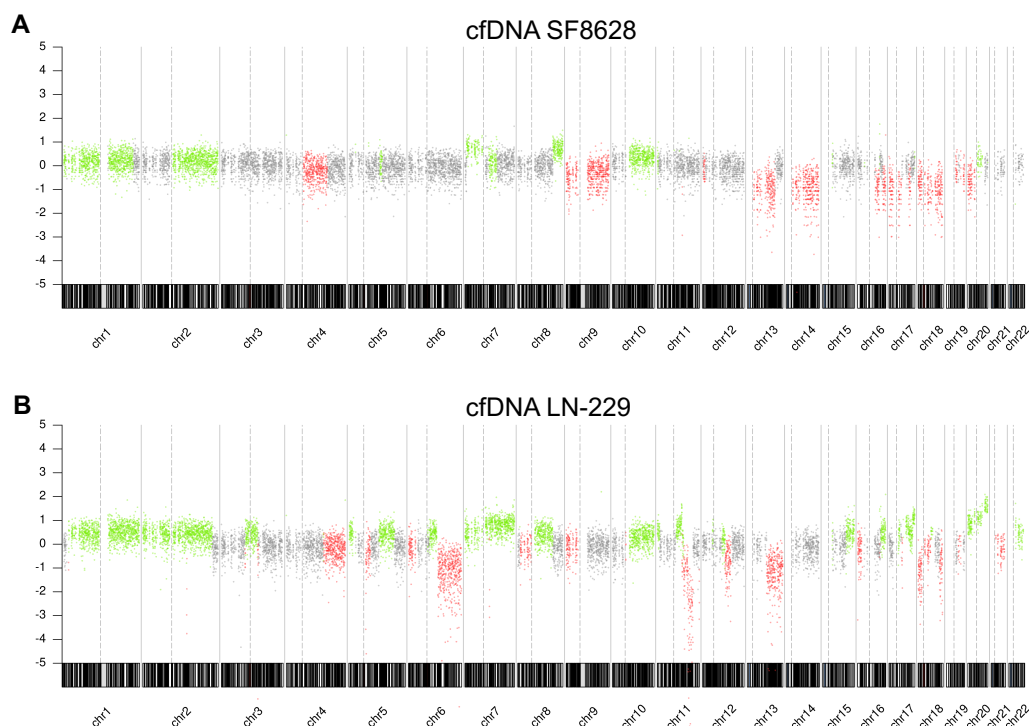
Figure 3.14 CNV plots of barcoded multiplexed cfDNA samples from cell lines from Nanopore data. (A) CNV plot from barcoded SF8628 cfDNA. (B) CNV plot from barcoded LN-229 cfDNA. Both cell lines were barcoded with an input of 100 ng. cfDNA - cell-free DNA, CNV - copy number variation.

As these results were promising, the same protocol was employed with cfDNA from patient samples that had also been previously sequenced individually. In Figure 3.15, barcoded cfDNA samples from patients and their respective natively sequenced samples are depicted (native sequencing for sample 1 in Figure 3.15 A, for sample 2 in Figure 3.15 B; barcoded demultiplexed for sample 1 in Figure 3.15 C, for sample 2 in Figure 3.15 D). Sample 1 is an ATRT sample (sample 91 in 3.4.1), sample 2 is a medulloblastoma sample (sample 16 in 3.4.1).

The CNV plots of the barcoded samples match those of the respective samples. Sample 1 shows losses in Chr. 9, 12, 20 and 22, which are clearly visible in the native CNV plot (Figure 3.15 A), as well as in the barcoded CNV plot (Figure 3.15 C), albeit less clearly. Sample 2 displays a very distinct CNV plot with gains in Chr. 1, 2 and 17, as well as losses in Chr. 8, 10, 16 and 22. These are clearly visible in both the native CNV plot (Figure 3.15 C) and the barcoded CNV plot (Figure 3.15 D). The input difference between the native and barcoded samples is rather stark in these examples. Sample 1 was sequenced with an input of 618 ng in the native setting and 100 ng in the barcoded setting, so an 6.18-fold reduction in input. For sample 2, the input was 10x higher in the barcoded sample than in the natively sequenced sample, with 100 ng as well. The sequencing output, however, was reduced drastically. Sample 1 in the barcoded experiment yielded less than 150 k reads, needing the larger window size setting for analysis, compared to 32 M in the natively sequenced sample. Sample 2 was well analyzable, but quality and quantity of data was nonetheless reduced at roughly 756 k reads compared to 9.5 M reads for the natively sequenced sample.

Both samples have been analyzed with the NanoDx workflow to compare methylation results with that of the native sequencing. Sample 1 did not achieve classification by methylation using NanoDx when sequenced natively (Figure 3.8, sample 91), even though 100,000 CpG sites were analyzed; the barcoded sample also did not achieve classification. 7,301 CpG sites were found, which was above the minimum requirement, but highest ranked entity was plexus tumor, subclass pediatric B with a score of only 0.04, which was below the set threshold and thus not counted as

classified. The medulloblastoma sample 2 had 50,000 CpG sites and a score of 0.28 for medulloblastoma, group 4 when sequenced natively (Figure 3.8, sample 16). When barcoded, only 18,036 CpG sites were read, which means that in the native sample 2.7 x the amount of CpG sites were read. Yet, the result is comparable as the barcoded sample achieved a classification score of 0.27 for medulloblastoma, group 4. Due to the data quality reduction, multiplexing was not further pursued in this work.
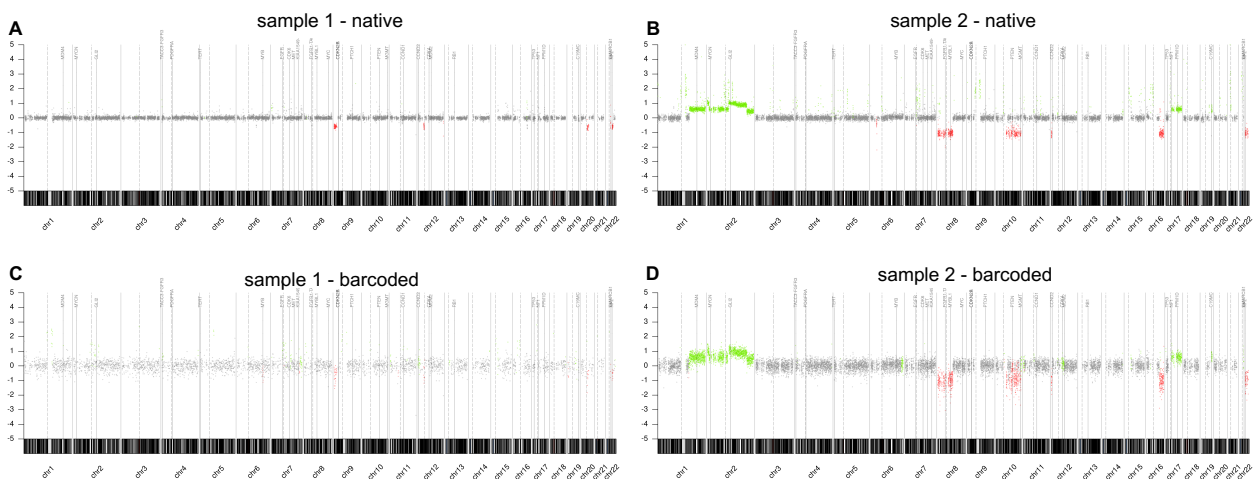
Figure 3.15 Barcoding cfDNA samples allows CNV analysis, yet a quality reduction can be observed in direct comparison to natively sequenced samples. (A) Sample 1 sequenced natively at 618 ng input. (B) Sample 2 sequenced natively at 10 ng input. (C) Sample 1 barcoded and demultiplexed, at 100 ng input. (D) Sample 2 barcoded and demultiplexed, at 100 ng input. cfDNA - cell-free DNA, CNV - copy number variation.

4. Discussion

As the current standard of brain tumor diagnostics relies on the availability of tumor tissue for analysis, a significant proportion of patients face risks of unclear diagnoses due to the inaccessibility of the tumor or the risks of surgery and anesthesia themselves. Especially in the context of pediatric and young adult patients, the need for novel non- or minimally invasive diagnostic methods is urgent. The aim is to secure a diagnosis to treat the patient accordingly, without the need to unnecessarily disturb the developing brain by a surgical intervention. In this work, several molecular analysis methods were explored for their use with CSF as an alternative to the surgical biopsies to perform initial diagnostics, but also for monitoring purposes.

4.1. ddPCR

ddPCR is a very sensitive approach to detect SNVs as each individual droplet serves as a singular reaction tube, and with thousands of droplets per well, increasing the sensitivity manifold compared to standard single tube PCR reactions [51]. Using ddPCR for liquid biopsies has been pioneered, and has recently become more interesting in the field of liquid biopsies in neurooncology, showing that this method has valid applications [52,53,86]. When tumors exhibit hotspot mutations that are relevant for diagnosis, ddPCR can sensitively and specifically confirm the presence of ctDNA by their detection in CSF samples. Additionally, the ease of designing probes and primers manually provides the opportunity to personalize assays for monitoring of patients when specific mutations occur, and for example sequencing panels do not include the mutations of interest [87].

In this work, cfDNA from CSF was analyzed to investigate the feasibility of the method on routine diagnostic samples. SNV detection is possible (Figure 3.2), even at low input (Figure 3.1). 4/27 samples did not show a positive signal for mutation when it was expected from the tumor tissue. This is, however, most likely due to low to no ctDNA content in the CSF at sampling time. CNV detection in cfDNA samples is also possible and informative (Figure 3.3 A), again even at low input (Figure 3.3 B).

It can be discussed whether the detection of both wildtype and mutation sequences in the sample are informative of the hetero-/homozygosity of the mutation. As there is little to no cfDNA present in the CSF of healthy humans, it can be assumed that most, if not all, cfDNA contained in a CSF sample from a patient with a brain tumor comes from that. This, in turn, means that if both wildtype and mutation is detected in roughly equal amounts in the cfDNA, the mutation occurs probably heterozygously. When only mutation sequence is detected, it can be assumed that the mutation is occurring homozygously, or that one allele is lost. However, when the wildtype detected sequences surpass those of the mutation, it is possible that there is another source of wildtype sequence, such as shedding of other cells into the CSF, or that the mutation occurs with low frequency in a heterogenous tumor. In some samples analyzed here, a mutation was expected, such as a *H3-3A* K27M mutation in a DMG, or a known *BRAF* V600E mutation in a pleomorphic xanthoastrocytoma, but only wildtype was detected. It could thus be that the tumors here exhibited the mutation with low frequency, shed cfDNA infrequently or that DNA from other sources diluted the mutated cfDNA to a point below the limit of detection. The lack of false-positives in the analyzed cohort is a great advantage, especially for methods with clinical applications, where positive detections of mutations can have therapeutical effects.

CNV detection using cfDNA from CSF works well, which allows further subtyping, risk stratifying or supporting a diagnosis, such as *Myc* amplifications in medulloblastoma [76] or *EGFR* amplifications in glioblastoma [88]. With the emergence of the new Bio-Rad QX600 system, the development of panels with six different channels for mutation detection is relatively easy and straightforward. This allows on the one hand the development of multiplexed panels for single samples for initial diagnosis, possibly investigating several SNVs and CNVs simultaneously, as well as the possibility to multiplex personalized assays, with primers and probes designed specifically for the patient as a monitoring tool.

4.2. Methylation arrays

As an open, uninformed approach to initially diagnose CNS tumors with their exact entity using cfDNA isolated from CSF, methylation arrays were tested. These are already widely used in the routine diagnostics with tissue biopsies, with an established and well recognized analysis pipeline [15,16]. Adapting an already established pipeline would be favorable over establishing a novel method, especially in a clinical routine setting, as implementing novel methods is challenging for the daily process, but also for eventual certification. cfDNA, however, does not necessarily behave the same as gDNA and the established protocol had to be adapted, especially considering the smaller input amount. Enzymatic conversion, initially developed for sequencing approaches, is less harsh compared to bisulfite conversion, meaning a smaller loss and lesser degradation of DNA during the experimental workflow is expected [89].

Initial testing of the here designed protocol with gDNA showed favorable results with inputs as low as 10 ng (Figure 3.4), so that 20 cfDNA samples were tested. Here, however, results were not up to diagnostic standard, with only 20% correctly classified cases using the classifier v11, and 30% using classifier v12 (Table 3.1). The CNV plots of most samples were not interpretable as they were very noisy (Figure 3.5). In routine tissue analysis, CNV plots are often an indicator for specific focal amplifications, like *EGFR* amplifications in glioblastoma [88], or losses, such as *CDKN2A/B* in gliomas [90,91], to reinforce classification by the random forest classifier based on the methylation. A possible reason for the low performance of this method could be the arbitrary selection of CpG sites that are analyzed in cfDNA. The DNA degrades within the CSF and the whole genome may not be uniformly present at all times, making the number and the kinds of CpGs sites analyzed random. It is possible that certain CpG sites necessary for classification were not present, resulting in low or very low scores. Perhaps the enzymatic conversion of the cfDNA results in slightly modified DNA structure (apart from the intended change to read methylation status), or slight cross-reactions between kits and reagents, so that CNV plot analysis resulted in those noisy plots that could not be interpreted.

The composition of CSF also differs at different times of puncture, resulting in possible impurities that could not be removed by cfDNA isolation and purification. Possible impurities or contaminants could also have an influence on the analysis with sensitive, yet broad approach methods like methylation arrays. The development of a reference based solely on CSF samples might improve classification results, yet this remains a difficult task as it is unclear if the method and protocol itself is successful, and additional novel bioinformatic tools may be needed. As both parts of the analysis, the classifier results and the CNV plots, did not yield results of sufficient quality to perform diagnostics with and improvement of the method proved to be difficult and lengthy, this method was not considered for further development, especially with alternatives, like varying sequencing approaches, being available.

4.3. TruSight Oncology 500 ctDNA

Sequencing panels have become a popular way to identify specific mutations in tumors to either confirm a diagnosis or identify therapeutical targets. As an open approach when the tumor entity is unclear and diagnosis is not yet made, a large sequencing panel covering a great variety of genes is of interest. For this reason, the TruSight Oncology 500 ctDNA was tested, as it spans over 500 genes and additionally gives the opportunity to identify gene fusions and CNVs for several genes. A total of 16 samples was tested, with different entities, mutations and cfDNA qualities included. The input ranged from 6.5 ng to 31 ng, with cfDNA proportions of total DNA of 0% to 99%. This reflects the reality of samples in the clinical routine. 62.5% of samples were a technical success, however only 6/16 (37.5%) delivered results matching the tumor tissue (Table 3.2). With hundreds of SNVs found for each sample, analysis remained difficult. Without prior knowledge of a suspected entity, filtering the found mutations is nearly impossible as all, none or just a small set could be relevant for the specific tumor. Broad deletions, such as seen in the ATRT samples TSO4 and TSO5 also cannot be detected by this panel. The deletion only came to attention after a retrospective analysis of the tissue for the specific genetic region, however this would not be the clinical goal of a minimally invasive diagnostic method. The cohort tested here is rather small and has a limited range of entities, yet the results are not convincing of this method. It remains unclear whether the input amount is influential, as the same samples have been tested with varying input amounts and the results went in both directions. Samples with low cfDNA percentages failed, with 60% cfDNA of total DNA being a suggested quality threshold as samples above this performed well technically, with only sample TSO16 being the exception. The results acquired here suggest that the panel works for top quality samples, yet the workflow does not seem very robust, and it defeats the purpose of an initial diagnosis tool when the tumor entity is still unknown. It is possible to confirm diagnoses with specific point mutations or fusions, but in this cohort, these often remained undetected and many others were found, which raises the question of artefacts and ambiguous results.

Although the diagnosis confirmation would be possible with the TruSight Oncology 500 ctDNA panel, it is unnecessarily large for this purpose and smaller, more neurooncologically targeted gene panels should be sufficient. Pagès *et al.* implemented a panel consisting of 46 genes that were extensively reported to contain hotspot mutations or fusions in pediatric brain tumors, and while they were not able to achieve satisfactory sensitivity, it nonetheless shows that a distinctly smaller sequencing panel will cover the most relevant genes [36]. Smaller sequencing panels focused on a specific entity have been shown to reproduce the same mutations in cfDNA as known from the tumor tissue, demonstrating that this technique is applicable for cfDNA with satisfactory results [54,92]. A large sequencing panel similar in size to the Tru Sight Oncology 500 ctDNA has been developed, initially for genomic DNA, and used successfully with cfDNA to confirm initial diagnosis when tissue analysis remained inconclusive, as well as to monitor tumor during treatment and its evolution [93–96]. Bale *et al.* demonstrate the utility of the large panel for a variety of tumors, also outside of the CNS [95], however as most tumor entities are not solely characterized by a mutation or fusion, further analyses would still be necessary, and a smaller panel might still be sufficient to confirm a suspected diagnosis. Additionally, large panels are expensive and not always feasible in the routine diagnostic as they tend to require larger sequencers, which, again, would be in favor of smaller panels. Another downside, just as for methylation arrays, is the use of flow cells that require a specific number of samples as to not waste consumables. As this method did not deliver satisfactory results and was not easily feasible outside of specific centers, it was not pursued for the development of a diagnostic method.

Even though this sequencing panel did not fulfil the expectations in terms of a novel diagnostic method, it nonetheless delivered interesting results. In samples TSO15 and TSO16, a strong *Myc* amplification was detected (Table 3.2). The patient experienced a relapse of a WNT-medulloblastoma, however the *Myc* amplification was only detected

in the primary tumor tissue. The possible reasons for this are diverse, with clonal heterogeneity, general tumor heterogeneity or the extrachromosomal accumulation of *Myc* being some of them. The finding of the *Myc* amplification raises the question in what way cfDNA studies could be expanded and how it can be informative of the tumor, and perhaps even elucidate some questions on tumor evolution.

4.4. Nanopore sequencing

A cohort of 197 cfDNA samples was analyzed with Nanopore sequencing as previous studies suggest that sequence and methylation data gained through Nanopore data is useful for tumor DNA detection and brain tumor classification [62,63]. A smaller subcohort of 129 analyzed cfDNA has been published in Afflerbach *et al.* [84]. The results presented there could be further supported and enhanced by analyzing the full 197 samples. The full cohort was diverse with over 30 entities, as well as several sample collection times. cfDNA used in sequencing was of varying quality, represented by the range of read lengths in addition to the range of cfDNA proportion of whole DNA content (Figure 3.7). This, however, represents the daily occurrences in the routine diagnostic, as samples arrive with unknown time between puncture and first processing in the laboratory, of varying quality depending on the puncture itself and with diverse questions, such as MRD detection, initial diagnosis, or exclusion of tumor involvement.

ctDNA was detected in 86/197 samples (43.7%), which was an improvement from the smaller cohort shown in Afflerbach *et al.* [84], where 39% of samples were positive for ctDNA after analysis. Not counting the technical failures, these statistics improve further to ctDNA detection in almost half of the analyzed samples (86/177, 48.6%). This underlines the use of the developed method for ctDNA detection and the potential complementation of other currently used methods in routine diagnostics.

The split into groups according to the time of sample collection (Figure 3.12) highlights the use of Nanopore sequencing for different clinical settings. The success rate with samples collected pre- and early post-surgery shows that the method can indeed complement the initial diagnosing process by providing insight into sequence aberrations as well as sometimes providing and exact classification. ctDNA detection rate in samples that were collected post-surgery is still relatively high, which emphasizes the use of the method for MRD and relapse detection. The use of cfDNA from CSF as MRD detection has been shown extensively by Liu *et al.* [50] using low-

coverage NGS, and anecdotally been reproduced with the use of Nanopore sequencing in this study (Figure 3.13) [84].

One great advantage of using Nanopore sequencing compared to other sequencing approaches is the possibility to simultaneously investigate methylation and sequence of cfDNA. As shown in Figure 3.10 A, CNV analysis allowed the detection of most samples with ctDNA, yet there are 10/87 samples (10.5%) with ctDNA detectable only by methylation analysis. While CNV analysis outperforms the methylation analysis, it is not able to make an accurate classification on its own, which in turn favors Nanopore sequencing over other sequencing only or methylation only approaches. Some samples without CNVs in the tissue biopsy were also analyzed, again highlighting the need for the additional methylation analysis. These samples remain harder to detect than those with CNVs, as the CNV analysis is more robust and generally performs better. Methylation analysis of Nanopore data has been used for the diagnosis of CNS tumors in several studies, showing the suitability of Nanopore methylation analysis for CNS tumors in general [63,97,98]. With the use of gDNA from a biopsy, Djirackor *et al.* were able to obtain results within the timeframe of the surgery, which allows the influencing of the surgical strategy [97]. Other machine learning besides random forest classifiers have been evaluated and tools for robust tumor diagnostics developed. Vermeulen *et al.* employed a neural network to diagnose a tumor based on its methylation profile in less than an hour after sequencing [99]. The sequencing of cfDNA on a Nanopore device behaves differently than that of gDNA due to its fragmentation, often also resulting in slower sequencing to reach the same coverage. Liquid biopsy diagnostics with the use of cfDNA might thus not necessarily profit from the extremely fast results that the novel tools can provide, however with the development of better and more diverse machine learning applications, the diagnostics from cfDNA will also improve and provide more reliable results.

One of the downsides of the method is its low coverage that can only be slightly improved by extending run times, however this proves uneconomic as flow cells are then un-reusable, as well as a relatively high error rate, especially compared to NGS approaches. This means that Nanopore sequencing does not allow the evaluation of SNVs and would require complementation of other methods, such as ddPCR.

Within the current workflow of the NanoDx analysis, the reference used is that published by Capper *et al.* [15], comprising brain tumor entities and some control tissue. This limits the current use of the developed method to samples where CNS tumor involvement is highly probable. Some cases from CNS-foreign tumors were included in the cohort, often with CNV aberrations, however these could then not be classified by the methylation analysis algorithm, somewhat skewing the results. To determine whether a lesion is a primary CNS tumor rather than a metastasis of an already known tumor, this might still be useful – but for cancers of unknown primary and additional assurance of primary vs metastasis, the improvement and constant extension of the reference is of importance. With 7/177 (4%) falsely classified cases, the rate is not very high, yet it is important to investigate these falsely classified samples closely. Adjusting the threshold for significant scores will improve the false classification rate, but it might also lower the number of overall classifications. For research purposes, a slightly lower threshold with a slightly higher number of false classifications is acceptable; for diagnostic purposes and subsequent clinical decision-making, classifications need to be as accurate as possible and thus a higher threshold would be preferable. The exact threshold for diagnostic purposes needs to be further validated, especially with extended and improved reference cohorts.

Another point to investigate before fully adapting the method into diagnostic routine is the evaluation of the limit of detection. The protocols by the manufacturer for Nanopore sequencing suggest an initial input of 1 µg, yet the method developed here provided sequencing results from samples with inputs of 3 ng or lower, probably due to the relative higher molarity of cfDNA. A definitive limit of detection is difficult to

establish as the results of this study suggest that if ctDNA is present, it can be detected, however the presence will only be known after analysis.

Of note, no case of pilocytic astrocytoma was detectable with the developed method (Figure 3.8), yet other benign tumors were detectable, even if only at lower numbers (Figure 3.8, Figure 3.10 B). It is unclear why this entity underperforms compared to all other entities. Remarkably, pilocytic astrocytoma cases investigated with the TSO500 panel remained also undetected with no mutation or fusion flagged in the results (Table 3.2). How the pilocytic astrocytoma differ in their biology from other tumors that might explain this phenomenon of the lack of detectability remains to be elucidated. One hint might be the frequent development of cysts [100] which might hinder the shedding of cfDNA into the CSF, hence evading detection via liquid biopsy. This issue might not be exclusive to pilocytic astrocytoma, but rather be an issue of low-grade tumors in general. This study is limited in sample size for what are considered benign tumors, but they generally contain significantly less ctDNA than malignant tumor samples (Figure 3.10 B). It is thus possible that other entities of low-grade tumors equally underperform when comparing them to malignant entities. Reasons for this general phenomenon still require explanations and further investigation, but it is conceivable that benign tumors generally have a lower cell turnover and the tendency to remain localized, thus also shedding less DNA into the CSF.

In a few samples, CNVs were found in the CSF biopsy that were not found in the matching tissue biopsy (Figure 3.9), or in the case of the longitudinally observed patient, only much later (Figure 3.13). This has also been observed by Liu *et al.* their longitudinal study for MRD detection in medulloblastoma [50]. This shows another advantage of using liquid biopsies at least in a complementary fashion, as the clonal heterogeneity of the tumor might be better depicted in the liquid than in the tissue biopsy alone. With tissue biopsies, there might be an initial surgical bias when taking

the biopsy, as well as an analytical bias when choosing the region of the tumor for molecular analyses in the diagnostic laboratory. When using the liquid biopsy, this sampling bias is not an issue as DNA fragments are mixed throughout, and depending on the volume of the sample, all fragments are eluted and analyzed. The use of liquid biopsies like this can also be informative of tumor evolution and particular risk factors, as seen in Figure 3.13 for patient L with ependymoma, posterior fossa group A.

Nanopore sequencing also provides the opportunity to multiplex samples and thus reduce the cost per sample. In pilot experiments shown in this study, a drastic quality reduction was seen compared to native sequencing of the cfDNA samples. Barcodes were well distinguishable and there was no cross-over between samples, suggesting that the barcoding protocol itself works well. CNVs could still be inferred from the reduced amount of data, which might be enough for monitoring, as it is already known what the aberrations are and what one needs to look for. Methylation analysis was also possible, however data reduction was noticeable here as well. Both samples tested with barcodes showed similar results to their natively sequenced counterparts, with one sample being accurately classified and the other one not classified. The amount of CpG sites was much lower than in the native sequencing results. As both CNV and methylation analysis is possible, yet with significantly lower data amounts, multiplexing might rather be an opportunity for reducing cost in a longitudinal monitoring setting instead of initial diagnostics. Initial diagnostics also tend to have a more pressing time frame than monitoring samples, meaning they would need to be run right away. Monitoring samples could be allowed to build a pool and then be run collectively. When a sample gets flagged as positive in a multiplexed sequencing run, it could then in turn be either sequenced again on its own, or a clinical follow-up could be one of the next steps to ensure a highly sensitive result.

4.5. Conclusion & Outlook

This study shows that there are several methods useful for diagnosis of brain tumors using liquid biopsies, especially CSF for CNS tumors. Nanopore sequencing constitutes the major part in this work as it allows the simultaneous analysis of DNA sequence and methylation, providing advantages over other sequencing approaches explored here, like the TSO500 or methylation arrays alone. The results are promising and show a significant sensitivity improvement over conventional CSF analyses that are usually just comprised of microscopic evaluation of the cells contained in the sample. Some entities are included with small sample sizes or singular cases, but the encouraging results of this first study pave the way to include this method in clinical trials and thus improve case numbers. Yet, the major downside of Nanopore sequencing is the low coverage that does not allow the investigation of specific SNVs. A recommendation for the implementation of liquid biopsy analysis in the routine diagnostic workflow could be to first apply Nanopore sequencing with low, but sufficient input. Retaining some cfDNA for further analysis in the form of ddPCR then allows specific mutation testing, as this method is very sensitive and only requires very little input. The combination of Nanopore sequencing for ctDNA detection, CNV analysis and methylation classification, with follow-up ddPCR testing to investigate SNVs gives a thorough insight into the tumor landscape without the need for a biopsy. A great part of molecular markers needed for specific diagnoses are covered by those two methods. With the advent of novel ddPCR machines that allow six-color multiplexing, the development of mutational panels relevant for a variety of tumor entities is possible, requiring even lower inputs of DNA than when all assays are conducted individually.

To improve ctDNA detection and classification of the exact tumor entity, development of a more advanced reference cohort is needed. Additionally, the use of other machine learning tools, such as neural networks, instead of random forest classifiers could improve the classification and shorten the analysis time. The reference is based on published data of methylation arrays covering 450,000 CpG sites [15], however the use

of 850,000 CpG site strong methylation arrays has become standard in the routine diagnostics. Building a reference using the newer methylation arrays would almost double the available sites for classification. Expanding the reference with more entities and different subtypes would also allow more exact diagnosis. The eventual goal would be to build one classification tool with not only CNS tumors, but also carcinomas and other entities, to diagnose any tumor.

Generally, the use of liquid biopsies as analyte gives a thorough insight into the tumor's characteristics and has the advantage of supplying more information on tumor heterogeneity that could potentially get lost in tissue biopsies due to surgical or analytical bias. Potential uses of other liquids such as plasma with the same analyses' workflows remain to be investigated, although this could prove to be difficult for diagnostics of brain tumors. With regards to other tumor entities though, it might be preferable and even more minimally invasive than CSF collection.

5. References

[1]   Louis DN, Perry A, Wesseling P, et al. The 2021 WHO Classification of Tumors of the Central Nervous System: a summary. Neuro-Oncol. 2021;23:1231–1251.

[2]   WHO Classification of Tumors Editorial Board, editor. Central nervous system tumours. 5th ed. Lyon: International Agency for Research on Cancer; 2021.

[3]   Jones DTW, Jäger N, Kool M, et al. Dissecting the genomic complexity underlying medulloblastoma. Nature. 2012;488:100–105.

[4]   Kool M, Korshunov A, Remke M, et al. Molecular subgroups of medulloblastoma: an international meta-analysis of transcriptome, genetic aberrations, and clinical data of WNT, SHH, Group 3, and Group 4 medulloblastomas. Acta Neuropathol (Berl). 2012;123:473–484.

[5]   Holdhof D, Johann PD, Spohn M, et al. Atypical teratoid/rhabdoid tumors (ATRTs) with SMARCA4 mutation are molecularly distinct from SMARCB1-deficient cases. Acta Neuropathol (Berl). 2021;141:291–301.

[6]   Johann PD, Erkek S, Zapatka M, et al. Atypical Teratoid/Rhabdoid Tumors Are Comprised of Three Epigenetic Subgroups with Distinct Enhancer Landscapes. Cancer Cell. 2016;29:379–393.

[7]   Siegel RL, Miller KD, Wagle NS, et al. Cancer statistics, 2023. CA Cancer J Clin. 2023;73:17–48.

[8]   Major N, Patel NA, Bennett J, et al. The Current State of Radiotherapy for Pediatric Brain Tumors: An Overview of Post-Radiotherapy Neurocognitive Decline and Outcomes. J Pers Med. 2022;12:1050.

[9]   Merchant TE, Conklin HM, Wu S, et al. Late Effects of Conformal Radiation Therapy for Pediatric Patients With Low-Grade Glioma: Prospective Evaluation of Cognitive, Endocrine, and Hearing Deficits. J Clin Oncol. 2009;27:3691–3697.

[10]   Ris MD, Packer R, Goldwein J, et al. Intellectual Outcome After Reduced-Dose Radiation Therapy Plus Adjuvant Chemotherapy for Medulloblastoma: A Children's Cancer Group Study. J Clin Oncol. 2001;19:3470–3476.

[11]   Paulino AC, Lobo M, Teh BS, et al. Ototoxicity After Intensity-Modulated Radiation Therapy and Cisplatin-Based Chemotherapy in Children With Medulloblastoma. Int J Radiat Oncol. 2010;78:1445–1450.

[12]   Vatner RE, Niemierko A, Misra M, et al. Endocrine Deficiency As a Function of Radiation Dose to the Hypothalamus and Pituitary in Pediatric and Young Adult Patients With Brain Tumors. J Clin Oncol. 2018;36:2854–2862.

[13] Remes TM, Suo-Palosaari MH, Arikoski PM, et al. Radiotherapy-induced vascular cognitive impairment 20 years after childhood brain tumor. Neuro-Oncol. 2023;noad186.

[14] Pajtler KW, Witt H, Sill M, et al. Molecular Classification of Ependymal Tumors across All CNS Compartments, Histopathological Grades, and Age Groups. Cancer Cell. 2015;27:728–743.

[15] Capper D, Jones DTW, Sill M, et al. DNA methylation-based classification of central nervous system tumours. Nature. 2018;555:469–474.

[16] Capper D, Stichel D, Sahm F, et al. Practical implementation of DNA methylation and copy-number-based CNS tumor diagnostics: the Heidelberg experience. Acta Neuropathol (Berl). 2018;136:181–210.

[17] Koelsche C, Schrimpf D, Stichel D, et al. Sarcoma classification by DNA methylation profiling. Nat Commun. 2021;12:498.

[18] Lyskjær I, De Noon S, Tirabosco R, et al. DNA methylation-based profiling of bone and soft tissue tumours: a validation study of the DKFZ Sarcoma Classifier. J Pathol Clin Res. 2021;7:350–360.

[19] Drexler R, Schüller U, Eckhardt A, et al. DNA methylation subclasses predict the benefit from gross total tumor resection in IDH-wildtype glioblastoma patients. Neuro-Oncol. 2023;25:315–325.

[20] Ramaswamy V, Hielscher T, Mack SC, et al. Therapeutic Impact of Cytoreductive Surgery and Irradiation of Posterior Fossa Ependymoma in the Molecular Era: A Retrospective Multicohort Analysis. J Clin Oncol. 2016;34:2468–2477.

[21] Thompson EM, Hielscher T, Bouffet E, et al. Prognostic value of medulloblastoma extent of resection after accounting for molecular subgroup: a retrospective integrated clinical and molecular analysis. Lancet Oncol. 2016;17:484–495.

[22] Pantel K, Alix-Panabières C. Circulating tumour cells in cancer patients: challenges and perspectives. Trends Mol Med. 2010;16:398–406.

[23] Schwarzenbach H, Hoon DSB, Pantel K. Cell-free nucleic acids as biomarkers in cancer patients. Nat Rev Cancer. 2011;11:426–437.

[24] Anfossi S, Babayan A, Pantel K, et al. Clinical utility of circulating non-coding RNAs — an update. Nat Rev Clin Oncol. 2018;15:541–563.

[25] Westphal, M, Pantel K, Ricklefs FL, et al. Circulating tumor cells and extracellular vesicles as liquid biopsy markers in neuro-oncology: prospects and limitations. Neuro-Oncol Adv. 2022;4:ii45–ii52.

[26] Bettegowda C, Sausen M, Leary RJ, et al. Detection of Circulating Tumor DNA in Early- and Late-Stage Human Malignancies. Sci Transl Med [Internet]. 2014 [cited 2022 Nov 17];6. Available from: https://www.science.org/doi/10.1126/scitranslmed.3007094.

[27] Lorente D, Olmos D, Mateo J, et al. Decline in Circulating Tumor Cell Count and Treatment Outcome in Advanced Prostate Cancer. Eur Urol. 2016;70:985–992.

[28] Beaver JA, Jelovac D, Balukrishna S, et al. Detection of Cancer DNA in Plasma of Patients with Early-Stage Breast Cancer. Clin Cancer Res. 2014;20:2643–2650.

[29] Heidrich I, Ačkar L, Mossahebi Mohammadi P, et al. Liquid biopsies: Potential and challenges. Int J Cancer. 2021;148:528–545.

[30] Alix-Panabières C, Pantel K. Liquid Biopsy: From Discovery to Clinical Application. Cancer Discov. 2021;11:858–873.

[31] Sakka L, Coll G, Chazal J. Anatomy and physiology of cerebrospinal fluid. Eur Ann Otorhinolaryngol Head Neck Dis. 2011;128:309–316.

[32] Hladky SB, Barrand MA. Mechanisms of fluid movement into, through and out of the brain: evaluation of the evidence. Fluids Barriers CNS. 2014;11:26.

[33] Betts JG, Young KA, Wise JA, et al. 13.3 Circulation and the Central Nervous System. Anat Physiol [Internet]. Houston, Texas: OpenStax; 2013. Available from: https://openstax.org/books/anatomy-and-physiology/pages/13-3-circulation-and-the-central-nervous-system.

[34] De Mattos-Arruda L, Mayor R, Ng CKY, et al. Cerebrospinal fluid-derived circulating tumour DNA better represents the genomic alterations of brain tumours than plasma. Nat Commun. 2015;6:8839.

[35] Escudero L, Llort A, Arias A, et al. Circulating tumour DNA from the cerebrospinal fluid allows the characterisation and monitoring of medulloblastoma. Nat Commun. 2020;11:5376.

[36] Pagès M, Rotem D, Gydush G, et al. Liquid biopsy detection of genomic alterations in pediatric brain tumors from cell-free DNA in peripheral blood, CSF, and urine. Neuro-Oncol. 2022;24:1352–1363.

[37] Müller C, Holtschmidt J, Auer M, et al. Hematogenous dissemination of glioblastoma multiforme. Sci Transl Med [Internet]. 2014 [cited 2022 Nov 17];6. Available from: https://www.science.org/doi/10.1126/scitranslmed.3009095.

[38] Ward Gahlawat A, Lenhardt J, Witte T, et al. Evaluation of Storage Tubes for Combined Analysis of Circulating Nucleic Acids in Liquid Biopsies. Int J Mol Sci. 2019;20:704.

[39] Maass KK, Schad PS, Finster AME, et al. From Sampling to Sequencing: A Liquid Biopsy Pre-Analytic Workflow to Maximize Multi-Layer Genomic Information from a Single Tube. Cancers. 2021;13:3002.

[40] Liu MC, Oxnard GR, Klein EA, et al. Sensitive and specific multi-cancer detection and localization using methylation signatures in cell-free DNA. Ann Oncol. 2020;31:745–759.

[41] Heitzer E, Auinger L, Speicher MR. Cell-Free DNA and Apoptosis: How Dead Cells Inform About the Living. Trends Mol Med. 2020;26:519–528.

[42] Lo YMD, Han DSC, Jiang P, et al. Epigenetics, fragmentomics, and topology of cell-free DNA in liquid biopsies. Science. 2021;372:eaaw3616.

[43] Jiang P, Lo YMD. The Long and Short of Circulating Cell-Free DNA and the Ins and Outs of Molecular Diagnostics. Trends Genet. 2016;32:360–371.

[44] Underhill HR, Kitzman JO, Hellwig S, et al. Fragment Length of Circulating Tumor DNA. Kwiatkowski DJ, editor. PLOS Genet. 2016;12:e1006162.

[45] Hudecova I, Smith CG, Hänsel-Hertsch R, et al. Characteristics, origin, and potential for cancer diagnostics of ultrashort plasma cell-free DNA. Genome Res. 2022;32:215–227.

[46] Mouliere F, Chandrananda D, Piskorz AM, et al. Enhanced detection of circulating tumor DNA by fragment size analysis. Sci Transl Med. 2018;10:eaat4921.

[47] Jiang P, Chan CWM, Chan KCA, et al. Lengthening and shortening of plasma DNA in hepatocellular carcinoma patients. Proc Natl Acad Sci [Internet]. 2015 [cited 2023 Oct 8];112. Available from: https://pnas.org/doi/full/10.1073/pnas.1500076112.

[48] Pentsova EI, Shah RH, Tang J, et al. Evaluating Cancer of the Central Nervous System Through Next-Generation Sequencing of Cerebrospinal Fluid. J Clin Oncol. 2016;34:2404–2415.

[49] Mouliere F, Mair R, Chandrananda D, et al. Detection of cell-free DNA fragmentation and copy number alterations in cerebrospinal fluid from glioma patients. EMBO Mol Med [Internet]. 2018 [cited 2021 Dec 30];10. Available from: https://onlinelibrary.wiley.com/doi/10.15252/emmm.201809323.

[50] Liu APY, Smith KS, Kumar R, et al. Serial assessment of measurable residual disease in medulloblastoma liquid biopsies. Cancer Cell. 2021;39:1519-1530.e4.

[51] Quan P-L, Sauzade M, Brouzes E. dPCR: A Technology Review. Sensors. 2018;18:1271.

[52] Cantor E, Wierzbicki K, Tarapore RS, et al. Serial H3K27M cell-free tumor DNA (cf-tDNA) tracking predicts ONC201 treatment response and progression in diffuse midline glioma. Neuro-Oncol. 2022;24:1366–1374.

[53] Li D, Bonner ER, Wierzbicki K, et al. Standardization of the liquid biopsy for pediatric diffuse midline glioma using ddPCR. Sci Rep. 2021;11:5098.

[54] O'Halloran K, Yellapantula V, Christodoulou E, et al. Low-pass whole-genome and targeted sequencing of cell-free DNA from cerebrospinal fluid in pediatric patients with central nervous system tumors. Neuro-Oncol Adv. 2023;5:vdad077.

[55] Chicard M, Iddir Y, Masliah Planchon J, et al. Cell-Free DNA Extracted from CSF for the Molecular Diagnosis of Pediatric Embryonal Brain Tumors. Cancers. 2023;15:3532.

[56] Pan C, Diplas BH, Chen X, et al. Molecular profiling of tumors of the brainstem by sequencing of CSF-derived circulating tumor DNA. Acta Neuropathol (Berl). 2019;137:297–306.

[57] Brown CG, Clarke J. Nanopore development at Oxford Nanopore. Nat Biotechnol. 2016;34:810–811.

[58] Carter J-M, Hussain S. Robust long-read native DNA sequencing using the ONT CsgG Nanopore system. Wellcome Open Res. 2018;2:23.

[59] Wang Y, Zhao Y, Bollas A, et al. Nanopore sequencing technology, bioinformatics and applications. Nat Biotechnol. 2021;39:1348–1365.

[60] Liu Y, Rosikiewicz W, Pan Z, et al. DNA methylation-calling tools for Oxford Nanopore sequencing: a survey and human epigenome-wide evaluation. Genome Biol. 2021;22:295.

[61] Martignano F, Munagala U, Crucitta S, et al. Nanopore sequencing from liquid biopsy: analysis of copy number variations from cell-free DNA of lung cancer patients. Mol Cancer. 2021;20:32.

[62] Katsman E, Orlanski S, Martignano F, et al. Detecting cell-of-origin and cancer-specific methylation features of cell-free DNA from Nanopore sequencing. Genome Biol. 2022;23:158.

[63] Kuschel LP, Hench J, Frank S, et al. Robust methylation-based classification of brain tumours using nanopore sequencing. Neuropathol Appl Neurobiol [Internet]. 2022 [cited 2022 Nov 6]; Available from: https://onlinelibrary.wiley.com/doi/10.1111/nan.12856.

[64] De Coster W, D'Hert S, Schultz DT, et al. NanoPack: visualizing and processing long-read sequencing data. Berger B, editor. Bioinformatics. 2018;34:2666–2669.

[65] Li H. Minimap2: pairwise alignment for nucleotide sequences. Bioinformatics. 2018;34:3094–3100.

[66] Li H. New strategies to improve minimap2 alignment accuracy. Bioinformatics. 2021;37:4572–4574.

[67] Danecek P, Bonfield JK, Liddle J, et al. Twelve years of SAMtools and BCFtools. GigaScience. 2021;10:giab008.

[68] Boeva V, Popova T, Bleakley K, et al. Control-FREEC: a tool for assessing copy number and allelic content using next-generation sequencing data. Bioinforma Oxf Engl. 2012;28:423–425.

[69] Adalsteinsson VA, Ha G, Freeman SS, et al. Scalable whole-exome sequencing of cell-free DNA reveals high concordance with metastatic tumors. Nat Commun. 2017;8:1324.

[70] Simpson JT, Workman RE, Zuzarte PC, et al. Detecting DNA cytosine methylation using nanopore sequencing. Nat Methods. 2017;14:407–410.

[71] Schwartzentruber J, Korshunov A, Liu X-Y, et al. Driver mutations in histone H3.3 and chromatin remodelling genes in paediatric glioblastoma. Nature. 2012;482:226–231.

[72] Louis DN, Perry A, Reifenberger G, et al. The 2016 World Health Organization Classification of Tumors of the Central Nervous System: a summary. Acta Neuropathol (Berl). 2016;131:803–820.

[73] Lassaletta A, Zapotocky M, Mistry M, et al. Therapeutic and Prognostic Implications of BRAF V600E in Pediatric Low-Grade Gliomas. J Clin Oncol. 2017;35:2934–2941.

[74] Pfister S, Remke M, Benner A, et al. Outcome Prediction in Pediatric Medulloblastoma Based on DNA Copy-Number Aberrations of Chromosomes 6q and 17q and the *MYC* and *MYCN* Loci. J Clin Oncol. 2009;27:1627–1636.

[75] Cho Y-J, Tsherniak A, Tamayo P, et al. Integrative Genomic Analysis of Medulloblastoma Identifies a Molecular Subgroup That Drives Poor Clinical Outcome. J Clin Oncol. 2011;29:1424–1430.

[76] Roussel MF, Robinson GW. Role of MYC in Medulloblastoma. Cold Spring Harb Perspect Med. 2013;3:a014308–a014308.

[77] Biegel JA, Zhou JY, Rorke LB, et al. Germ-line and acquired mutations of INI1 in atypical teratoid and rhabdoid tumors. Cancer Res. 1999;59:74–79.

[78] Hasselblatt M, Nagel I, Oyen F, et al. SMARCA4-mutated atypical teratoid/rhabdoid tumors are associated with inherited germline alterations and poor prognosis. Acta Neuropathol (Berl). 2014;128:453–456.

[79] Tomlins SA, Rhodes DR, Perner S, et al. Recurrent Fusion of *TMPRSS2* and ETS Transcription Factor Genes in Prostate Cancer. Science. 2005;310:644–648.

[80] Barbieri CE, Baca SC, Lawrence MS, et al. Exome sequencing identifies recurrent SPOP, FOXA1 and MED12 mutations in prostate cancer. Nat Genet. 2012;44:685–689.

[81] Zehir A, Benayed R, Shah RH, et al. Mutational landscape of metastatic cancer revealed from prospective clinical sequencing of 10,000 patients. Nat Med. 2017;23:703–713.

[82] Robinson D, Van Allen EM, Wu Y-M, et al. Integrative Clinical Genomics of Advanced Prostate Cancer. Cell. 2015;161:1215–1228.

[83] Castro E, Goh C, Olmos D, et al. Germline *BRCA* Mutations Are Associated With Higher Risk of Nodal Involvement, Distant Metastasis, and Poor Survival Outcomes in Prostate Cancer. J Clin Oncol. 2013;31:1748–1757.

[84] Afflerbach A-K, Rohrandt C, Brändl B, et al. Classification of Brain Tumors by Nanopore Sequencing of Cell-Free DNA from Cerebrospinal Fluid. Clin Chem. 2023;hvad115.

[85] Baroni LV, Sundaresan L, Heled A, et al. Ultra high-risk PFA ependymoma is characterized by loss of chromosome 6q. Neuro-Oncol. 2021;23:1360–1370.

[86] Izquierdo E, Proszek P, Pericoli G, et al. Droplet digital PCR-based detection of circulating tumor DNA from pediatric high grade and diffuse midline glioma patients. Neuro-Oncol Adv. 2021;3:vdab013.

[87] Kojic M, Maybury MK, Waddell N, et al. Efficient detection and monitoring of pediatric brain malignancies with liquid biopsy based on patient-specific somatic mutation screening. Neuro-Oncol. 2023;25:1507–1517.

[88] Brennan CW, Verhaak RGW, McKenna A, et al. The Somatic Genomic Landscape of Glioblastoma. Cell. 2013;155:462–477.

[89] Vaisvila R, Ponnaluri VKC, Sun Z, et al. Enzymatic methyl sequencing detects DNA methylation at single-base resolution from picograms of DNA. Genome Res. 2021;31:1280–1289.

[90] Appay R, Dehais C, Maurage C-A, et al. CDKN2A homozygous deletion is a strong adverse prognosis factor in diffuse malignant IDH-mutant gliomas. Neuro-Oncol. 2019;noz124.

[91] Reis GF, Pekmezci M, Hansen HM, et al. *CDKN2A* Loss Is Associated With Shortened Overall Survival in Lower-Grade (World Health Organization Grades II–III) Astrocytomas. J Neuropathol Exp Neurol. 2015;74:442–452.

[92] Martínez-Ricarte F, Mayor R, Martínez-Sáez E, et al. Molecular Diagnosis of Diffuse Gliomas through Sequencing of Cell-Free Circulating Tumor DNA from Cerebrospinal Fluid. Clin Cancer Res. 2018;24:2812–2819.

[93] Miller AM, Szalontay L, Bouvier N, et al. Next-generation sequencing of cerebrospinal fluid for clinical molecular diagnostics in pediatric, adolescent and young adult brain tumor patients. Neuro-Oncol. 2022;24:1763–1772.

[94] Miller AM, Shah RH, Pentsova EI, et al. Tracking tumour evolution in glioma through liquid biopsies of cerebrospinal fluid. Nature. 2019;565:654–658.

[95] Bale TA, Yang S-R, Solomon JP, et al. Clinical Experience of Cerebrospinal Fluid–Based Liquid Biopsy Demonstrates Superiority of Cell-Free DNA over Cell Pellet Genomic DNA for Molecular Profiling. J Mol Diagn. 2021;23:742–752.

[96] Cheng DT, Mitchell TN, Zehir A, et al. Memorial Sloan Kettering-Integrated Mutation Profiling of Actionable Cancer Targets (MSK-IMPACT). J Mol Diagn. 2015;17:251–264.

[97] Djirackor L, Halldorsson S, Niehusmann P, et al. Intraoperative DNA methylation classification of brain tumors impacts neurosurgical strategy. Neuro-Oncol Adv. 2021;3:vdab149.

[98] Patel A, Dogan H, Payne A, et al. Rapid-CNS2: rapid comprehensive adaptive nanopore-sequencing of CNS tumors, a proof-of-concept study. Acta Neuropathol (Berl). 2022;143:609–612.

[99] Vermeulen C, Pagès-Gallego M, Kester L, et al. Ultra-fast deep-learned CNS tumour classification during surgery. Nature. 2023;622:842–849.

[100] Collins VP, Jones DTW, Giannini C. Pilocytic astrocytoma: pathology, molecular mechanisms and markers. Acta Neuropathol (Berl). 2015;129:775–788.

6. Abstract

Diagnosing a central nervous system (CNS) tumor relies heavily on histopathological and molecular analysis of tumor tissue. This is not always feasible as tumor tissue cannot always be obtained safely, with especially difficult situations in pediatric patients. There is a great need for minimally invasive CNS tumor diagnostics that can molecularly diagnose the tumor, and its development was the aim of this work.

For this, cerebrospinal fluid (CSF) was investigated, specifically cell-free DNA (cfDNA) as an analyte isolated from it.

As a first attempt, droplet digital PCR (ddPCR) was established. It proves to be an informative approach, for specific single nucleotide variants as well as copy number variations of defined genes. It is very sensitive and in none of the 29 analyzed patient samples, a false positive was observed.

Methylation arrays and next-generation sequencing approaches would in theory allow an uninformed approach to make an initial diagnosis. Yet, both methods were not ideal for the analysis of cfDNA and did not deliver satisfactory results that would allow an implementation of this method into routine diagnostics.

Nanopore sequencing permits the analysis of sequence as well as methylation simultaneously. The protocol was adapted for the use with short, fragmented DNA. Copy number variation plots calculated from the sequence were used to capture gains and losses, and the methylation was used to classify the tumor exactly using a random forest classifier. 197 samples were analyzed and in 48.6% of all technically successful samples, tumor-derived cfDNA could be found. This approach grants the possibility to diagnose a tumor without prior knowledge of the tissue, and the use in long-term monitoring settings.

A novel, minimally-invasive diagnostic method for CNS tumors has thus been developed that has potential to be adapted into clinical routine.

7. Zusammenfassung

Um einen Tumor des zentralen Nervensystems (ZNS) zu diagnostizieren, wird für histopathologische und molekulare Analysen eine Gewebsbiopsie benötigt. Diese ist nicht immer verfügbar, da nicht immer eine sichere Entnahme gewährleistet werden kann, mit besonderen Schwierigkeiten bei pädiatrischen Patient:innen. Es besteht ein großer Bedarf an minimal-invasiven Methoden, die eine genaue molekulare Analyse des Tumors, und somit eine exakte Diagnose, erlauben. Dafür wurde in dieser Arbeit Liquor, insbesondere zell-freie DNA als Analyt, untersucht.

In einem ersten Ansatz wurde die *droplet digital PCR* (ddPCR) etabliert. Sie stellte sich als informative Methode für Punktmutationen und Kopienzahlveränderungen von Genen heraus. Die Methode ist sehr sensitiv und in keiner der 29 analysierten Patient:innenproben wurde ein falsch-positives Signal beobachtet.

Methylierungsarrays und *Next-Generation*-Sequenzierungsansätze sind theoretisch in der Lage, bei einer initialen Diagnose zu helfen, ohne dass vorher etwas über den Tumor bekannt ist. Die Ergebnisse der hier getesteten Methoden waren allerdings nicht überzeugend.

Nanopore-Sequenzierung erlaubt die zeitgleiche Aufnahme von DNA-Sequenz und Methylierung. In dieser Arbeit wurde das Protokoll für kurze, stark fragmentierte DNA angepasst. Kopienzahlprofile, die mithilfe der Sequenz berechnet wurden, wurde ausgewertet, um Verluste und Zugewinne nachzuweisen; die Methylierung wurde mit Hilfe eines Random Forest Klassifikationsverfahrens analysiert. 197 Liquorproben wurden analysiert und in 48.6% aller technisch einwandfreien Proben konnte zell-freie DNA, die vom Tumor stammte, nachgewiesen werden. Die Methode erlaubt es, eine initiale Diagnose ohne vorherige Informationen oder Verdachtsdiagnosen zu erstellen.

Es wurde eine neue, minimal-invasive diagnostische Methode für ZNS-Tumoren etabliert, die das Potential hat, in die klinische Routinediagnostik implementiert zu werden.

8. Appendix

8.1. Supplementary figures
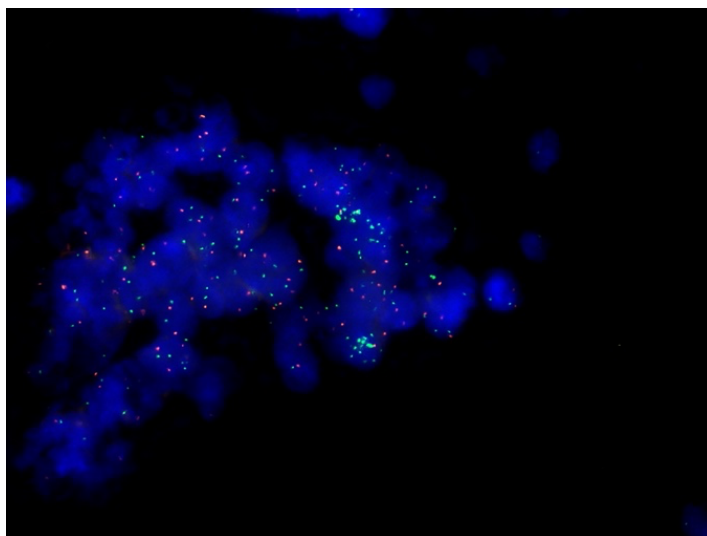
Supplementary Figure 1 FISH of tumor tissue of patient 1 with a medulloblastoma, showing focal amplifications of Myc (green) in occasional cells. Control centromere of chromosome 8 in red. FISH - fluorescence in situ hybridization.
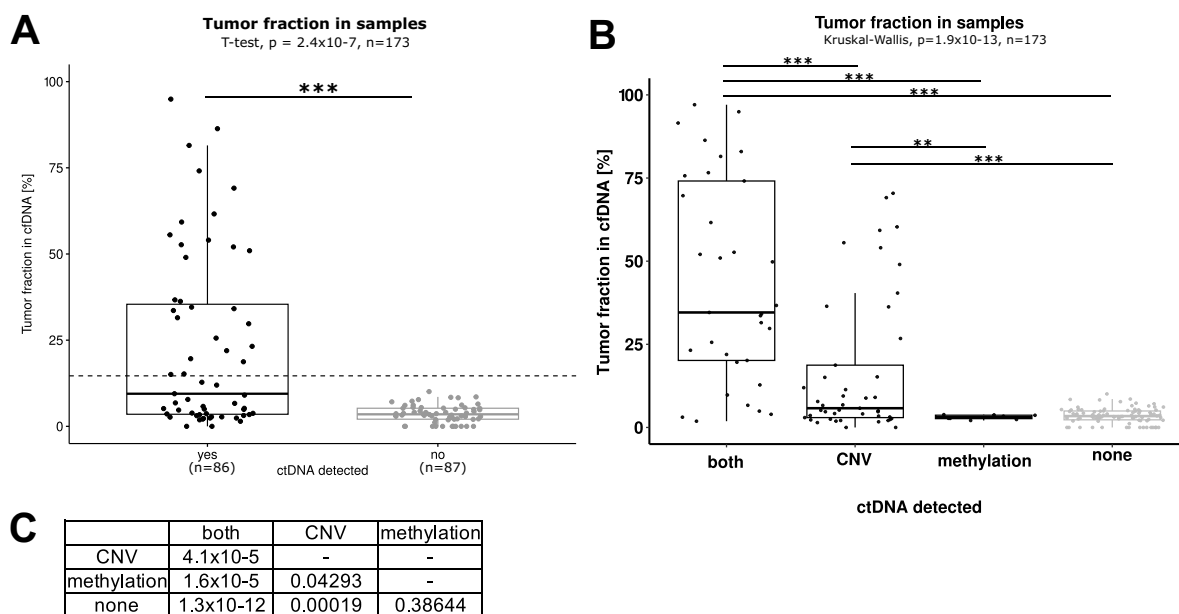
Supplementary Figure 2 Calculated tumor fractions are statistically significantly different between samples with detected ctDNA and without and between detection methods. (A) A statistically significant higher tumor fraction was observed in samples with detectable ctDNA (t-test, p = 2.4x10-7, n=173). (B) Statistical differences were observed for tumor fractions between ctDNA detection methods (Kruskal-Wallis, p = 1.9x10-13, n=173), with exact p-values of differences between detection methods as calculated by Wilcoxon-test in (C).

8.2. Supplementary tables

Supplementary Table 1 with clinical, sequencing and analysis details of all cfDNA samples analyzed by Nanopore sequencing on the following pages.

Supplementary Table 1 Clinical, sequencing and analysis details on all 197 cfDNA samples analyzed by Nanopore sequencing.

ID	multiple samples per patient	malignancy	entity	disease status	age [years]	collection time	days post-surgery	CSF volume [mL]	ng cfDNA per mL CSF	technical	tumor cells	cell count per mL	total reads [M]	passed reads [M]	failed reads [M]	% passed reads	mean read length [bp]	Gb	coverage	CpGs	input [ng]	CNV	NanoDx	NanoDx score	class NanoDx	ctDNA	cfDNA % of total DNA	tumor fraction by ichorCNA	corresponding ID in Afflerbach et al.
1	no	malignant	Medulloblastoma	active	5	pre	NA	NA	22.18	pass	FALSE	NA	0.642	0.447	0.195	69.64	354.0	0.37	0.116	5451	10.64	TRUE	FALSE	0.046	too low	yes	43	0.078	1
2	yes	malignant	Medulloblastoma	active	12	post	439	2.0	11.99	pass	FALSE	1.33	0.343	0.183	0.160	53.36	417.2	0.32	0.101	2261	39.50	TRUE	TRUE	0.161	TRUE	yes	31	0.341	2
3	no	malignant	Medulloblastoma	unknown	8	post	915	2.0	10.80	pass	FALSE	0.67	1.113	0.678	0.435	60.92	544.0	2.08	0.649	808	12.00	FALSE	NA	NA	NA	no	58	0.034	3
4	yes	malignant	Medulloblastoma	active	15	post	97	4.0	12.51	pass	FALSE	1.00	3.023	2.029	0.994	67.12	347.3	2.83	0.885	26537	14.00	NA	FALSE	0.147	CTRL	NA	51	0.020	4
5	no	malignant	Medulloblastoma	unknown	5	early post	NA	2.0	68.67	fail	FALSE	2.67	0.002	0.001	0.001	64.57	0.0	0.00	0.001	NA	20.60	NA	NA	NA	NA	NA	0	NA	5
6	yes	malignant	Medulloblastoma	active	14	pre	NA	3.0	7.40	fail	FALSE	0.67	0.945	0.016	0.930	1.65	958.4	0.11	0.033	NA	11.50	NA	NA	NA	NA	NA	30	0.022	6
7	yes	malignant	Medulloblastoma	active	15	post	121	3.0	8.66	pass	FALSE	0.00	1.160	0.551	0.609	47.52	295.9	0.44	0.137	3381	11.55	FALSE	FALSE	0.090	CTRL	no	56	0.072	7
8	yes	malignant	Medulloblastoma	active	14	early post	NA	3.0	17.68	fail	FALSE	4.67	0.161	0.075	0.086	46.47	384.2	0.15	0.046	494	15.02	NA	NA	NA	NA	NA	47	0.029	8
9	yes	malignant	Medulloblastoma	active	14	post	50	2.0	16.20	pass	FALSE	1.33	2.676	1.006	1.669	37.61	368.7	0.83	0.259	16320	18.00	FALSE	FALSE	0.121	CTRL	no	60	0.024	9
10	yes	malignant	Medulloblastoma	active	12	post	666	5.0	6.44	pass	FALSE	1.33	2.507	0.429	2.078	17.10	399.3	1.05	0.329	1538	13.44	TRUE	FALSE	0.038	too low	yes	54	NA	10
11	yes	malignant	Medulloblastoma	active	15	post	181	5.0	13.84	fail	FALSE	0.33	2.699	0.125	2.574	4.65	364.5	0.44	0.138	NA	15.40	NA	NA	NA	NA	NA	53	0.043	11
12	yes	malignant	Medulloblastoma	active	37	early post	NA	4.0	342.50	pass	FALSE	1.67	6.907	5.186	1.721	75.09	738.9	5.27	1.646	100000	41.10	FALSE	FALSE	0.187	CTRL	no	57	0.000	12
13	yes	malignant	Medulloblastoma	active	13	post	722	3.0	9.00	pass	FALSE	0.33	1.502	1.116	0.386	74.31	404.9	3.29	1.027	532	36.21	FALSE	NA	NA	NA	NA	28	0.023	13
14	yes	malignant	Medulloblastoma	active	16	post	294	2.0	8.80	pass	FALSE	1.33	0.283	0.146	0.137	51.61	451.5	0.25	0.077	1097	15.47	NA	FALSE	0.092	CTRL	yes	44	0.213	14
15	yes	malignant	Medulloblastoma	active	13	post	792	3.5	12.95	fail	FALSE	0.33	0.050	0.030	0.020	60.13	294.4	0.05	0.016	119	15.54	NA	NA	NA	NA	NA	39	0.510	15
16	no	malignant	Medulloblastoma	active	5	early post	NA	3.0	166.73	pass	FALSE	1.33	9.565	8.408	1.157	87.90	388.2	5.00	1.564	100000	10.00	TRUE	TRUE	0.388	TRUE	yes	75	0.058	16
17	yes	malignant	Medulloblastoma	unknown	14	post	238	2.0	18.48	pass	FALSE	2.00	0.220	0.117	0.103	53.15	257.7	0.16	0.050	353	16.26	NA	NA	NA	NA	yes	91	0.021	17
18	yes	malignant	Medulloblastoma	unknown	14	post	266	2.0	12.22	pass	FALSE	1.00	0.300	0.203	0.096	67.91	395.0	0.45	0.142	1009	25.29	FALSE	FALSE	0.080	CTRL	no	61	0.616	18
19	yes	malignant	Medulloblastoma	active	13	early post	NA	2.0	7.34	pass	FALSE	0.00	7.666	4.381	3.286	57.14	359.8	2.69	0.841	69998	13.86	TRUE	TRUE	0.086	TRUE	yes	40	0.949	19
20	yes	malignant	Medulloblastoma	active	13	post	94	4.0	30.00	pass	FALSE	0.67	0.679	0.250	0.429	36.86	341.0	0.17	0.053	2534	12.00	TRUE	TRUE	0.117	TRUE	yes	66	0.052	20
21	no	malignant	Medulloblastoma	unknown	1	post	34	2.0	57.15	pass	FALSE	24.00	0.931	0.378	0.553	40.63	375.7	0.28	0.087	4213	10.16	TRUE	FALSE	0.104	CTRL	yes	20	0.052	21
22	no	malignant	Medulloblastoma	unknown	9	post	605	3.0	15.35	pass	FALSE	0.33	0.475	0.190	0.285	40.00	568.6	0.50	0.155	157	12.82	NA	NA	NA	NA	NA	10	0.152	22
23	no	malignant	Medulloblastoma	unknown	40	post	652	8.0	6.93	fail	FALSE	5.33	1.265	0.009	1.257	0.68	0.0	0.10	0.031	NA	10.16	NA	NA	NA	NA	NA	0	0.032	23
24	no	malignant	Medulloblastoma	active	7	post	18	3.0	3.17	fail	FALSE	NA	0.002	0.000	0.002	0.00	0.0	0.00	0.001	NA	30.08	NA	NA	NA	NA	NA	0	NA	24
25	no	malignant	Medulloblastoma	active	17	early post	NA	2.0	75.38	pass	FALSE	6.33	8.152	5.711	2.441	70.06	325.7	2.13	0.666	100000	10.11	TRUE	FALSE	0.089	CTRL	yes	75	0.152	25
26	no	malignant	Medulloblastoma	active	6	post	292	2.0	10.46	pass	FALSE	15.33	0.689	0.370	0.319	53.69	286.0	0.47	0.145	512	12.56	FALSE	FALSE	0.096	CTRL	no	42	0.032	26
27	yes	malignant	Medulloblastoma	active	12	early post	NA	3.0	37.58	pass	FALSE	6.00	1.515	0.935	0.580	61.73	305.9	0.45	0.141	24585	41.75	FALSE	TRUE	0.160	TRUE	yes	74	0.346	27
28	no	malignant	Medulloblastoma	active	34	early post	NA	3.0	21.60	pass	FALSE	3.67	3.023	2.637	0.386	87.23	463.7	2.92	0.912	82690	14.28	FALSE	FALSE	0.078	CTRL	no	74	0.052	28
29	yes	malignant	Medulloblastoma	active	4	early post	NA	3.0	66.10	pass	FALSE	26.00	0.979	0.284	0.696	28.97	594.9	0.54	0.168	8512	10.58	FALSE	FALSE	0.037	CTRL	no	11	0.049	29
30	yes	malignant	Medulloblastoma	active	4	pre	NA	9.0	75.25	pass	FALSE	4.67	2.079	1.543	0.536	74.20	750.5	2.32	0.725	63053	10.54	FALSE	FALSE	0.100	CTRL	no	18	0.000	30
31	no	malignant	Medulloblastoma	unknown	6	post	481	3.0	23.85	pass	FALSE	0.67	1.084	0.580	0.504	53.53	439.1	1.87	0.585	1495	10.49	FALSE	FALSE	0.055	CTRL	no	61	0.084	31
32	yes	malignant	Medulloblastoma	active	41	early post	NA	4.0	8.10	pass	FALSE	324.33	0.488	0.271	0.217	55.58	247.4	0.11	0.034	4635	9.72	FALSE	TRUE	0.074	TRUE	yes	20	0.038	32
33	yes	malignant	Medulloblastoma	unknown	11	post	1566	2.0	7.45	pass	FALSE	0.33	0.748	0.522	0.226	69.80	261.4	1.37	0.426	1696	11.92	FALSE	TRUE	0.115	CTRL	no	55	0.027	33
34	yes	malignant	Medulloblastoma	active	12	post	205	2.0	16.20	pass	FALSE	0.33	0.861	0.335	0.526	38.89	320.7	0.80	0.250	3503	10.26	TRUE	TRUE	0.084	TRUE	yes	15	0.220	34
35	no	malignant	Medulloblastoma	unknown	3	post	62	200.0	29.50	pass	FALSE	2.33	4.573	1.156	3.417	25.27	434.9	0.86	0.269	35319	11.80	TRUE	TRUE	0.084	TRUE	yes	30	0.028	35
36	no	malignant	Medulloblastoma	active	8	pre	NA	3.0	46.38	pass	TRUE	3.67	4.274	2.958	1.316	69.21	329.9	1.47	0.460	78349	27.90	FALSE	TRUE	0.147	TRUE	yes	11	0.256	36
37	yes	malignant	Medulloblastoma	active	1	pre	NA	10.0	11.88	pass	FALSE	0.33	1.586	1.269	0.317	80.00	502.6	1.60	0.500	38999	9.98	FALSE	NA	0.143	NA	no	NA	0.091	37
38	no	malignant	Medulloblastoma	unknown	1	early post	NA	4.0	17.30	pass	FALSE	0.00	0.766	0.359	0.407	46.87	412.9	0.27	0.083	16549	10.38	TRUE	TRUE	0.069	TRUE	yes	28	0.830	38
39	no	malignant	Medulloblastoma	active	12	early post	NA	3.0	13.15	pass	NA	3.67	1.369	0.743	0.626	54.26	379.1	1.57	0.491	10639	18.41	TRUE	TRUE	0.032	TRUE	yes	26	0.367	39
40	no	malignant	Medulloblastoma	active	17	early post	NA	5.0	3.50	pass	NA	0.67	1.652	1.207	0.446	73.03	513.7	3.04	0.949	11028	14.67	TRUE	FALSE	0.382	too low	no	41	0.050	40
41	yes	malignant	Medulloblastoma	active	9	early post	NA	4.5	13.10	pass	FALSE	1.33	5.525	4.562	0.963	82.58	1414.6	7.53	2.352	805399	97.80	TRUE	TRUE	0.196	TRUE	yes	54	0.091	41
42	yes	malignant	Medulloblastoma	active	36	post	NA	2.0	815.00	pass	FALSE	NA	6.495	5.300	1.195	81.60	326.4	2.28	0.713	87457	26.40	FALSE	FALSE	0.089	CTRL	no	35	0.067	42
43	yes	malignant	Medulloblastoma	active	46	pre	NA	3.0	66.00	pass	NA	66.67	4.774	3.564	1.210	74.65	324.0	2.51	0.783	31592	17.36	TRUE	TRUE	0.093	TRUE	yes	54	0.052	43
44	no	malignant	Medulloblastoma	active	17	pre	NA	2.0	12.40	pass	FALSE	0.67	0.712	0.556	0.156	78.09	902.1	0.00	0.000	3379	6.52	TRUE	FALSE	0.089	CTRL	yes	35	0.052	44
45	yes	malignant	Medulloblastoma	active	1	post	84	3.0	4.08	pass	FALSE	0.33	0.775	0.414	0.361	53.47	568.8	0.91	0.284	8427	11.79	FALSE	FALSE	0.093	CTRL	no	29	0.000	45
46	yes	malignant	Medulloblastoma	unknown	6	post	107	3.0	9.83	pass	FALSE	0.33	0.508	0.336	0.171	66.27	620.6	0.57	0.179	11390	11.79	FALSE	FALSE	0.065	too low	no	40	0.062	46
47	no	malignant	Medulloblastoma	unknown	NA	NA	NA	8.0	392.50	pass	NA	36.67	11.718	10.098	1.620	86.17	490.6	6.40	2.001	50000	31.40	NA	NA	0.084	NA	no	55	0.053	NA
48	yes	malignant	Medulloblastoma	active	6	post	33	3.0	52.25	pass	FALSE	NA	14.123	12.255	1.868	86.77	258.4	5.32	1.662	91625	20.90	TRUE	TRUE	0.292	TRUE	yes	81	0.527	48
49	yes	malignant	Medulloblastoma	active	3	pre	NA	14.0	25.63	pass	FALSE	1.00	9.183	7.986	1.197	86.96	219.4	2.49	0.777	32399	20.50	TRUE	TRUE	0.190	TRUE	yes	89	0.196	49
50	no	malignant	Medulloblastoma	active	3	early post	NA	2.0	250.00	pass	TRUE	8.00	2.993	2.456	0.537	82.07	458.2	1.55	0.484	66371	25.00	FALSE	FALSE	0.046	too low	no	4	0.055	NA
51	yes	malignant	Medulloblastoma	unknown	3	early post	NA	4.0	4.50	pass	FALSE	1.00	5.207	4.364	0.843	83.82	382.2	2.43	0.759	50000	14.95	TRUE	TRUE	0.070	TRUE	yes	NA	0.098	NA
52	no	malignant	Medulloblastoma	unknown	NA	post	NA	3.0	4.93	pass	NA	NA	5.561	4.884	0.676	87.84	384.3	3.64	1.136	50000	8.87	TRUE	TRUE	0.180	TRUE	yes	28	0.766	NA
53	no	malignant	Medulloblastoma	unknown	10	NA	NA	2.0	45.00	pass	FALSE	NA	2.799	2.063	0.736	73.69	756.1	2.48	0.776	50000	15.12	FALSE	FALSE	0.070	CTRL	no	6	0.061	NA
54	no	malignant	Medulloblastoma	unknown	6	NA	NA	2.0	27.25	pass	FALSE	NA	4.917	4.264	0.653	86.73	573.0	2.91	0.910	50000	15.28	FALSE	TRUE	0.100	TRUE	yes	34	0.019	NA
55	yes	malignant	Medulloblastoma	unknown	4	NA	NA	3.0	3.63	pass	TRUE	NA	0.886	0.622	0.264	70.18	398.0	1.48	0.463	1570	6.82	FALSE	TRUE	0.060	too low	yes	71	0.041	NA
56	yes	malignant	Medulloblastoma	unknown	12	pre	NA	3.0	77.00	pass	NA	66.67	4.774	3.564	1.210	74.65	324.0	2.51	0.783	31592	NA	TRUE	FALSE	0.220	TRUE	yes	54	0.034	NA
57	yes	malignant	Medulloblastoma	unknown	NA	NA	NA	4.0	NA	pass	NA	2.33	2.259	1.638	0.621	72.52	411.4	2.91	0.908	23595	NA	FALSE	FALSE	0.050	too low	no	35	0.047	NA
58	no	malignant	Medulloblastoma	unknown	5	NA	NA	4.0	NA	pass	FALSE	NA	6.723	5.109	1.613	76.00	320.7	5.45	1.703	NA	NA	FALSE	TRUE	0.060	too low	no	29	0.049	NA
59	no	malignant	Medulloblastoma	unknown	8	NA	NA	NA	NA	pass	FALSE	NA	0.556	0.333	0.223	59.93	230.6	0.66	0.207	2264	NA	TRUE	FALSE	0.060	too low	yes	40	0.017	NA
60	no	malignant	Medulloblastoma	unknown	20	NA	NA	4.5	NA	pass	FALSE	6.33	1.413	1.065	0.348	75.36	1142.2	2.40	0.750	47685	10.20	FALSE	TRUE	0.090	CTRL	no	81	0.054	NA
61	no	malignant	Medulloblastoma	unknown	3	NA	NA	8.0	1612.50	pass	FALSE	5.33	13.651	9.956	3.695	72.93	232.5	3.28	1.026	71982	38.70	TRUE	TRUE	0.910	TRUE	yes	89	0.498	NA
62	no	malignant	Medulloblastoma	unknown	7	NA	NA	3.0	4.18	pass	FALSE	NA	2.266	1.596	0.670	70.44	260.6	0.58	0.181	13920	6.68	TRUE	TRUE	0.200	TRUE	yes	6	0.757	NA
63	no	malignant	Medulloblastoma	unknown	12	NA	NA	2.0	4.65	pass	FALSE	0.33	8.496	5.900	2.596	69.44	253.1	2.08	0.650	13780	8.74	FALSE	FALSE	0.070	CTRL	no	34	0.040	NA
64	no	malignant	Medulloblastoma	unknown	35	post	38	2.5	3.64	pass	NA	NA	0.916	0.434	0.482	47.36	453.2	0.29	0.090	10293	9.00	FALSE	TRUE	0.040	too low	yes	53	0.068	NA
65	no	malignant	Medulloblastoma	unknown	4	NA	NA	4.0	1.93	pass	FALSE	2.33	0.802	0.430	0.372	53.65	626.7	0.38	0.117	12785	7.00	FALSE	FALSE	0.110	CTRL	no	33	0.000	NA

ID	multiple samples per patient	entity	malignancy	disease status	age [years]	collection time	days post-surgery	CSF volume [mL]	ng cfDNA per mL CSF	technical	tumor cells	cell count per mL	total reads [M]	passed reads [M]	failed reads [M]	% passed reads	mean read length [bp]	Gb	coverage	CpGs	input [ng]	CNV	NanoDx	NanoDx score	class NanoDx	ctDNA	cfDNA % of total DNA	tumor fraction by ichorCNA	corresponding ID in Afflerbach et al.
66	no	Ependymoma	malignant	unknown	1	post	145	NA	10.15	fail	FALSE	0.00	0.195	0.023	0.172	11.92	672.9	0.58	0.181	NA	9.54	FALSE	FALSE	NA	NA	NA	NA	NA	50
67	yes	Ependymoma	malignant	active	5	early post	NA	2.0	51.00	pass	FALSE	1.67	13.598	11.632	1.965	85.55	323.8	5.28	1.651	100000	20.40	FALSE	FALSE	0.047	too low	no	33	0.061	51
68	no	Ependymoma	malignant	active	4	pre	NA	2.0	270.00	pass	FALSE	2357.33	1.035	0.186	0.849	17.93	682.9	0.23	0.070	7682	48.00	TRUE	FALSE	0.106	CTRL	yes	6	0.050	52
69	yes	Ependymoma	malignant	unknown	5	post	21	2.0	15.59	pass	FALSE	4.33	2.665	1.385	1.280	51.96	496.9	1.46	0.457	35441	15.38	FALSE	FALSE	0.055	too low	yes	30	0.490	53
70	yes	Ependymoma	malignant	active	1	post	78	2.0	63.54	pass	FALSE	0.00	1.408	0.395	1.014	28.02	755.8	1.08	0.339	747	24.78	FALSE	NA	NA	NA	no	NA	0.065	54
71	yes	Ependymoma	malignant	unknown	1	early post	NA	4.0	30.15	pass	FALSE	16.00	1.318	0.188	1.130	14.24	533.2	0.16	0.050	4455	10.72	TRUE	FALSE	0.075	CTRL	yes	13	0.015	55
72	yes	Ependymoma	malignant	unknown	1	post	140	4.0	47.75	pass	NA	NA	1.381	0.475	0.906	34.37	344.5	1.00	0.311	981	33.43	FALSE	NA	NA	NA	no	NA	0.027	56
73	yes	Ependymoma	malignant	unknown	6	post	283	3.0	9.80	pass	FALSE	1.33	1.106	0.678	0.428	61.30	265.8	1.99	0.623	1223	10.00	FALSE	FALSE	0.110	CTRL	no	23	0.037	57
74	yes	Ependymoma	malignant	active	5	early post	NA	4.0	19.68	pass	FALSE	13.67	11.526	9.493	2.033	82.37	387.0	4.90	1.531	342758	25.68	FALSE	FALSE	0.110	CTRL	no	28	0.000	58
75	yes	Ependymoma	malignant	unknown	5	early post	NA	3.0	12.85	pass	FALSE	8.33	5.486	2.526	2.959	46.05	305.1	1.32	0.412	61998	14.04	FALSE	FALSE	0.075	CTRL	no	45	0.029	59
76	no	Ependymoma	malignant	active	6	pre	NA	3.0	7.27	fail	FALSE	2.33	0.237	0.076	0.161	32.18	357.0	0.13	0.041	NA	7.27	NA	NA	NA	NA	NA	54	0.046	60
77	no	Ependymoma	malignant	unknown	6	post	1315	3.0	4.63	fail	FALSE	2.33	0.000	0.000	0.000	0.00	NA	0.00	0.000	NA	8.70	FALSE	NA	NA	NA	NA	8	NA	61
78	yes	Ependymoma	malignant	active	2	post	389	4.0	1.50	pass	FALSE	0.00	1.433	0.201	1.232	14.00	359.3	0.38	0.120	1109	3.00	FALSE	FALSE	0.127	CTRL	no	2	0.053	62
79	yes	Ependymoma	malignant	unknown	6	post	520	3.0	3.60	pass	FALSE	1.00	0.614	0.377	0.237	61.47	285.3	0.94	0.294	635	6.48	FALSE	NA	NA	NA	no	12	0.053	63
80	yes	Ependymoma	malignant	unknown	8	post	1067	3.0	18.95	pass	FALSE	10.00	0.787	0.585	0.202	74.31	311.5	0.62	0.194	857	9.85	TRUE	NA	NA	NA	yes	45	0.363	64
81	no	Ependymoma	malignant	unknown	67	NA	NA	2.0	9.80	pass	FALSE	NA	3.125	0.329	2.796	10.52	665.8	1.23	0.384	959	10.19	FALSE	NA	NA	NA	no	40	0.038	65
82	no	Ependymoma	malignant	unknown	49	post	9818	350.0	931.25	pass	FALSE	NA	15.570	13.076	2.493	83.99	351.6	5.51	1.722	18217	100.00	FALSE	FALSE	0.098	CTRL	no	46	0.000	66
83	no	Ependymoma	malignant	unknown	8	post	NA	0.9	5.40	pass	FALSE	NA	0.886	0.572	0.314	64.55	365.8	1.56	0.488	288	5.00	FALSE	FALSE	0.080	FALSE	no	NA	0.051	NA
84	no	Ependymoma	malignant	unknown	1	NA	NA	NA	25.25	pass	FALSE	NA	0.631	0.291	0.340	46.14	453.4	0.88	0.274	1797	15.15	FALSE	FALSE	0.060	too low	no	NA	0.000	NA
85	no	Ependymoma	malignant	unknown	41	post	41	NA	183.50	pass	NA	NA	1.627	1.062	0.565	65.25	632.4	1.00	0.311	43207	100.00	FALSE	FALSE	0.170	CTRL	no	41	0.041	NA
86	no	Ependymoma	malignant	unknown	0	pre	NA	4.0	192.00	pass	FALSE	826.67	21.665	17.691	3.974	81.66	311.9	7.53	2.353	100000	76.80	FALSE	TRUE	0.102	TRUE	yes	89	0.049	78
87	no	ATRT	malignant	unknown	14	post	23	15.0	61.50	pass	FALSE	1.33	1.420	0.800	0.620	56.33	478.1	0.63	0.196	18286	17.22	FALSE	FALSE	0.082	CTRL	no	11	0.038	79
88	no	ATRT	malignant	active	2	early post	NA	3.0	56.00	pass	NA	6.00	4.505	3.874	0.631	86.00	473.2	2.80	0.874	100000	22.40	FALSE	FALSE	0.050	too low	yes	8	0.000	80
89	no	ATRT	malignant	active	3	early post	NA	4.0	51.00	pass	FALSE	NA	3.940	3.125	0.815	79.30	315.7	1.81	0.566	50257	10.20	TRUE	FALSE	0.035	too low	yes	54	0.027	81
90	no	ATRT	malignant	active	1	post	NA	4.0	19.75	pass	FALSE	NA	8.220	6.226	1.995	75.74	275.6	2.25	0.704	119330	95.00	TRUE	TRUE	0.117	TRUE	yes	77	0.031	82
91	no	ATRT	malignant	unknown	2	pre	NA	700.0	80.31	pass	TRUE	826.67	31.999	28.015	3.984	87.55	588.3	10.00	6.694	1663380	100.00	TRUE	FALSE	0.028	too low	yes	21	0.000	83
92	yes	ATRT	malignant	active	4	early post	NA	6.0	188.00	pass	FALSE	0.67	0.766	0.381	0.385	49.72	293.7	0.17	0.052	7849	15.04	FALSE	TRUE	0.139	TRUE	yes	71	0.024	84
93	yes	ATRT	malignant	unknown	4	post	57	2.0	139.75	pass	FALSE	0.33	1.559	0.141	1.417	9.07	326.6	0.11	0.033	2192	11.18	FALSE	TRUE	0.071	TRUE	yes	46	0.021	85
94	yes	ATRT	malignant	active	4	pre	NA	1.0	835.00	pass	FALSE	NA	20.166	17.057	3.109	84.58	238.5	4.88	1.526	50000	33.40	TRUE	FALSE	0.070	too low	no	10	0.040	NA
95	yes	ATRT	malignant	unknown	4	post	NA	4.0	131.50	pass	NA	NA	7.694	5.856	1.838	76.11	294.3	4.03	1.259	91523	21.04	FALSE	FALSE	0.030	too low	no	62	0.038	NA
96	yes	ATRT	malignant	unknown	2	NA	NA	4.0	49.75	pass	NA	NA	5.039	1.916	3.123	38.02	464.3	1.54	0.482	50000	NA	FALSE	FALSE	0.050	too low	no	4	0.028	NA
97	no	ATRT	malignant	unknown	2	NA	NA	7.0	54.00	pass	NA	NA	3.009	2.502	0.507	83.14	609.4	2.24	0.701	23473	21.60	FALSE	NA	0.040	NA	NA	NA	0.000	NA
98	yes	ATRT	malignant	unknown	2	post	NA	3.0	NA	pass	NA	1.67	1.790	1.420	0.370	79.32	577.6	3.50	1.092	5333	NA	TRUE	FALSE	0.090	too low	no	NA	0.032	NA
99	no	ATRT	malignant	unknown	2	NA	NA	NA	15.75	pass	FALSE	NA	0.877	0.546	0.332	62.21	237.9	0.60	0.188	26465	14.00	FALSE	FALSE	0.048	too low	NA	49	0.054	98
100	no	Lymphoma	malignant	active	75	pre	NA	10.0	15.75	pass	FALSE	0.00	4.209	3.311	0.897	78.68	292.3	2.26	0.707	4723	13.35	FALSE	FALSE	0.086	FALSE	yes	31	0.128	99
101	no	Lymphoma	malignant	unknown	65	post	1427	5.0	13.35	pass	FALSE	15.33	1.686	0.982	0.704	58.25	308.2	3.07	0.958	2361	17.22	TRUE	TRUE	0.081	TRUE	yes	NA	0.066	100
102	no	Lymphoma	malignant	active	83	post	1447	7.0	14.35	pass	FALSE	3.00	0.433	0.209	0.225	48.17	369.0	0.50	0.156	24360	11.85	FALSE	FALSE	0.077	CTRL	no	27	0.030	101
103	no	Lymphoma	malignant	unknown	80	post	NA	7.0	19.75	pass	FALSE	0.33	3.832	3.545	0.287	92.51	301.7	0.97	0.303	50000	6.16	FALSE	NA	0.077	NA	yes	14	0.030	102
104	no	Lymphoma	malignant	unknown	56	post	NA	3.0	4.40	pass	FALSE	3.67	0.506	0.313	0.193	61.82	1586.6	0.87	0.273	50000	15.05	FALSE	FALSE	NA	CTRL	no	NA	0.026	NA
105	yes	Lymphoma	malignant	unknown	60	post	NA	6.0	113.25	pass	FALSE	24.00	3.828	1.683	2.145	43.96	1419.6	3.37	1.053	34862	15.86	FALSE	FALSE	0.050	too low	yes	8	0.114	NA
106	no	Lymphoma	malignant	active	83	post	NA	6.0	26.88	pass	FALSE	49.00	8.079	7.167	0.911	88.72	595.4	6.37	1.992	7955	15.05	TRUE	FALSE	0.030	too low	no	10	0.022	NA
107	no	Lymphoma	malignant	active	49	post	NA	2.0	27.50	pass	FALSE	14.00	5.664	4.008	1.656	70.76	271.8	2.69	0.842	3543	14.30	TRUE	TRUE	0.080	TRUE	yes	NA	0.697	NA
108	no	Lymphoma	malignant	unknown	74	NA	NA	4.0	79.50	pass	FALSE	12.00	3.653	1.367	2.285	37.44	253.5	0.84	0.263	8338	NA	TRUE	TRUE	0.180	TRUE	yes	32	0.915	NA
109	yes	Lymphoma	malignant	unknown	52	early post	NA	NA	49.75	pass	NA	NA	0.298	0.164	0.133	55.20	1106.4	0.27	0.083	50000	12.00	FALSE	FALSE	0.050	too low	yes	27	0.021	NA
110	no	Lymphoma	malignant	unknown	52	NA	NA	6.0	4.53	pass	NA	2.00	15.172	12.338	2.834	81.32	222.4	3.40	1.062	100000	28.40	TRUE	NA	0.070	NA	no	41	0.024	NA
111	no	Lymphoma	malignant	unknown	NA	NA	NA	NA	NA	pass	NA	0.67	0.320	0.062	0.258	19.45	237.9	0.15	0.048	27	44.30	TRUE	TRUE	0.910	TRUE	yes	31	0.970	NA
112	no	Pilocytic Astrocytoma	benign	active	5	pre	NA	3.5	5.08	pass	FALSE	22.33	5.346	4.343	1.003	81.25	533.5	3.96	1.237	1255	14.00	FALSE	FALSE	0.103	CTRL	no	26	0.071	67
113	no	Pilocytic Astrocytoma	benign	unknown	11	post	3913	2.0	17.45	fail	FALSE	0.67	0.588	0.190	0.398	32.31	595.5	0.53	0.166	237	17.45	FALSE	NA	NA	NA	NA	26	0.020	68
114	no	Pilocytic Astrocytoma	benign	unknown	6	early post	NA	3.0	131.36	pass	FALSE	0.00	1.707	0.731	0.976	42.81	246.5	1.43	0.448	274	10.10	FALSE	FALSE	0.086	CTRL	no	77	0.073	69
115	no	Pilocytic Astrocytoma	benign	active	3	pre	NA	3.0	5.08	pass	FALSE	NA	0.197	0.112	0.085	56.70	462.1	0.42	0.130	17149	8.12	FALSE	NA	NA	NA	no	45	NA	70
116	no	Pilocytic Astrocytoma	benign	active	6	pre	NA	11.0	10.47	pass	FALSE	3.00	0.001	0.000	0.001	0.00	523.3	0.00	0.000	10929	9.87	FALSE	NA	NA	NA	no	30	0.030	71
117	no	Pilocytic Astrocytoma	benign	unknown	33	post	16	3.0	3.70	pass	NA	NA	1.397	0.917	0.480	65.66	302.8	0.75	0.235	2613	10.00	FALSE	FALSE	0.075	CTRL	no	NA	0.028	72
118	yes	Pilocytic Astrocytoma	benign	active	1	pre	NA	2.0	17.98	pass	FALSE	NA	1.290	0.587	0.703	45.50	573.0	1.20	0.375	1749	10.07	FALSE	FALSE	0.058	too low	no	8	0.019	73
119	no	Pilocytic Astrocytoma	benign	active	20	pre	NA	8.0	28.75	pass	FALSE	2.33	0.327	0.226	0.102	68.95	724.7	0.70	0.218	1200	10.35	FALSE	FALSE	0.057	TRUE	no	32	0.032	74
120	no	Pilocytic Astrocytoma	benign	active	7	pre	NA	2.0	31.63	pass	FALSE	0.67	0.769	0.200	0.569	25.99	647.4	0.64	0.200	194	17.56	TRUE	TRUE	0.073	TRUE	no	27	0.033	75
121	no	Pilocytic Astrocytoma	benign	active	3	pre	NA	4.0	10.90	pass	FALSE	NA	0.815	0.113	0.702	13.86	580.9	0.33	0.104	5912	15.26	FALSE	FALSE	0.089	CTRL	no	10	0.041	76
122	no	Pilocytic Astrocytoma	benign	active	4	early post	NA	NA	6.23	pass	FALSE	4.33	0.243	0.129	0.114	52.99	344.1	0.38	0.120	100	9.28	FALSE	NA	0.070	NA	no	31	0.042	77
123	no	Pilocytic Astrocytoma	benign	unknown	11	NA	NA	3.0	12.03	pass	FALSE	2.00	5.185	4.011	1.175	77.35	832.8	4.04	1.263	7136	12.50	FALSE	FALSE	0.400	FALSE	yes	NA	NA	NA
124	no	Glioblastoma	malignant	unknown	70	post	142	10.0	16.09	pass	FALSE	0.67	1.610	0.123	1.487	7.64	311.2	0.13	0.041	20471	10.01	FALSE	FALSE	0.056	too low	NA	46	NA	92
125	no	Glioblastoma	malignant	unknown	48	post	99	5.0	14.53	pass	FALSE	2.00	2.998	0.623	2.375	20.77	308.6	1.02	0.318	801	14.50	FALSE	NA	NA	NA	yes	25	0.691	93
126	no	Glioblastoma	malignant	unknown	59	post	289	6.0	3.65	fail	NA	0.00	0.001	0.000	0.001	0.00	273.1	0.00	0.000	NA	9.85	FALSE	NA	NA	NA	NA	40	NA	94
127	no	Glioblastoma	malignant	active	40	pre	NA	2.0	14.00	pass	FALSE	1.67	4.703	2.405	2.298	51.14	215.8	1.61	0.503	1506	15.12	TRUE	TRUE	0.072	TRUE	yes	NA	0.202	95
128	no	Glioblastoma	malignant	unknown	70	pre	NA	2.0	14.40	fail	FALSE	0.67	0.511	0.281	0.230	54.93	278.1	0.83	0.259	NA	17.28	TRUE	NA	NA	NA	NA	43	0.151	96
129	no	Glioblastoma	malignant	active	43	pre	NA	3.0	9.35	fail	FALSE	0.67	0.010	0.005	0.005	53.15	0.0	0.00	0.001	NA	11.22	NA	NA	NA	NA	NA	21	NA	97
130	no	Glioblastoma	malignant	active	42	pre	NA	4.0	7.53	pass	FALSE	NA	1.308	0.464	0.844	35.45	510.1	1.03	0.321	NA	10.85	FALSE	FALSE	0.050	too low	no	27	0.030	NA

ID	multiple samples per patient	entity	malignancy	disease status	age [years]	collection time	days post-surgery	CSF volume [mL]	ng cfDNA per mL CSF	technical	tumor cells	cell count per mL	total reads [M]	passed reads [M]	failed reads [M]	% passed reads	mean read length [bp]	Gb	coverage	CpGs	input [ng]	CNV	NanoDx	NanoDx score	class NanoDx	ctDNA	cfDNA % of total DNA	tumor fraction by ichorCNA	corresponding ID in Afflerbach et al.
131	no	Glioblastoma	malignant	unknown	67	NA	NA	NA	NA	pass	FALSE	68.00	2.366	1.913	0.453	80.87	278.3	0.64	0.199	21401	NA	FALSE	FALSE	0.060	CTRL	no	NA	0.043	NA
132	no	Glioblastoma	malignant	unknown	53	NA	NA	2.0	4.30	pass	FALSE	41.33	5.185	4.424	0.761	85.33	616.7	3.15	0.984	100000	8.08	FALSE	FALSE	0.050	CTRL	no	NA	0.037	NA
133	no	Glioblastoma	malignant	unknown	74	NA	NA	NA	NA	pass	NA	32.67	10.916	9.014	1.902	82.58	500.7	5.43	1.698	50000	27.80	FALSE	FALSE	0.090	CTRL	no	NA	0.000	NA
134	no	Glioblastoma	malignant	active	NA	pre	NA	2.4	163.00	pass	NA	NA	12.377	10.456	1.921	84.48	228.2	2.83	0.884	45887	20.00	TRUE	TRUE	0.090	TRUE	yes	60	0.232	NA
135	no	unknown	unknown	unknown	22	pre	NA	3.0	14.67	fail	FALSE	0.33	0.004	0.002	0.002	61.56	0.0	0.01	0.002	NA	11.00	NA	NA	NA	NA	NA	19	NA	107
136	no	unknown	unknown	active	16	NA	NA	4.0	6.03	fail	FALSE	2.33	0.315	0.017	0.298	5.51	0.0	0.04	0.013	NA	8.04	NA	NA	NA	NA	NA	0	0.152	108
137	no	unknown	unknown	unknown	53	pre	NA	11.0	4.90	pass	FALSE	0.00	0.579	0.334	0.245	57.67	683.5	0.83	0.259	3145	8.82	TRUE	FALSE	0.075	CTRL	yes	14	0.031	109
138	no	unknown	unknown	unknown	69	NA	NA	1.0	4.10	pass	FALSE	0.00	0.750	0.538	0.212	71.69	1556.8	1.74	0.545	7	7.38	FALSE	FALSE	0.640	CTRL	no	NA	NA	NA
139	no	unknown	unknown	unknown	83	NA	NA	2.0	NA	pass	FALSE	1.33	0.931	0.303	0.627	32.61	1021.6	0.97	0.302	11531	NA	FALSE	FALSE	NA	NA	no	NA	0.031	NA
140	no	unknown	unknown	unknown	14	NA	NA	2.0	5.00	pass	FALSE	72.00	1.623	0.630	0.992	38.86	1780.8	2.26	0.708	80550	10.00	TRUE	FALSE	0.150	too low	yes	44	0.025	NA
141	no	unknown	unknown	unknown	60	NA	NA	4.0	NA	pass	NA	72.00	13.616	10.404	3.212	76.41	262.7	3.51	1.096	80550	10.00	TRUE	FALSE	0.880	CTRL	no	57	0.000	NA
142	no	unknown	unknown	unknown	NA	NA	NA	4.0	4.68	pass	FALSE	72.00	4.867	3.894	0.974	80.00	213.1	1.16	0.363	50000	10.00	TRUE	TRUE	0.880	TRUE	yes	57	0.315	NA
143	no	unknown	unknown	unknown	17	post	NA	3.0	10.40	fail	FALSE	NA	0.438	0.071	0.366	16.28	279.6	0.18	0.055	NA	12.48	NA	NA	NA	NA	NA	36	NA	110
144	no	Diffuse Midline Glioma	malignant	active	9	pre	NA	4.0	197.25	pass	FALSE	NA	0.813	0.544	0.269	66.91	513.7	0.42	0.130	15911	26.30	FALSE	TRUE	0.071	TRUE	yes	0	0.336	86
145	no	Diffuse Midline Glioma	malignant	active	62	pre	NA	4.0	14.74	fail	FALSE	0.33	0.000	0.000	0.000	0.00	0.0	0.00	0.000	NA	9.83	NA	NA	NA	NA	NA	18	NA	87
146	yes	Diffuse Midline Glioma	malignant	active	19	pre	NA	4.0	12.85	pass	FALSE	0.33	0.784	0.468	0.316	59.67	349.0	0.94	0.294	1614	10.28	FALSE	FALSE	0.055	too low	no	50	0.025	88
147	no	Diffuse Midline Glioma	malignant	unknown	26	post	32	3.0	1155.00	pass	FALSE	NA	3.322	2.793	0.529	84.07	1511.1	4.53	1.414	100000	30.00	FALSE	FALSE	0.357	CTRL	no	4	0.035	89
148	no	Diffuse Midline Glioma	malignant	active	33	pre	NA	5.0	23.80	pass	FALSE	0.67	2.031	0.151	1.880	7.42	451.7	0.31	0.095	584	10.47	FALSE	FALSE	NA	NA	no	48	0.000	90
149	yes	Diffuse Midline Glioma	malignant	active	19	post	446	8.0	NA	pass	FALSE	0.67	21.329	18.399	2.930	86.26	363.4	7.70	2.405	469511	49.00	TRUE	FALSE	0.036	too low	no	85	0.054	91
150	no	Diffuse Midline Glioma	malignant	unknown	62	post	NA	2.0	8.60	pass	FALSE	0.67	1.370	0.831	0.539	60.64	362.2	2.32	0.725	4838	12.04	TRUE	FALSE	0.040	NA	yes	31	0.047	NA
151	no	Diffuse Midline Glioma	malignant	unknown	NA	NA	NA	6.0	705.00	pass	NA	NA	8.549	7.105	1.444	83.11	1000.6	8.30	2.594	100000	84.60	TRUE	TRUE	0.620	TRUE	yes	3	0.521	NA
152	no	Breast Carcinoma	malignant	unknown	73	NA	NA	3.0	NA	pass	FALSE	0.33	4.824	3.316	1.507	68.75	376.1	5.42	1.695	46124	NA	TRUE	FALSE	0.100	CTRL	NA	NA	0.047	NA
153	no	Breast Carcinoma	malignant	unknown	64	NA	NA	5.0	44.10	pass	TRUE	6.00	0.636	0.077	0.559	12.08	1605.7	0.25	0.078	5745	20.00	TRUE	FALSE	0.950	FALSE	yes	4	0.556	NA
154	no	Breast Carcinoma	malignant	unknown	86	NA	NA	2.5	15.26	pass	TRUE	34.00	0.690	0.548	0.142	79.48	697.8	0.49	0.153	14050	21.80	FALSE	FALSE	0.080	too low	no	11	0.011	NA
155	no	Breast Carcinoma	malignant	unknown	43	NA	NA	1.7	NA	pass	FALSE	34.00	8.847	7.500	1.346	84.78	264.0	2.38	0.744	48556	22.08	TRUE	FALSE	0.950	TRUE	yes	86	0.540	NA
156	no	Breast Carcinoma	malignant	unknown	NA	NA	NA	5.5	8.90	pass	NA	NA	11.127	9.622	1.505	86.48	274.8	3.06	0.955	39224	20.00	TRUE	FALSE	0.070	TRUE	yes	30	0.120	NA
157	no	Craniopharyngioma	benign	active	NA	pre	NA	3.0	NA	pass	NA	NA	3.395	2.169	1.226	63.88	216.4	0.68	0.212	1749	10.80	FALSE	FALSE	0.078	CTRL	no	8	0.033	NA
158	yes	Craniopharyngioma	benign	active	54	post	746	4.0	30.75	pass	FALSE	70.67	6.533	5.295	1.238	81.04	295.1	2.48	0.775	12672	22.14	FALSE	TRUE	0.093	TRUE	yes	52	0.038	103
159	yes	Craniopharyngioma	benign	active	54	post	752	4.0	33.25	pass	TRUE	60.00	12.658	10.426	2.232	82.37	251.6	3.67	1.148	195418	26.60	FALSE	FALSE	0.117	TRUE	yes	35	0.037	104
160	yes	Craniopharyngioma	benign	unknown	54	early post	NA	6.0	52.13	pass	TRUE	218.67	5.013	4.403	0.610	87.83	360.1	3.60	1.126	57512	15.60	FALSE	FALSE	0.096	CTRL	yes	30	0.048	105
161	yes	Craniopharyngioma	benign	active	54	post	807	18.0	18.43	pass	TRUE	140.00	11.236	9.765	1.471	86.91	436.5	5.91	1.847	100000	14.47	FALSE	FALSE	0.129	CTRL	no	20	0.037	106
162	no	Germ Cell Tumor	malignant	unknown	11	post	14	2.0	44.78	pass	FALSE	2.00	3.258	2.070	1.189	63.52	228.8	0.56	0.174	10930	9.95	FALSE	FALSE	0.030	too low	yes	86	0.187	114
163	no	Germ Cell Tumor	malignant	active	22	pre	NA	2.0	16.50	pass	FALSE	6.00	0.315	0.128	0.187	40.60	640.0	0.23	0.073	651	13.20	FALSE	FALSE	0.050	NA	no	50	0.085	115
164	no	Germ Cell Tumor	malignant	active	11	pre	NA	3.0	3.88	pass	NA	NA	1.529	0.779	0.750	50.95	279.1	0.92	0.287	2378	6.98	TRUE	TRUE	0.030	too low	yes	NA	0.088	NA
165	no	Germ Cell Tumor	malignant	unknown	11	NA	NA	4.0	7.20	pass	NA	0.33	11.738	7.568	4.170	64.48	206.3	3.47	1.084	43435	NA	TRUE	FALSE	0.040	too low	yes	NA	0.404	111
166	no	ETMR	malignant	unknown	1	post	123	2.0	7.20	fail	FALSE	0.33	0.006	0.000	0.006	0.00	702.9	0.00	0.000	184	1.88	NA	NA	0.030	NA	NA	8	NA	NA
167	yes	ETMR	malignant	active	1	post	46	4.0	46.75	pass	NA	NA	16.522	13.287	3.235	80.42	302.4	5.06	1.581	100000	37.40	TRUE	TRUE	0.182	TRUE	yes	59	0.864	112
168	yes	ETMR	malignant	active	1	early post	NA	11.0	31.59	pass	FALSE	NA	16.552	12.912	3.640	78.01	449.0	9.84	3.076	100000	10.00	FALSE	TRUE	0.148	TRUE	yes	55	0.741	113
169	no	Glioma	malignant	active	15	pre	NA	9.0	3.20	pass	NA	64.00	1.561	0.810	0.751	51.91	482.7	0.88	0.275	13707	5.76	FALSE	FALSE	0.080	FALSE	yes	NA	0.032	NA
170	no	Oligodendroglioma	malignant	unknown	36	NA	NA	10.0	10.23	pass	FALSE	1.33	4.193	3.316	0.877	79.08	416.4	2.37	0.741	73877	12.27	FALSE	FALSE	0.030	too low	yes	50	0.000	NA
171	no	Glioma	malignant	unknown	49	pre	NA	1.0	5.30	pass	NA	64.00	6.719	4.776	1.943	71.08	293.9	1.90	0.593	57879	4.66	FALSE	NA	0.110	too low	NA	NA	0.045	NA
172	no	Pineoblastoma	malignant	active	4	pre	NA	3.0	3.80	pass	FALSE	3.67	0.646	0.250	0.396	38.73	858.7	0.84	0.263	1022	6.84	FALSE	FALSE	0.060	CTRL	NA	NA	0.040	NA
173	yes	Chordoma	NA	active	4	early post	NA	4.0	74.25	pass	FALSE	0.33	5.867	4.561	1.306	77.75	596.2	5.15	1.610	100000	23.76	FALSE	FALSE	0.070	CTRL	no	6	0.000	NA
174	no	DLGNT	benign	unknown	4	post	37	2.0	14.67	pass	FALSE	416.00	0.991	0.638	0.352	64.44	500.7	1.42	0.442	1064	11.41	FALSE	FALSE	0.067	CTRL	yes	28	0.000	120
175	no	DLGNT	benign	unknown	13	NA	NA	8.0	408.75	pass	FALSE	2.00	3.522	2.519	1.004	71.51	362.2	2.10	0.655	87225	32.70	TRUE	FALSE	0.050	too low	yes	64	0.603	NA
176	no	Lung Carcinoma	malignant	active	51	pre	NA	7.0	4.35	pass	NA	NA	13.813	10.133	3.680	73.36	298.8	5.95	1.860	1104	10.00	TRUE	NA	0.050	NA	yes	40	0.065	123
177	no	Lung Carcinoma	malignant	unknown	61	NA	NA	1.0	6.25	pass	FALSE	5.33	0.482	0.209	0.274	43.30	476.8	0.63	0.197	74654	10.00	TRUE	TRUE	0.059	too low	yes	50	0.815	NA
178	no	Oligodendroglioma	malignant	unknown	42	pre	NA	9.0	6.75	pass	FALSE	1.67	0.815	0.484	0.331	59.42	256.9	0.31	0.096	8290	9.45	TRUE	TRUE	0.187	TRUE	yes	50	0.036	116
179	no	Oligodendroglioma	malignant	active	41	pre	NA	2.0	17.45	pass	FALSE	NA	13.852	11.890	1.963	77.84	239.9	2.14	0.669	155930	17.45	TRUE	FALSE	0.153	too low	yes	92	0.298	117
180	no	Pineoblastoma	malignant	active	16	pre	NA	3.0	337.50	pass	FALSE	1.00	3.218	2.510	0.708	77.99	330.6	2.21	0.691	34042	40.50	FALSE	FALSE	0.070	FALSE	yes	NA	0.704	125
181	no	Pineoblastoma	malignant	unknown	3	NA	NA	4.0	3.10	pass	NA	NA	2.510	2.847	0.708	59.17	330.6	2.21	1.842	100000	76.70	FALSE	FALSE	0.139	CTRL	yes	NA	0.083	118
182	no	Plexus Papilloma	benign	unknown	9	post	21	2.0	NA	pass	TRUE	NA	4.813	2.847	0.991	59.17	1682.3	5.89	1.842	100000	76.70	TRUE	TRUE	0.050	too low	no	6	0.000	118
183	no	Plexus Papilloma	benign	active	1	pre	NA	2.0	8.28	pass	FALSE	2.00	3.522	2.519	1.004	71.51	362.2	2.10	0.655	66471	20.54	TRUE	FALSE	0.050	too low	yes	64	0.095	119
184	no	Prostate Carcinoma	malignant	unknown	NA	NA	NA	8.0	145.50	pass	NA	NA	13.813	10.133	3.680	82.80	298.8	5.95	1.860	500000	32.70	TRUE	FALSE	0.070	FALSE	yes	NA	0.364	NA
185	no	Prostate Carcinoma	malignant	unknown	56	pre	NA	5.0	7.00	pass	FALSE	1.00	2.110	1.381	0.729	65.45	815.0	4.72	1.474	12669	10.00	FALSE	FALSE	0.040	too low	yes	40	0.019	NA
186	yes	Acoustic Neurinoma	NA	NA	50	pre	NA	7.0	12.85	pass	FALSE	31.00	6.140	4.518	1.623	73.57	350.6	3.27	1.022	50000	15.42	TRUE	FALSE	0.040	FALSE	yes	25	0.000	NA
187	no	Astrocytoma	benign	active	1	pre	NA	4.0	3.43	pass	NA	5.33	2.468	0.745	1.723	30.19	419.7	0.90	0.280	12834	6.17	FALSE	FALSE	0.040	NA	no	NA	0.049	NA
188	no	Rhabdomyosarcoma Embryonal	malignant	active	8	early post	NA	2.0	11.85	pass	FALSE	0.33	0.523	0.317	0.207	60.52	184.0	0.31	0.097	197	14.22	TRUE	NA	0.048	NA	yes	25	0.034	121
189	no	Glioneuronal Tumor	benign	active	3	pre	NA	750.0	179.35	pass	FALSE	8.67	2.630	1.006	1.624	38.26	327.2	0.45	0.142	23401	13.56	FALSE	FALSE	0.110	too low	no	18	0.040	122
190	no	Leptomeningeal Tumor	NA	unknown	7	NA	NA	4.0	17.98	pass	NA	NA	0.185	0.106	0.079	57.29	282.3	0.05	0.016	672	14.38	FALSE	FALSE	0.110	FALSE	yes	NA	0.030	NA
191	no	MN1-altered Glioma	malignant	unknown	17	NA	NA	2.0	32.38	pass	NA	NA	0.348	0.104	0.244	29.80	563.6	0.14	0.045	3111	19.43	FALSE	NA	0.109	NA	yes	15	0.101	NA
192	no	MN1-altered Glioma	malignant	active	6	pre	NA	2.0	10.25	pass	FALSE	11.67	4.461	3.503	0.958	78.52	717.4	3.60	1.125	500000	10.25	FALSE	FALSE	0.109	CTRL	yes	16	0.033	124
193	no	Paranasal Sinus Cancer	malignant	unknown	60	NA	NA	7.0	66.75	pass	NA	5.33	0.334	0.064	0.270	19.22	527.4	0.20	0.063	123	19.03	TRUE	FALSE	0.040	too low	yes	NA	0.288	NA
194	no	Pleomorphic Xanthoastrocytoma	malignant	active	16	post	666	3.0	17.74	pass	FALSE	2.00	0.334	0.064	0.270	19.22	432.9	0.20	0.063	123	19.03	NA	FALSE	NA	NA	no	56	NA	126

ID	multiple samples per patient	entity	malignancy	disease status	age [years]	collection time	days post-surgery	CSF volume [mL]	ng cfDNA per mL CSF	technical	tumor cells	cell count per mL	total reads [M]	passed reads [M]	failed reads [M]	% passed reads	mean read length [bp]	Gb	coverage	CpGs	input [ng]	CNV	NanoDx	NanoDx score	class NanoDx	ctDNA	cfDNA % of total DNA	tumor fraction by ichorCNA	corresponding ID in Afflerbach et al.
195	no	RGNT	benign	unknown	53	pre	NA	1.0	24.30	pass	FALSE	NA	0.280	0.188	0.092	67.24	383.1	0.29	0.090	2437	9.72	TRUE	FALSE	0.092	FALSE	yes	NA	0.021	127
196	no	SEGA	benign	active	14	pre	NA	3.0	41.75	pass	FALSE	1.67	0.978	0.257	0.722	26.22	394.1	0.21	0.064	8318	10.02	FALSE	FALSE	0.177	CTRL	no	5	0.044	128
197	no	Stomach carcinoma	malignant	unknown	61	post	NA	7.0	39.63	pass	TRUE	16.00	11.531	10.174	1.356	88.24	432.9	6.29	1.965	100000	31.70	TRUE	FALSE	0.031	too low	yes	40	0.593	129

9. List of Publications

Part of this thesis has been published in:

Afflerbach AK, Rohrandt C, Brändl B, Sönksen M, Hench J, Frank S, Börnigen D, Alawi M, Mynarek M, Winkler B, Ricklefs F, Synowitz M, Dührsen L, Rutkowski S, Wefers AK, Müller FJ, Schoof M, Schüller U. Classification of Brain Tumors by Nanopore Sequencing of Cell-Free DNA from Cerebrospinal Fluid. Clinical Chemistry. 2023 Aug 25:hvad115. doi: 10.1093/clinchem/hvad115. Epub ahead of print. PMID: 37624932.

Co-Authorship during PhD program:

Schoof M, Godbole S, Albert T, Dottermusch M, Walter C, Ballast A, Qin N, Baca Oliveira M, Göbel C, Neyazi S, Holdhof D, Kresbach C, Peter L, Epplen GD, Thaden V, Blattner-Johnson M, Modemann F, Mynarek M, Rutkowski S, Sill M, Varghese J, **Afflerbach AK**, Eckhardt A, Münter D, Struve N, Jones D, Remke M, Neumann J, Kerl K, Schüller U. Mouse modeling of pediatric HGG-MYCN reveals intratumoral heterogeneity including neuronal and oligodendroglial lineage signatures. Nature Commun. *accepted for publication.*

Other publications:

Afflerbach AK, Kiri MD, Detinis T, Maoz BM. Mesenchymal Stem Cells as a Promising Cell Source for Integration in Novel In Vitro Models. Biomolecules. 2020 Sep 10;10(9):1306 doi: 10.3390/biom10091306. PMID: 32927777.

10. Danksagung

11. Curriculum Vitae

Persönliche Angaben

Name	Ann-Kristin Afflerbach
Geburtsdatum	09.04.1996
Geburtsort	Hamburg, Deutschland

Ausbildung

seit 04/2021	PhD Programm Nicht-Medizin, Medizinische Fakultät, Universität Hamburg
10/2018 – 09/2020	Master of Science Molecular Biosciences – Major Neuroscience, Ruprecht-Karls Universität Heidelberg
10/2015 – 09/2018	Bachelor of Science Molecular Life Sciences, Universität Hamburg
04/2015 – 09/2015	Bachelor of Science Biotechnologie, Hochschule für Angewandte Wissenschaften Hamburg
09/2014 – 11/2014	Bachelor of Science Sustainable Development, University of St. Andrews
07/2014	Abitur, Gymnasium Osterbek, Hamburg

Berufserfahrung

seit 10/2020	wissenschaftliche Mitarbeiterin Forschungsinstitut Kinderkrebs-Zentrum Hamburg, Pädiatrische Hämatologie und Onkologie, Universitätsklinikum Hamburg-Eppendorf
04/2020 – 09/2020	wissenschaftliche Hilfskraft Pharmakologisches Institut, Universitätsklinikum Heidelberg
10/2019 – 12/2019	Praktikantin AG Biomedical Engineering – Dr. Maoz Tel Aviv University
04/2019 – 07/2019	Praktikantin AG Neurotransmitter – Dr. Jung-Klawitter Universitätsklinikum Heidelberg
01/2019 – 04/2019	Praktikantin AG Experimentelle Neuroregeneration – Dr. Puttagunta Universitätsklinikum Heidelberg
10/2018 – 02/2019	wissenschaftliche Hilfskraft Nationales Centrum für Tumorerkrankungen, Universitätsklinikum Heidelberg
10/2018 – 12/2018	Praktikantin AG Klinische Kooperationseinheit Neuropathologie – Prof. Dr. von Deimling / Dr. Pusch Deutsches Krebsforschungszentrum Heidelberg
11/2017 – 09/2018	studentische Hilfskraft Bode Chemie GmbH
04/2017 – 10/2017	studentische Hilfskraft Eurofins BioTesting Services Nord GmbH
06/2016 – 03/2017	studentische Hilfskraft Bode Chemie GmbH

12. Eidesstattliche Erklärung

Ich versichere ausdrücklich, dass ich diese Arbeit selbständig und ohne fremde Hilfe verfasst, andere als die von mir angegebenen Quellen und Hilfsmittel nicht benutzt und die aus den benutzten Werken wörtlich oder inhaltlich entnommenen Stellen einzeln nach Ausgabe (Auflage und Jahr des Erscheinens), Band und Seite des benutzten Werkes kenntlich gemacht habe. Ferner versichere ich, dass ich die Dissertation bisher nicht einem Fachvertreter an einer anderen Hochschule zur Überprüfung vorgelegt oder mich anderweitig um Zulassung zur Promotion beworben habe. Ich erkläre mich einverstanden, dass meine Dissertation vom Dekanat der Medizinischen Fakultät mit einer gängigen Software zur Erkennung von Plagiaten überprüft werden kann.

Unterschrift: _____